8-2016

X-ray fluorescence for quantification of lead and strontium in vivo

Aaron James Specht
Purdue University

Graduate School Form
30 Updated 12/26/2015

PURDUE UNIVERSITY
GRADUATE SCHOOL
Thesis/Dissertation Acceptance

This is to certify that the thesis/dissertation prepared

By Aaron Specht

Entitled
X-RAY FLUORESCENCE FOR QUANTIFICATION OF LEAD AND STRONTIUM IN VIVO

For the degree of Doctor of Philosophy

Is approved by the final examining committee:

Linda H Nie
Chair

Wei Zheng

Keith M Stantz

Marc Weisskopf

To the best of my knowledge and as understood by the student in the Thesis/Dissertation Agreement, Publication Delay, and Certification Disclaimer (Graduate School Form 32), this thesis/dissertation adheres to the provisions of Purdue University's "Policy of Integrity in Research" and the use of copyright material.

Approved by Major Professor(s): Linda H Nie

Approved by: Wei Zheng 06/30/2016
Head of the Departmental Graduate Program Date

X-RAY FLUORESCENCE FOR QUANTIFICATION OF LEAD AND STRONTIUM IN VIVO

A Dissertation

Submitted to the Faculty

of

Purdue University

by

Aaron James Specht

In Partial Fulfillment of the

Requirements for the Degree

of

Doctor of Philosophy

August 2016

Purdue University

West Lafayette, Indiana

For my wife, parents, sisters, and brother.

ACKNOWLEDGEMENTS

I am most grateful for the support and guidance from my advisor Dr. Linda Nie. She helped steer me in the right directions both professionally and scholarly to be able to accomplish my goals, and she is a source of inspiration for my future. She was always willing to help and never had a closed door for any of my small problems, and would dedicate as much time as she could to lending her guidance for experiments and problem solving. I hope to be able to reflect many of the same qualities in my life as a scientist to be as admirable as she was to all of our lab members.

I would also like to thank my other committee members Dr. Wei Zheng, Dr. Keith Stantz, and Dr. Marc Weisskopf. The work presented here was only possible through their teachings, critiques, suggestions, and support.

I would also like to thank my fellow lab members that have helped me throughout my studies and helped to direct my future, Dr. Farshad Mostafaei, Dr. Yingzi Liu, Dan Sowers, Yufei Wang, Xinxin Zhang, and Mindy Hsieh. Their support and guidance has helped me throughout my graduate study at Purdue and will serve me in the future as well.

Lastly, I would like to thank my wife and family. With their love and support I was able to become the man I am today. I would have never had the chances I did without any of you by my side.

TABLE OF CONTENTS

Page

Page

Page

LIST OF TABLES

Table Page

LIST OF FIGURES

Figure Page

Figure Page

ABSTRACT

Specht, Aaron James. Ph.D., Purdue University, August 2016. X-ray Fluorescence for Quantification of Lead and Strontium In Vivo. Major Professor: Linda H. Nie.

Lead (Pb) is a toxicant well known for its effects on almost every organ system in the body. Pb use in industry has declined since removal of Pb from gasoline, but many developing countries still have significant use of Pb. Exposure to Pb has been linked with diseases causing neurodegeneration and thus have lasting effects long after the initial exposure. Another metal, strontium (Sr), has been linked with bone disease in particular situations and shown to have uses in treating osteoporosis as a supplement. However, there are no studies of the effects of Sr using a meaningful biomarker. The most commonly used biomarkers for Pb and Sr exposures are blood Pb and Sr; however, blood tests are unable to identify long-term exposure levels due to the short half-life of these metals in blood. Bone stores of Pb and Sr have a half-life of years to decades and serve as a biomarker of long-term exposure. X-ray fluorescence has been used to measure bone Pb and Sr. However, current systems have limitations with radioisotope sources, bulky equipment, and long measurement times. A portable XRF device capable of measurement of bone Pb and Sr, overcomes the limitation of the current systems and has been developed in this work. The detection limit of the portable XRF for bone Pb and Sr was found to be 11 ppm and 5 ppm respectively at 5 mm of skin thickness. The portable XRF

will have limitations of measurement based on an individual's skin thickness. The device was calibrated using standard phantoms and validated with in-lab samples, which demonstrated good agreement between KXRF and portable XRF measurements with strong correlations between goat bone, cadaver bone, and phantom measurements. In a population study of Pb poisoned children the portable XRF was further validated and a significant correlation between KXRF measured bone Pb and portable XRF measured bone Pb was identified; however, the device had limitations based on anatomical differences unaccounted for in children from our calibration. Adaptations of our calibration to account for the differences in children's bone can be used to further improve on the results we obtained. Pb biokinetics was studied in these children, and the blood Pb half-life in the children was calculated to be about 10 days, which is much short than the 30 day half-life identified for adults. Bone Sr was measured in these children and a significant correlation with age was identified, indicating the Sr accumulates in bone. A novel high-energy x-ray tube based KXRF measurement system was tested for its feasibility of in vivo measurement of metals in bone using Monte Carlo (MC) simulation. The novel system shows a combination of the advantages of the portable XRF with a smaller scale device, x-ray tube source, and room temperature detector, as well as the advantages of the KXRF of minimal soft tissue signal degradation with more applicability to a wider range of populations. This device, with an optimized x-ray tube and uranium target of 0.056 mm, was found to have a detection limit for bone Pb measurement of about 3.6 ppm and could be adapted for measurements of multiple metals.

CHAPTER 1. INTRODUCTION

1.1 Pb and Sr Toxicity

Pb has presented a perseverant problem to environmental health despite our control standards and continues to especially affect many communities in developing countries. Pb is a toxicant that affects many part of the human body. Pb exposure occurs via oral cavity, inhalation, or dermal exposures, but dermal exposures are much less efficient. The absorption of Pb depends on the age of the individual with children absorbing 5-10 times more Pb from an oral dose than an average adult would. In adults about 94% of the Pb burden will accumulate in the bones, whereas children will only reflect about 73% of their Pb burden in bone [1]. Blood Pb is primarily in the red blood cells. Pb can act similarly to calcium in many interactions in the body, which is why it is so easily stored in bone. Pb acts primarily as an oxidative stressor to cause changes in organ systems.

Pb replaces calcium in many interactions in the body, and thus can affect nearly every system. Pb exposure has been linked to many severe diseases and health risks including cardiovascular disease, neurodegenerative disease, and even mortality[2-4]. Pb has many adverse health effects in the body primarily affecting the central nervous system [5, 6]. Neurodegenerative disease is of particular concern, as millions of adults

with Pb exposure from leaded gasoline are aging and will be impacted by Pb associated neurodegenerative disease in the coming years. The population associated with this exposure is about 25 million people with effects lasting until the year 2050 [4]. Low-level Pb exposures have been linked to cognitive effects in children [5, 6]. This is of importance as well since these exposures can be obtained environmentally. Occupational exposures are widespread in industry and more proper protections need to be in place to ensure the safety of workers. A study from the CDC showed that over 11,000 workers in the US were still exposed to dangerous levels of Pb with blood Pb values greater than 40 μg/dl, and almost 3,000 of those workers have had those blood Pb levels consistently for multiple years [7]. The protections put in place for occupational workers are apparently lacking as these high blood Pb levels persist. With its ranging effects over the body, even at environmental exposure levels, persistent occupational exposure, and association with long-term neuro-degeneration, bone Pb is a primary target for in vivo XRF technology, which needs to be expanded for future identification of long-term chronic exposure and associated health risk.

Pb is used in many different manufacturing and production environments. Pb has properties that make it versatile for use in many different industries and is still used in electronics, battery manufacturing, Pb alloy bearings, ammunition, and many other applications. Most of the Pb consumption in the US comes from its use in batteries. In developing countries Pb use is not as strictly enforced and Pb is used in things such as gasoline and insecticides. Leaded gasoline is still used as an aviation fuel for particular planes world-wide and releases over 100 tons of Pb each year [8].

Sr may have beneficial and negative effects primarily on bone with exposures being commonplace for most populations. XRF has been used in the study of many metals including Pb for many years [9, 10].The documented health effects of Sr over exposure are limited to changes in the bone. In a study where children ingested food grown in soil with high levels of Sr there was a significant effect on developing bones of the children leading to rickets in the children [11]. The subjects in this study also had a lack of vitamin D and protein in their diets, which likely increased Sr metabolism and the effects observed in the over-exposed population. Sr is known to act similarly to calcium with 99% of the Sr in the body accumulating in the bone [12, 13]. However, beyond effects in bone, other adverse health effects have not been studied for Sr alone.

Sr related health effects from over-exposure generally occur in specific populations with confounding issues such as diet. Everyone is exposed to some levels of Sr from food consumption and aerosols. Sr in soil and uptake in plants accounts for the majority of Sr exposures worldwide and high levels of Sr in soil are common. Sr is a naturally occurring element in the earth's crust and oceans.

Sr has been shown to be beneficial for many people suffering from osteoporosis [14, 15]. Studies showed that using a dose of 2 grams per day of Sr ranelate lowered the incidence of non-vertebral fractures in post-menopausal women [15, 16]. This again results from is similarities with calcium in the body, allowing Sr to replace calcium in bone and strengthen the bone structure. Osteoporotic fractures account for 2.8 million disability-adjusted life years in the Americas and Europe [17]. Thus Sr supplementation as a preventative care measure could potentially help thousands of people; however, proper studies of the effects of Sr are needed to ensure safety in these treatments.

1.2 Biomarkers of Pb and Sr Exposure

1.2.1 Traditional Methods of Pb Exposure Assessment

The traditional biomarker for Pb exposure is blood Pb. Other biomarkers for Pb exposure are bone, urine, plasma, and hair. Hair and finger prick blood Pb samples are prone to contamination, and plasma levels are difficult to measure as the concentrations are generally near the detection limit of the measurement instruments. Urine Pb is an estimation of recent exposure levels and can vary based on volume of urine [18]. Biomarkers are generally chosen to reflect certain biological responses or total body burden of the toxicant. In that sense, blood Pb is an appropriate measure of a persons current exposure levels and potential health risk. The limitations of blood Pb are evident when we look at whole body Pb burden and long-term health effects. Blood Pb only reflects less than 2% of the total body Pb burden with the majority of Pb accumulating in bone [19]. The half-life of Pb in blood is about 30 days [1]. This has implications in the variability of blood Pb over a short period of time. It is possible for a blood Pb level to change fairly drastically over the course of weeks. Blood Pb has a positive response with exposure, but this relationship too can be less clear, as different ages and diet in subjects can drastically change uptake of Pb in the body [20]. Blood Pb has the further complication of analysis using inductively coupled plasma mass spectrometry (ICP-MS) and atomic absorption spectrometry (AAS). These processes require a significant time investment in taking and analyzing each sample, while maintaining a Pb free environment.

1.2.2 Traditional Methods of Sr Exposure Assessment

Sr exposure can be monitored a number of different ways. Similarly to Pb, Sr can be monitored using a blood sample; however this likely reflects the acute exposure. This is done by simply taking a blood sample and analyzing it using a detection system such as AAS or ICP-MS. Similarly, urine, hair, and bone and be studied using a tissue sample and AAS or ICP-MS. Urine, hair, and blood have less relevance to tracking of exposure because of the accumulation of Sr body burden primarily being in bone. Since Sr deposition occurs primarily in the bone, bone biopsy has been used to determine Sr exposure, primarily in studies determining efficacy for treatment of osteoporosis [21]. Bone biopsy is difficult and painful procedure for patients and is generally avoided. A device using dual photon absorptiometry (DPA) has been used to estimate levels of Sr in bone [22]. This device uses two radioisotopes, which complicates the licensing procedures, requires the submersion of the subject's measurement site in water, and a 10-minute measurement time. It also produces results in a measure of percentage Sr, which is difficult unit for further comparisons to other biomarkers of exposure.

1.2.3 Bone Pb and Sr as a Biomarker

Bone has many advantages over blood biomarkers, but also has some limitations. Bone Pb better reflects exposure, especially a cumulative exposure. It has a long half-life of between 10-30 years, and accounts for between 70-90% of the total body Pb burden depending on the age of the subject [1, 19]. The same can be assumed to be similar for Sr

since 99% of Sr accumulates in bone [12, 13]. This long half-life has been used to better illuminate health effects of Pb with delayed symptoms. Bone Pb and Sr is traditionally measured through a KXRF bone measurement device. Bone Pb and Sr could also be obtained through a bone biopsy; however, as mentioned previously this is a painful procedure that would not likely be done multiple times. KXRF measured bone Pb and Sr measurements have the advantage of being an assessment of cumulative exposure and the measurements can be taken in vivo.

1.3 X-ray Fluorescence (XRF)

1.3.1 Principles of X-ray Fluorescence

XRF is a process that can be used to quantify elements in a particular sample using radiation. An incoming radioactive source, which is usually photons, interacts with the sample by means of the photoelectric effect transferring the photon energy to an electron. This will eject an inner shell electron as long as the photon energy is greater than the binding energy of the electron orbital, which typically is from the K or L shell for XRF. An electron from an outer orbital within the atom then de-excited into the orbital the electron was ejected and releases the difference in energy between the two orbitals, which has an energy specific to an individual element. That energy release is the characteristic x-rays, and is collected by a detector.

Each step in the process is governed by specific calculated probabilities. The initial photoelectric interaction depends on the ability of the source radiation to penetrate

to the sample without significant attenuation, and interact by photoelectric absorption rather than either Compton scatter or Rayleigh (coherent) scatter. After a photoelectric interaction, the characteristic yield will determine the probability of a particular energy line being represented from the element. Lastly, there is the probability of the isotropic characteristic x-ray to be produced in the direction of our detector and the absorption of the x-ray in the detector itself. These are all well studied physics interactions and easily calculated events, which justifies the ability to use Monte Carlo simulation methods to test many of these processes.

Beyond the physics, the calibration procedures for XRF are standard and important to the understanding of the process itself. The interaction probabilities will all increase linearly with increasing amount of a particular element. Thus, a linear relationship between the events or counts in the detector for a particular characteristic x-ray will relate to an increase of similar magnitude of concentration of that particular element in the measured sample. Through calibration using samples of known levels of a particular element in similar structural matrices to a test sample, we can determine the concentrations associated with each level of counts.

The detectors used for XRF also need to be specifically chosen for each purpose. Detectors with materials able to produce higher energy resolution are most valuable for use in XRF, since each element has characteristic energies. A high energy resolution allows us to discern more easily between a particular element's energy and background or noise surrounding. Each element observed in a sample will be represented in the energy spectrum with a Gaussian peak centered at the characteristic energy. The width of the Gaussian peak is determine by the resolution of the detector and will determine the

ability to resolve the characteristic x-rays from background and other characteristic peaks of energy close to the peak of interest.

XRF technology is unique in its ability to quantify exposure levels in vivo. The tissue type observed through these techniques can be chosen specifically to aid in identifying health effects from exposure. For Pb, bone is used as the measurement site for its previously mentioned biological half-life of 10 to 30 years, and its accumulation of up to about 90% of the total body Pb burden [1]. Utilizing the physics principles and optimizing detector and calibration procedures we are able to do measurements of many elements in vivo.

1.3.2 In Vivo X-ray Fluorescence Systems for Bone Pb and Sr Measurements

The first in vivo measurement done using XRF was monitoring iodine in thyroid in 1968 [23]. The first bone Pb measurement using KXRF was completed in 1976 by Ahlgren et al. [24]. These methods used a Co-57 source and were able to be optimized to the Cd-109 source with a HPGe detector in 1985 by Somervaille et al. [25]. This method was further optimized by increasing the detector size from 16 mm to 51 mm diameter increasing the acquired signal greatly [26]. The device by Gordon et al. is the typical instrument found in most labs. One final iteration of improvements led to the design of the clover-leaf KXRF measurement system, which has four 16mm HPGe detectors and uses a stronger source than the previous iteration, to lower the minimum detectable limit even more [27, 28]. Bone Sr has been measured more recently using similar equipment as bone Pb with

HPGe detectors with Cd-109 source in a 90-degree and 180-degree geometry and extra shielding around the source and detectors [10].

Current KXRF technology has limitations based on the instrumentation, which restricts the populations available for measurement. Current KXRF systems utilize a Cd-109 radioisotope and high-purity germanium (HPGe) detector system to perform bone Pb measurements. Radioisotopes in general require site-specific licensing procedures that limit the facilities available for using the system. Thus, even if the system is transported elsewhere, the site needs to go through the licensing procedure with the NRC to approve use of the radioisotope. Normally, each site would then buy a source as well, which also is problematic, as there are few sellers of the source. Then, the site would need a health physics or radiation safety officer willing to go through the licensing process and perform annual inspections on the source.

Another pitfall of the KXRF measurement systems is the size. The HPGe detectors require cooling using liquid nitrogen, which drastically increases the size and weight of the system, making transportation much more difficult and requiring dedicated space and cooling for the system. The site for measurements needs to have access to liquid nitrogen every week to refill the Dewar of the detector. These are all costs that are recurring and for some sites without access to liquid nitrogen, delivery of liquid nitrogen weekly is going to be necessary for the duration of the detectors use.

Finally, the measurement itself requires 30 minutes. For large populations, this can be a significant time investment for research personnel. 30 minutes can be a long time for a measurement of certain populations, especially in children or adults with Alzheimer's or dementia who may have difficulty sitting still.

Since KXRF has so many limitations, alternatives were explored using L-shell XRF (LXRF). LXRF for bone Pb measurement was first developed in 1983 using an I-125 source [29]. An x-ray tube source utilizing polarized x-rays was then developed for LXRF measurement of Pb in bone [30, 31]. Finally an x-ray tube source with secondary target was developed for LXRF measurements [32-34]. Using an x-ray tube source eliminated the licensing restrictions of the KXRF system; however, these methods all found variability in soft-tissue thickness to be a significant problem and did not have proper methods to correct for this in their calibrations. Finally, the development of the work described in this thesis identified a calibration with correction for soft-tissue thickness to allow for measurements using our LXRF system in vivo [35, 36].

The previous LXRF technologies had limitations primarily with calibration to overcome varying soft tissue thickness over bone. In addition to this, geometry factors play a much larger role with LXRF than KXRF. KXRF uses a high-energy source that will penetrate further into the bone and the characteristic x-rays produced isotropically will be of high energy as well and able to exit the bone into the detector without significant attenuation from surrounding soft tissue structures. LXRF using the much lower energy has an attenuation factor about 20 times that of the KXRF energies. This represents only millimeters of penetration or measurement depth for the characteristic x-rays released in the material. Combine this with the fact that these LXRF devices are utilizing x-ray tubes, which will have a small beam size limiting the area of irradiation to a specific location. This is where I believe the studies done by Todd had their shortcomings, and likely has contributions to the other previous LXRF devices as well [32-34]. The geometry is so sensitive to the fact that the detector has to be placed

precisely where the maximum number of characteristic x-rays will be able to escape, but most importantly it needs to be consistently in the exact same geometry for every measurement. Even a 1.5 mm difference in source detector geometry would represent a change in the signal by a factor of 2. This is evident in Todd's studies, which revealed a reproducibility that was unacceptable for measurement [32]. In the work described here, we have correctly isolated the geometry and have the detector and source in a stable reproducible setup allowing us to overcome previous device limitations.

The soft tissue attenuation presented another significant problem for LXRF measurements. Measurements of soft tissue were needed along with the LXRF measurements in order to properly account for the attenuation. This step in itself added uncertainty to the measurement. A study by Rosen et al. demonstrated this in a population study of children and was able to successfully measure bone Pb using LXRF with ultrasound measurements [37]. The need for a proper calibration including soft tissue thickness is evident by these methods, which limited the detection limit, increased uncertainty, and required extraneous instrumentation in studies using LXRF bone Pb measurements. The work presented here will detail specific calibration procedures utilized with our developed system that allows for appropriate correction for soft-tissue thickness and overcomes the limitations of previous LXRF measurement systems.

To address the disadvantages of KXRF and overcome the limitations of LXRF this thesis will present the development of a novel portable LXRF device and a portable KXRF device with advantages using an x-ray tube source, detector without liquid nitrogen cooling, and significantly reduced measurement times.

1.4 Overall Goals and Specific Aims

The goals in my project were to develop and validate use of a portable XRF device for in vivo measurement of bone Pb and bone Sr, and to determine the feasibility of a high-energy x-ray tube XRF device for use with in vivo applications. The portable XRF can then be used for monitoring cumulative Pb exposure levels in populations to assess the health effects associated with exposure. To achieve the overall objective four specific aims for this doctoral work were accomplished:

Aim 1: Calibrate and validate the portable XRF system for *in vivo* Pb quantification and improve upon previous XRF technology. We developed and validated a portable system to quantify Pb concentration in tibia bones. We used a portable x-ray tube system from Thermo Fisher generally used for environmental and industry samples, optimized the device settings for use *in vivo*, developed calibration methods, and validated the device with phantoms, goat bone, and cadaver bone. The work for this aim was published in a paper by Specht et al in 2014 [38].

Aim 2: Validate the portable XRF bone Pb measurement system using a comparison with KXRF data in a Pb poisoned children study. We measured tibia Pb in a population study of Pb poisoned children with both KXRF and portable XRF. We quantified Pb concentrations in their tibia bones with the portable XRF and KXRF systems and compared the results. We identified differences in Pb biokinetics in children. The work for this aim was published in a paper by Specht et al in 2016 [36].

Aim 3: Validate the portable XRF system for *in vivo* bone Sr quantification. Using the same system as for Pb, we developed and validated a system to quantify Sr in

tibia bone. We created phantoms for use in calibration of Sr with the portable device. We used optimized settings and calibration methods from Pb. We did an analysis for Sr with the data collected in the Pb poisoned children population study, and identified sex differences of Sr accumulation with age.

Aim 4: Develop a novel XRF device for quantifying metals. We developed a higher energy x-ray tube system for use with quantifying metals using MCNP. We simulated the design of a novel higher energy XRF system. We identified optimized settings of the x-ray tube and detector to maintain advantages of previous systems with a low detection limit.

1.5 Significance

Metal exposure has increased dramatically through the years with increased development of industry, agriculture, and manufacturing. Pb has been a centerpiece for metal exposure with its numerous adverse health effects especially within the central nervous system [39]. Pb exposures have decreased with the removal of Pb from gasoline. However, Pb exposure and toxicity remains an important public health issue as: low level Pb exposure has been increasingly correlated with adverse health effects[2, 3, 40-43], high exposures remain commonplace in occupational workers [7], and significant internal exposure persists for individuals from the leaded gasoline era [4]. For these exposed population, we need to identify cumulative effects of Pb to determine whether current public health and treatment initiatives are correctly focused.

Traditionally, blood Pb is used as a biomarker to determine Pb exposures, but blood Pb has a half-life of 30 days; bone Pb with its half-life of years to decades better reflects lifetime exposure levels [1, 44] and for many, particularly chronic, conditions has proven to be a much more relevant biomarker. Current Cd-109 KXRF systems have been used to study cumulative Pb exposure for over two decades, but it requires radioisotopes, long acquisition times, and a large amount of space [9, 45]. Radioisotopes require extensive licensing procedures from each site with an active system and significant maintenance from health physicists. This and other space limitations have severely restricted the use of this approach in research with only a few research groups having conducted such studies. In this thesis we use a portable XRF device to overcome the disadvantages in portability and measurement time. This device was validated alongside KXRF bone Pb measurement and with these measurements of bone and blood Pb we investigated the biokinetics of Pb in children.

This project is significant because: it will develop a system for Pb measurement with improved portability and without radioisotope restrictions. Development of this system will allow for measurement of populations previously inaccessible by traditional KXRF systems due to radioisotope restrictions or portability requirements, which will help identify at risk populations for public health initiatives, and make this line of research available to a far wider research community than currently, and with expanded development be applicable for measurement of other metals in other tissues.

1.6 Structure of This Dissertation

The structure of this dissertation is organized by the following order: Chapter one consists of introduction and background information; chapter 2 addresses the portable XRF optimization and validation with in lab samples with study results from my publication [38]; chapter 3 addresses the Pb poisoned children population study biokinetics and validation findings with study results from my publication [36]; chapter 4 focuses on the calibration and validation for bone Sr measurements with the portable XRF and population study results; chapter 5 focuses on the development of a novel XRF device for Pb quantification with simulation results; chapter 6 has an overall summary of the studies and future directions for further study.

CHAPTER 2. SIMULATION, OPTIMIZATION, AND VALIDATION OF PORTABLE XRF FOR BONE PB QUANTIFICATION

2.1 Introduction

The portable XRF offers many advantages over previous bone Pb measurement technologies. Optimization of the portable XRF needs to be completed to determine the settings that properly fit with the technology to get the lowest limit of detection for in vivo measurements. The minimum detection limit (MDL) will define the usefulness of the technology and gauge its ability to measure the general population. Along with system optimization, optimization of our calibration procedures using different approaches will allow us to determine the spectral features and analysis manipulations that can be done to further minimize our detection limit. Previous technologies have the advantage of a system, calibration, and analysis process that has been tested and refined for almost a decade. Calibration and optimization for the portable XRF will require a different approach to previous technologies, as soft tissue thickness needs to be accounted for, preferably using spectral features and physics theory. With a proper calibration, validation is an easier process that can be used to help explore the limitations and potential problems of the device itself or the calibration used.

When exploring our potential calibration methods we revisited the physics of XRF and the anatomical make-up of an in vivo measurement. The energy of the portable XRF limited us to the probable interactions in a sample of Rayleigh scattering, Compton scattering, and photoelectric effect, which together determine the total attenuation as seen in Figure 2.1 from NIST [46].

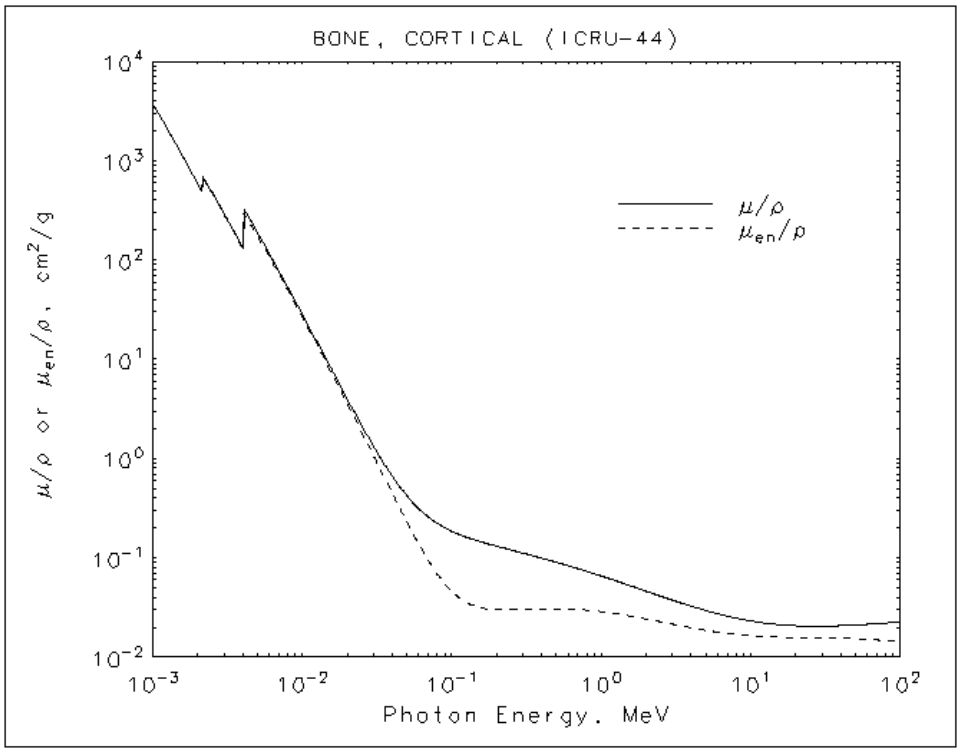

Figure 2.1 Plot of total attenuation cross section for cortical bone from NIST [46].

The photoelectric effect dominates at lower energies with a slowly increasing Compton scattering probability as the energy increases. As mentioned previously the photoelectric interaction will generate all of our signal from x-ray fluorescence measurements and Compton scattering events will lead to an increase in background around that signal.

Along with that the cross-sections will change depending on the material composition of the bone or soft tissue. At the energies useful for XRF, the photoelectric cross section changes as such with energy and atomic number,

$$\sigma_{PE} \propto \rho \frac{Z^3}{E^3}$$

, where σ_{PE} is the cross section, Z is effective atomic number of the material, ρ is the density of the material, and E is the energy. The Compton scattering cross section at the energies for XRF typically have only one dependency, which is a linear relation with density. Our calibration methods will attempt to use some of these relations to identify which interactions have the most relevance to overcome the many changing variables that encompass in vivo measurements. Finally, the calibration can then be tested using in lab samples to further validate the device, optimization, and calibration.

2.2 Materials and Methods

2.2.1 Portable XRF Bone Pb Measurement System

The portable XRF devices used in this work were from Thermo Fischer Scientific Inc. (XL3t and XL3t GOLDD+, Billerica, MA). Traditionally these devices are used to quantify elements in soil and rock samples for mining purposes. Advances to the detector and geometry allowed us to apply these devices for in vivo measurements. The devices

both have a power output of 2 watts, a 50 kV max x-ray tube voltage, with silver anode. The XL3t is equipped with a Silicon (Si) PIN diode detector with 8 mm^2 area, whereas the XL3t GOLDD+ is equipped with a Si drift detector with 25 mm^2 area. Both detectors had thickness of 1 mm. This represents a 300% increase in size for the detector, which will increase the characteristic x-ray signal collected by the detector. This does not equate to a 300% decrease of the detection limit, because there is a gap between the detector and the sample. The characteristic x-rays are produced isotropically, which makes the increase of detector size limited by the gap combined with the amount of solid angle the detector size covers, which will be much less than 300%. The company controls the release of the exact specifications for these devices, but they claimed a better geometry to further decrease detection limit was also introduced in the GOLDD+ device.

We can speculate on the changes between devices to decrease the detection limit for different elements. In order to use geometry to decrease the detection limit a couple of optimizations needed to take place. First, they could optimize the angle of the detector to be perpendicular to any characteristic x-ray source, thus allowing for a greater coverage of solid angle, for more signal collection. Second, they could minimize the distance between the detector and sample to decrease the effect of the inverse square degradation of signal and increase solid angle coverage. Both systems are quite compact, so it was likely a combination of these optimizations, and possibly some changes to the angle of the x-ray beam to accommodate the changes.

We performed an optimization of the device both for the x-ray settings and filtration of the x-ray beam. The device had a set number of filters that we could apply to the x-ray beam allowing us to change the energy spectrum of the emitting x-rays. For

maximal output of characteristic x-rays you would ideally want to set the energy as close to the binding energy of the element of interest as possible. Since this process is through the photoelectric effect, the cross section will decrease with increasing energy, so being right at the edge of the binding energy maximizes the amount of photoelectric interactions. In the KXRF system they do this very well using 88.035 keV of Cd-109 for the 88.01 keV binding energy of the Pb k-shell. However, with an x-ray tube this process is more difficult, as x-ray tubes will produce a spectrum of energies. X-ray tubes can have increased average energy using filtration of the x-ray beam.

Filtration of an x-ray beam is done using external filters after the target (anode) and in the target itself. The x-ray beam in the portable XRF uses a transmission x-ray tube, which produces the beam in the same direction as the electrons were accelerated. This is contrary to traditional x-ray machines in the hospital, which use an angled anode to produce a beam 90^0 from the original electron beam. A transmission x-ray tube generally will have more filtration in the target from self-absorption events. Thus the x-ray beam has a higher average energy. The optimization of the target thickness in these devices was done for many different elements and not just Pb and Sr, which we are particularly interested in. Thus without the external filters the x-ray beam produced in these devices was not very well optimized for our purposes.

For our optimization, we used measurements of phantoms and a calculation of the minimum detection limit (MDL) as our standard for determining the optimized settings. We discuss the MDL calculation in the results section of this chapter. We found the optimized settings to be using 50 kV 40 μA and a filter of silver and iron with our measurement time of 3 minutes. The dose of the device was estimated from previous

TLD measurements taken at 50 kV 25 μA with the same filter. Since the only change was to the current, the dose should scale proportionally to the increase in current, because increases in current will just increase the output of the x-ray beam, and not the energy spectrum of the x-ray beam. The entrance skin dose was then estimated to be 31mSv to a 1 cm^2 area of skin [47]. We used 1 cm^2 to be conservative in our estimates, but the NRC standard is for a 10 cm^2 area of skin for dose estimations, and the limit is 500 mSv to the skin of the whole body or to the skin of any extremity for a radiation worker. The whole body effective dose was then estimated similarly to be 3.6 μSv [47]. This can be compared to the dose of a standard AP chest x-ray of about 100 μSv. The risk of this radiation dose to any member of the public would be negligible.

2.2.2 KXRF Bone Pb Measurement System

In our study, we used the most advanced KXRF cloverleaf system discussed previously. The cloverleaf KXRF bone Pb measurement system utilized four 16 mm HPGe detectors, DSA-1000's for signal processing, and used Genie 2k spectroscopy software for data collection. The device has a previously measured detection limit of around 2-3 μg/g bone mineral [27]. The system's four detectors are placed around the Cd-109 radioisotope source, and the system uses a 180^0 geometry. The Cd-109 energy is 88.035 keV and the binding energy for Pb is about 88.01 keV, which allows a special analysis method using coherent scattering. Since the coherent scattering will reflect the interactions in the bone, based primarily on effective atomic number of the materials, it can be used as a normalization factor to determine the amount of bone mineral that was irradiated. This

also allows us to determine the units in μg per gram bone mineral, which is more valuable than a determination solely of parts per million, because it can be related back with more biological significance.

The Cd-109 source usually starts at about 135 mCi and will decay over time with its half-life of about 3 months. The source is placed in a holder with most of the point source pointing forwards to few millimeter copper collimator to reduce dose from the competing decay processes from the Cd-109, since the 88.035 keV gamma release only represents ~3% of the branching ratio for the radioisotope decay scheme. With decreasing source strength the integrity of each measurement in comparison to previous can be maintained by decreasing the distance between the source and measurement site, which can be monitored by using the dead time of the detector as an indicator.

The measurements were taken for 30 minutes, processed with the digital electronics, and spectra analyzed using our in-house peak fitting software to calculate the final Pb concentrations. The whole body effective radiation dose of each measurement was assessed to be 0.26 μSv for adults and 10 μSv for children [48]. The Cd-109 source has a more significant dose given to the bone marrow of subjects, which has a higher tissue-weighting factor in children, so will result in a higher dose value.

2.2.3 Monte Carlo (MC) Simulation

MC simulation is a tool that uses a large number of probability calculations to determine the impact of certain processes on systems. In our case, we have physics equations determining the probability of interactions for each interaction based on energy and

material. We can input a number of particles that are defined to go through those interactions and based on the probabilities the MC simulation determines how they interact. Finally, we can look at a particular outcome or interaction specifically to compare with experimental result.

We used a standard software package from Los Alamos National Lab called Monte Carlo N-Particle transport code (MCNP). This software has more updated low energy interactions, which is needed for doing any validation with the portable XRF. MCNP uses a simple input syntax, where the user defines objects using corresponding intersections between different functions such as six planes intersecting to form a cube. The user can then set each object to a material that can be specified using mass percentages. Finally, the user can define a source, which can be electrons, photons, or neutrons that then will produce particles of a particular energy or spectrum of energies to interact with the objects.

MCNP allowed us to input the objects and geometry from the portable XRF exactly, so that we could better understand the x-ray source produced in the system and define calibration standards for our system to work with. Using the simulation we can determine from physics interaction theory whether our methods and materials were appropriate and if not how we should change them.

2.2.4 Phantom, Goat Bone, and Cadaver Bone Samples

In-lab samples were used in this study to verify the accuracy of our chosen calibration method and to calibrate the device itself. Phantom materials made of plaster-of-Paris are

commonly used for XRF bone measurement calibrations, so we used a set of phantoms with known Pb doped concentrations at 0, 5, 10, 15, 20, 30, 50, 75, and 100 ppm for our calibration. Since we knew soft tissue thickness would become an issue with the lower energy portable XRF, we wanted our calibration to attempt to combat this, so we used Lucite plates in increments of about 0.5 mm up to 6 mm in conjunction with our bone phantoms to determine the affect of soft tissue on the measurements.

Goat bones were obtained from goats that orally ingested Pb of various levels. The goat bones were grinded down and compacted into the form of small discs for measurement and then placed in vacuum-sealed bags to prevent contamination. They had concentrations of 0.2, 9.6, 16.1, and 31.4 ppm as measured by our KXRF bone Pb measurement system. We used these along with the Lucite slabs to determine if the bone matrix had any effect on our calibration method. We also used the Lucite slabs at 0, 1, 2, 3, 4, and 5 mm with the goat bones to determine the validity of our correction for soft tissue thickness and the calibration method that correctly adjusted for it.

We had 10 cadaver bone samples with 3 having intact soft tissue thickness over the tibia bone. They were also placed in vacuum-sealed bags to prevent contamination of the bones and the portable XRF. The bones had varying Pb concentrations ranging between 3.6 and 23.1 ppm with most of the bones being around 20 ppm. We used these to further verify the bone matrix equivalence to in vivo for our calibration and for reproducibility measures of our portable XRF. We used Lucite slabs of 0, 1, 2, and 3 mm in conjunction with the cadaver bones to determine the accuracy of measruements made with soft tissue thickness for human bone.

2.2.5 Calibration Methods for the Portable XRF

2.2.5.1 Traditional Peak Fitting

Traditional peak fitting is the standard way to calibrate a device for quantification using calibration standards. We used Matlab for fitting of our spectra. We combined a Gaussian peak fit for the Pb peaks with an exponential function to represent the background under the peaks. We set the ranges for the variables in the fitting to values to reflect the volatility of each variable. For example, the amplitude of the Gaussian was set between ±100, which reflected the counts for about 500 ppm. The background variables were ranged through ±infinity, because they are more likely to change drastically for different spectra. The peak location was set to be within one sigma of the energy of the characteristic x-ray energy, and the width was determined using tests with the detector.

The Gaussian peak width was set to reflect the resolution of the detector for the portable XRF. We did this using two methods 1) using a large peak from Sr measured from our plaster-of-Paris phantom (~1000 ppm) to determine the resolution and then converting that to the energy of the Pb peak regions, and 2) using the 100 ppm Pb phantom to determine the width of the peak at the Pb regions. These two methods were in agreement and we used a range of ±20% of the indicated width to account for variations in background level and surrounding noise that may distort the width of the Gaussian peak.

Traditional peak fitting using this method worked well as long as the peak was visible over the background and, as we will see later, had less influence from variables from the in vivo situation. For measurements we did a soft tissue or Lucite correction for these values by identifying the tissue thickness and determining signal degradation from that particular thickness of tissue. For this we used a function both to identify soft tissue thickness and to signal degradation of the ppm versus counts function as derived from the traditional peak fitting calibration.

2.2.5.2 Background Subtraction

The background subtraction method was a unique calibration method identified to try to combine the correction for soft tissue and traditional calibration line to quantify Pb signal. We found that the background and the Compton scattering peak attributed to the Ag characteristic x-rays from the x-ray tube target were well correlated. The physics confirms this, as the characteristic Pb or other elemental x-rays will arise from photoelectric interactions within the sample, and the other interactions will all lead to background in the spectrum. Compton scattering is the primary interaction other than photoelectric absorption, so the Compton scattering peak from the Ag x-rays is a demonstration of the cross section for Compton scattering in that particular sample being measured, and can then be used as a reflection of the background obtained in that particular sample.

For this calibration we would do measurements of the 0 ppm and 100 ppm phantoms for 0, 1, 2, 3, 4, and 5mm of Lucite thickness. Lucite thickness was reflected in the spectra using the Compton scattering peak from the Ag target x-ray. This would then allow us to create functions to define the background from the 0 ppm phantom measurements and how the background counts changes with increasing Compton scattering counts. The function of background and Compton counts is in Figure 2.2 below. Then we could similarly look at net counts of the Pb peak as it relates to Compton scattering counts over increasing Lucite thickness, such as in Figure 2.3 below.

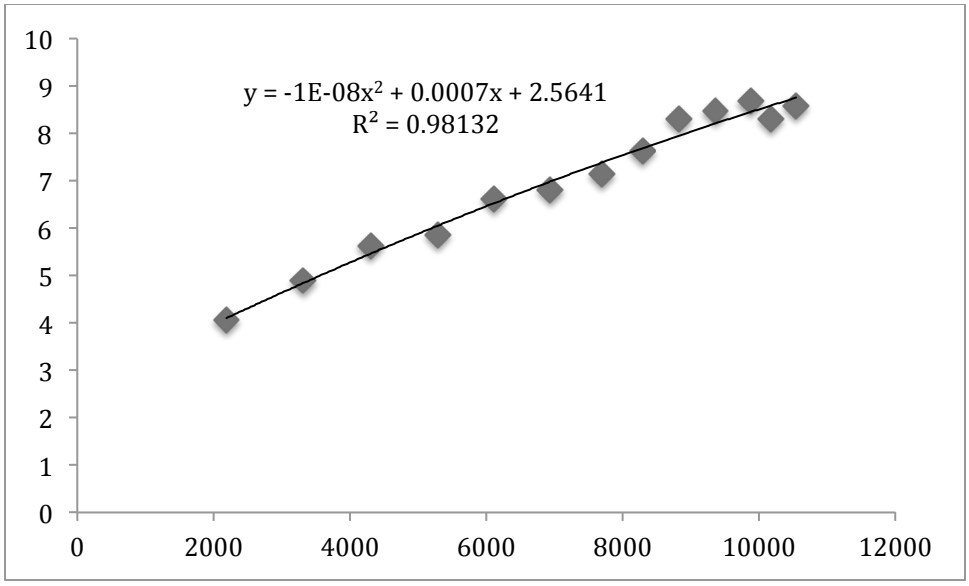

Figure 2.2 Background counts under Pb L-alpha region versus Compton scattering counts at varying thicknesses of Lucite.

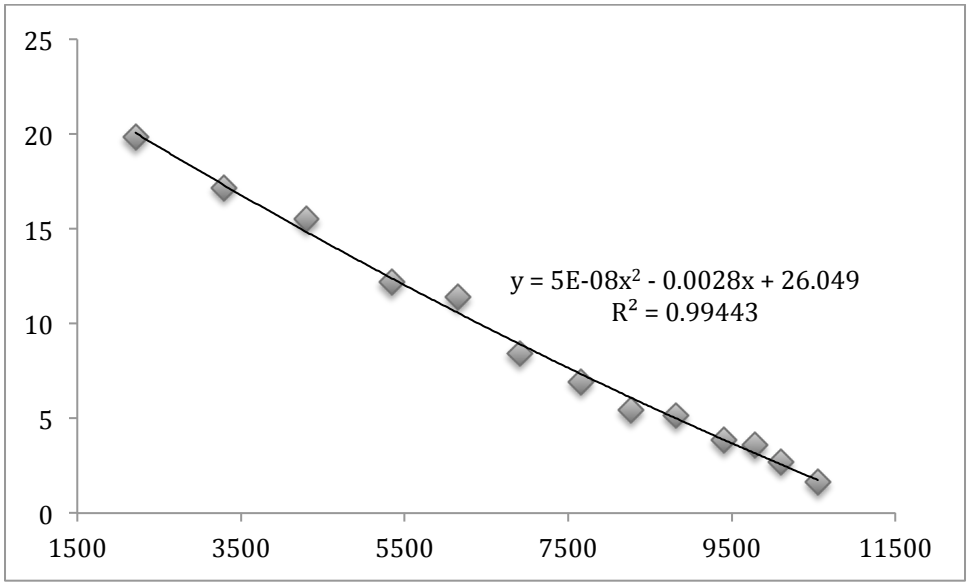

Figure 2.3 Net Pb L-alpha peak counts versus Compton scattering counts at varying Lucite thicknesses.

The background function deviates more from the estimation at higher Lucite thicknesses, which may be an indication of higher background levels arising from interactions other than Compton scattering. Besides that deviation, the functions show good agreement with high correlation values.

2.2.5.3 Bone Calibration

Bone calibration was tested to determine whether the bone matrix would have a greater impact on the measurements. This method was the same as the background subtraction method previously discussed; however, this method used the goat bone samples of 0.2 and 31.4 ppm instead of the 0 and 100 ppm phantoms respectively. Using this had the advantage of using a bone matrix that would be very consistent with human bone and

thus any changes in the spectra that would be because of the matrix would be reflected in this substitution of phantoms.

2.2.5.4 Bone Adjustment

The final calibration method we explored tried to directly adjust each measurement for the differences in effective atomic number and density of the sample. This was done by correlating the Compton scattering peaks of the goat bone and phantom, as seen in Figure 2.4, so that any measurement done on normal bone could then have this function applied to allow for use with a normal phantom calibration. This was done because bone calibration seemed like a more reasonable approach to calibration, but had the great disadvantage of having a low Pb concentration goat bone of 31.4 ppm to use in the calibration process. This calibration method was supposed to correct for the bone matrix without giving up the advantage of the higher concentration standards in the calibration line.

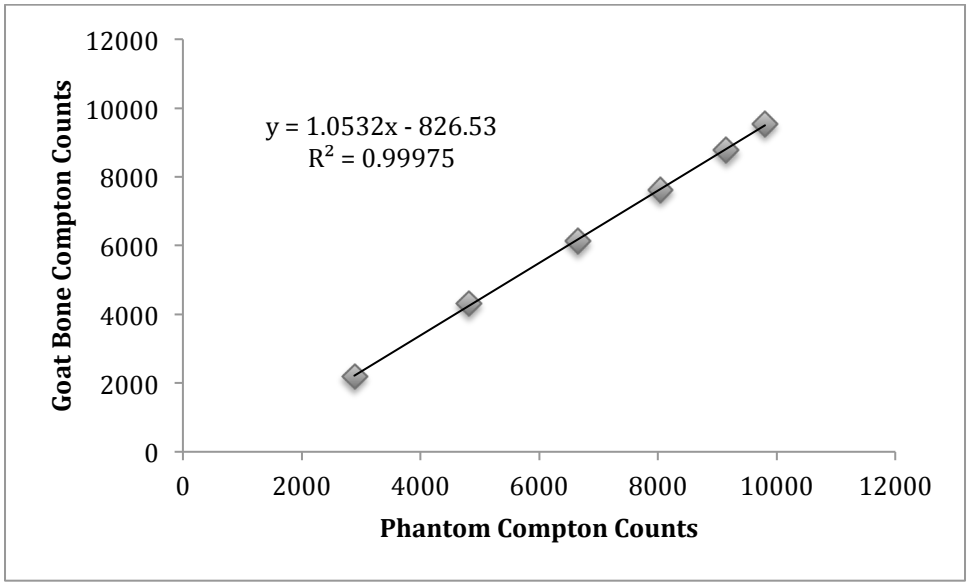

Figure 2.4 Goat bone versus phantom Compton scattering counts function.

2.3 Results

2.3.1 Portable XRF Spectrum

Figure 2.5 shows the resultant portable XRF spectrum from a measurement of an intact human cadaver bone with 1.3 mm soft tissue. As shown in the spectrum the Compton scattering peak comes from the x-ray tube silver characteristic x-rays undergoing Compton scattering in our sample. This is the peak that we have correlated with background and signal degradation from inverse square and attenuation using our background subtraction method. It is also the peak that correlates well with soft tissue thickness, so in a sample with more soft tissue, this peak will appear larger. The Pb peaks at 10.5 keV and 12.6 keV are visible in this spectrum with only 1.3 mm of soft tissue

thickness and 14.3 ppm of Pb. This spectrum demonstrates the difficulty in using traditional peak fitting methods, since with more soft tissue, there will be more background and the Pb peaks will become increasingly noisier.

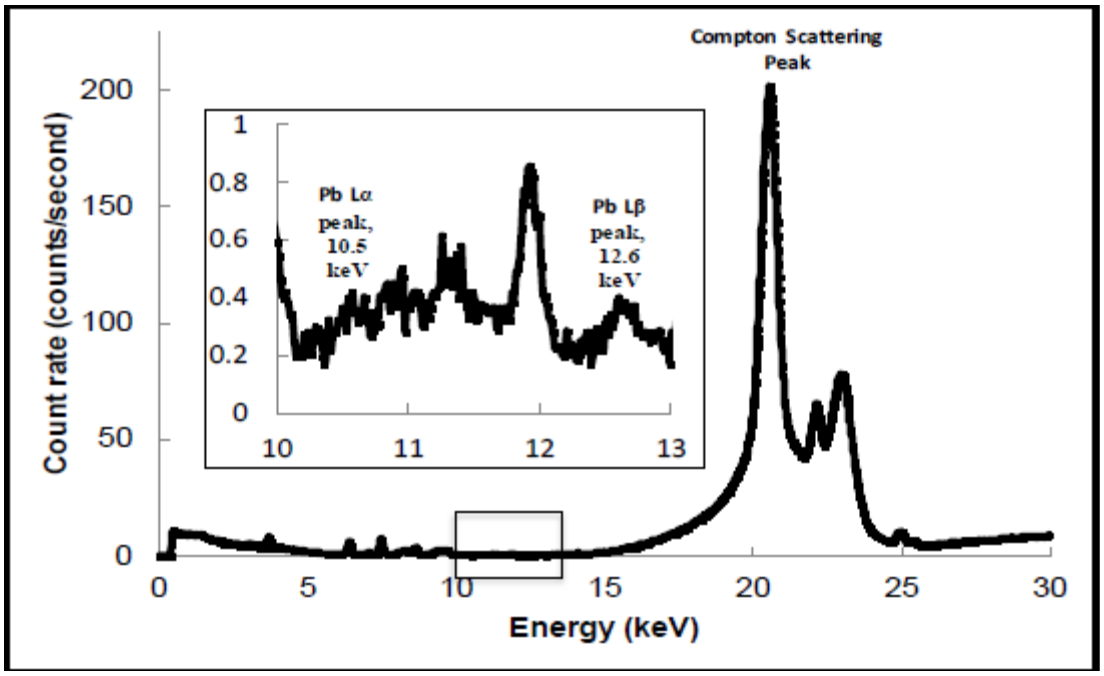

Figure 2.5 Example portable XRF spectrum when measuring cadaver bone with overlying soft tissue.

2.3.2 MC Validation of Phantom Materials

We used a MC simulation of the portable XRF itself to determine the validity of our choices for phantom materials. This allowed us to test the measurement on a sample of known soft tissue and bone elemental mass percentages, and then test it with our Lucite and plaster-of-Paris phantom materials without changing any of the settings or geometry. According to the simulation there was no significant changes between bone and soft

tissue and plaster-of-Paris and Lucite. There were minimal spectral changes to the Compton peak when changing between bone and plaster-of-Paris, but these were less than a 5% change, which is about equal to the uncertainty from the simulation itself. This result if true, would validate the use of the phantom material for our calibration, since we would also be testing other calibration methods using materials more comparable to bone matrix. Figure 2.6 shows the spectrum comparison between bone and phantom, demonstrating their equivalence.

When testing the differences between Lucite and soft tissue, we used composition information taken from NIST for soft tissue. We tested this using simulation at varying thicknesses from 0, 1, 2, 3, 4, and 5 mm. Figure 2.7 shows the resultant differences observed for the 5 mm values are about 20%. We attempted to verify this result using the cadaver bone with intact soft tissue thickness in comparison to our Lucite plates, and found the resultant spectrum shown in Figure 2.8 with better agreement than the simulation led us to believe. This compares both plaster-of-Paris and Lucite to cadaver bone with intact soft tissue thickness, which should be equivalent to the in vivo measurements. The difference between these spectra was less than 5% as compared by taking a ratio of above and below the Compton scattering energies.

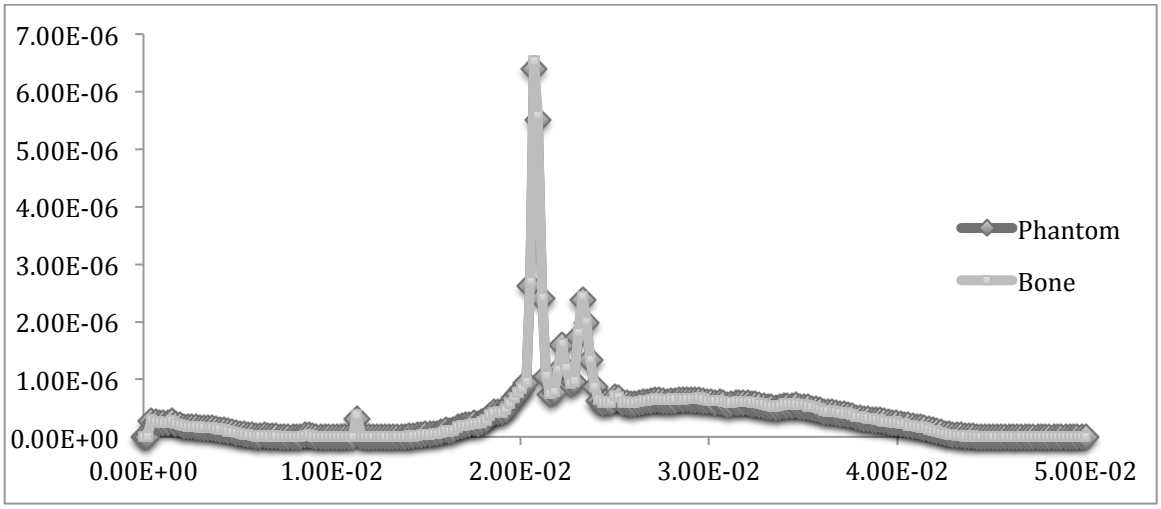

Figure 2.6 Bone and plaster-of-Paris bone phantom spectrum comparison.

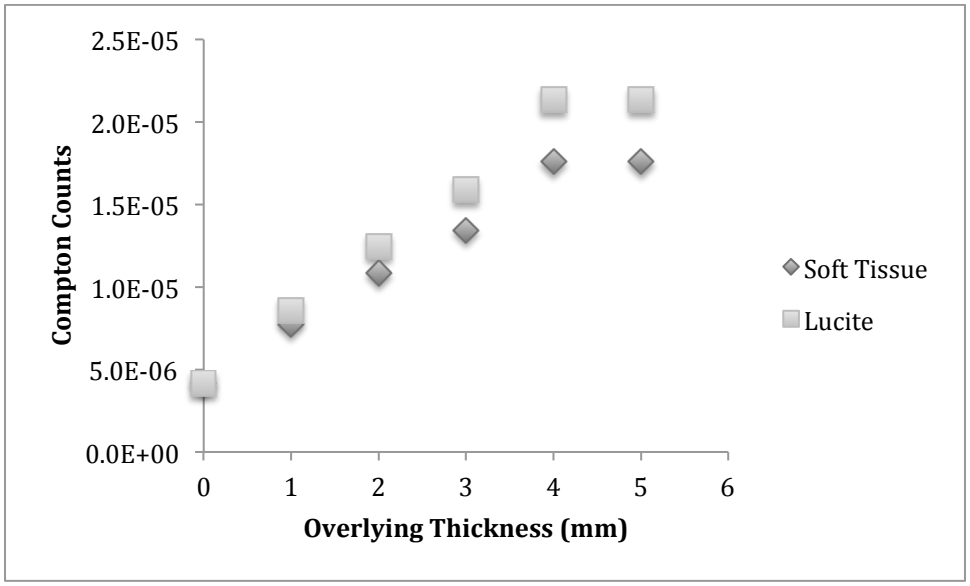

Figure 2.7 Comparison between the Compton scattering peak area for varying Lucite and soft tissue thicknesses using simulation.

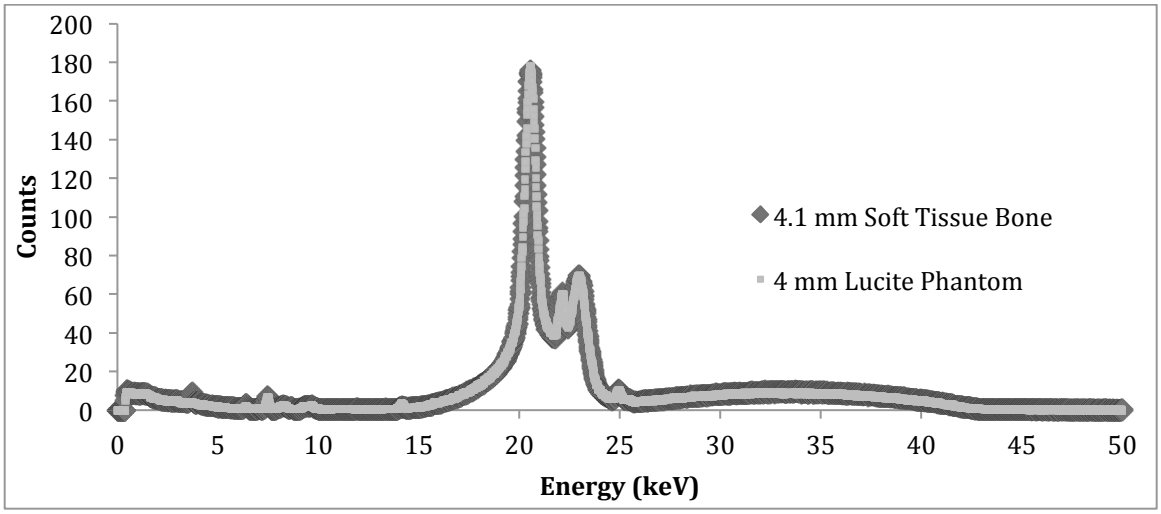

Figure 2.8 Comparison of experimental phantom and Lucite to cadaver bone and intact soft tissue thickness showing differences of <5%.

2.3.3 Soft Tissue and Compton Correlations

A Correlation between soft tissue thickness and Compton scattering counts from the Ag x-ray was identified. We sought to validate this finding using MC simulation and our phantom measurements. We did measurements with MC simulation using Lucite and plaster-of-Paris, and produced a correlation with Compton scattering counts from the peak at 20.5 keV. We did this same thing experimentally using Lucite slabs and our plaster-of-Paris phantoms. We normalized the MC simulation results, so that they would be comparable, and the comparison can be seen in Figure 2.9. The disagreement in higher thicknesses could arise from a discrepancy from our Lucite slab thickness measurements, how the simulation handled Compton scattering interactions, or uncertainty from the simulation. Uncertainty in the simulation was about 5% per channel in our spectrum. Given the discrepancy in the simulation results of soft tissue and Lucite, this likely

reflects a similar error in how the Lucite is simulated or the Compton scattering cross-section with Lucite is calculated. This discrepancy would not affect our calibration, because we are not directly using the estimated soft-tissue thickness for anything, but only how it relates to the rest of the spectrum.

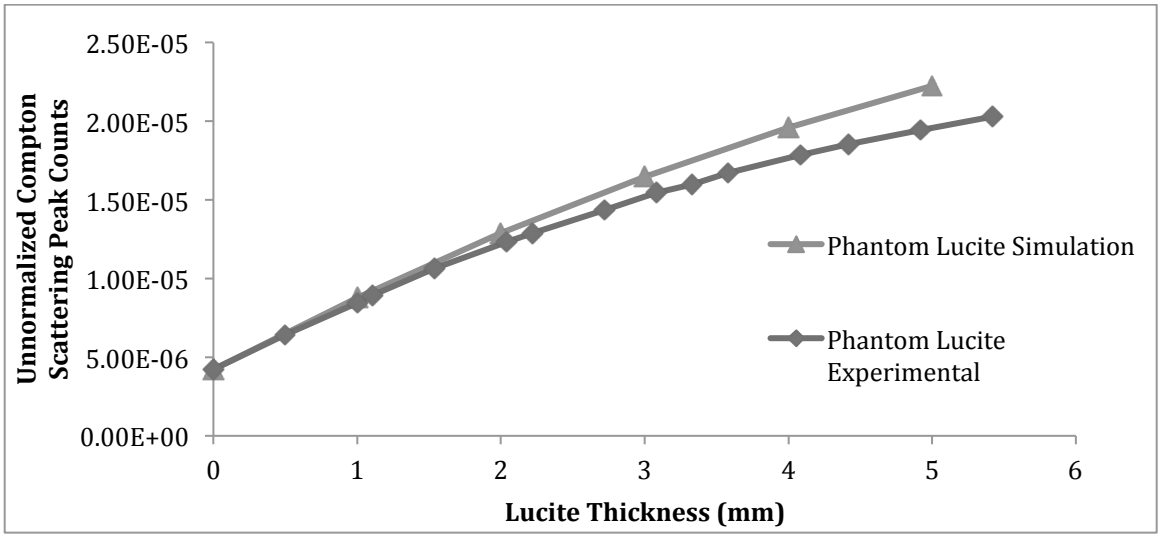

Figure 2.9 Compton scattering counts versus Lucite thickness comparison between simulation and experimental results.

2.3.4 Minimum Detection Limit Optimization

We did multiple tests for the minimum detection limit optimization using both MC simulations and experimental results. Our MC simulations were looking at a number of parameters for optimization. We have max energy of the x-ray tube and filters, as our variables to modify, and used dose and signal produced from a 100 ppm sample as our parameters to minimize and maximize for optimization. What we found is shown in Table 2.1. The best settings without accounting for detector limitations were 40 kV 50

μA with a filter of aluminum and iron which produced the best results, and the settings of 50 kV 40μA with a filter of Ag and iron being 1.5 times lesser with our parameters of dose and signal. This unfortunately was not the case, as simulation does not reproduce the experimental setup flaws such as detector resolving time (dead time), which is why it was necessary to do further testing with the experimental setup.

Table 2.1 MC simulation optimization of x-ray tube settings results.

	50 keV 40 μA Ag Filter	50 keV 40 μA Al Filter	40 keV 50 μA Ag Filter	40 keV 50 μA Al Filter
Total Dose (MeV)	9.91E-08	1.40E-07	5.84E-08	7.05E-08
Unnormalized Signal	2.52E-06	1.67E-06	2.30E-06	3.24E-06
Signal/Sqrt(Dose)	2.40E+05	1.34E+05	3.56E+05	4.57E+05

Using experimental tests we needed to test our results. We did this by using a calculation of minimum detection limit for each setting after measuring a 0 ppm and 100 ppm phantom. The detection limit was calculated as

$$DL = 2 \times \sigma_{0\ ppm} = 2 \times \sqrt{\frac{1}{\frac{1}{\sigma^2_{\alpha,0ppm}} + \frac{1}{\sigma^2_{\beta,0ppm}}}}$$

, where

$$\sigma_{(\alpha,\beta)0ppm} = 100ppm \times \frac{\sqrt{\frac{BKG_{0ppm}}{180s}}}{Gross_{100ppm} - BKG_{0ppm}}$$

, and BKG_{0ppm} is the background count rate under the L_α or L_β peak for the 0 ppm phantom and $GROSS_{100ppm}$ is the total count rate under the L_α or L_β peak for the 100 ppm phantom.

These tests revealed that the settings with 50 μA produced results that were better than those from 40 μA, but the dead time of the detector was up to over 70% in some cases for 50 μA. This is unacceptable especially for a phantom measurement. It is generally accepted that phantom measurements should have about ~15% dead time, because in vivo will always become significantly higher with the increased scatter from soft tissue and larger sample size. We thus went on taking into account the dead time in our measurements as another parameter for optimization. We found that 50 kV 40 μA with a Ag and iron filter produced the best results.

We measured the detection limit of both our portable XRF devices to quantify the improvements made in the device detector and geometry and those measurements can be seen in Table 2.2 below.

Table 2.2 Detection limit comparison between XL3 and XL3t GOLDD+.

Soft Tissue Thickness (mm)	Detection Limit XL3t GOLDD+ (ppm)	Detection Limit XL3 (ppm)
0mm	1.2	2.0
1mm	1.8	3.5
2mm	2.9	5.9
3mm	4.6	9.6
4mm	8.0	12.8
5mm	11.0	14.7

2.3.5 Validation of Portable XRF

Measurements were made to validate the portable XRF system against the standard KXRF systems for *in vivo* bone Pb measurements. Phantoms, goat bones, and cadaver bones with 0, 1, 2, and 3 mm of Lucite were measured by both the portable XRF system and KXRF bone Pb measurement systems, with goat bone also being measured at 4 and 5 mm of Lucite thickness. Table 2.3 shows the measured phantom Pb concentrations at different Lucite thicknesses. The correlation (R-squared) between the expected concentrations and those measured with portable XRF system ranges from 0.991 to 0.999 for soft tissue thicknesses of 0 to 3 mm, demonstrating a good agreement of Pb concentrations determined by KXRF and portable XRF for bare and Lucite covered phantoms. An example of this is seen in Figure 2.10 with the 3 mm Lucite thickness phantom measurements. The quantified results are also accurate and deviations from the standard phantom concentration is reflected in our calculated uncertainty values.

Table 2.3 Phantom Pb concentrations calculated using the background subtraction method.

	Lucite Thickness			
Standard Phantom ppm	0mm	1mm	2mm	3mm
0	-0.38±0.8	-0.1±1.3	-2.22±2.1	3.31±3.31
5	4.83±0.86	3.57±1.34	9.61±2.19	7.37±3.37
10	10.23±0.9	10.5±1.39	11.23±2.19	17.83±3.42
15	14.9±0.94	13.3±1.4	20.37±2.27	13.39±3.41
20	19.52±0.97	19.17±1.46	21.25±2.27	17.37±3.46
30	31.32±1.06	30.09±1.53	30.35±2.36	32.34±3.56
50	47.45±1.17	52.76±1.7	49.43±2.48	48.54±3.7
75	75.56±1.33	77.44±1.85	74.49±2.65	74.34±3.82
100	96.96±1.44	108.65±2.02	105.26±2.84	101.73±4.06

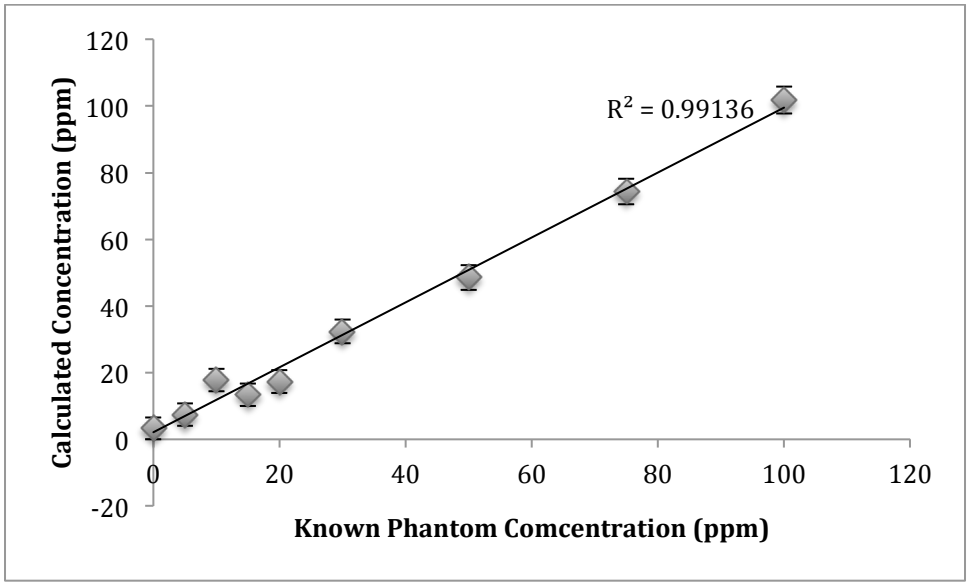

Figure 2.10 Phantom calculated concentration versus known concentration for measurements with 3 mm of Lucite thickness.

Table 2.4 and 2.5 demonstrate the ability of the three calibration methods to quantify bare cadaver bone Pb values. Table 2.4 shows the Pb concentration in bare cadaver bone calculated using the three calibration methods. Table 2.5 shows the bone Pb concentrations for cadaver Bone covered with 3 mm of Lucite. Without Lucite the calibration methods tend to be fairly similar, but with the introduction of Lucite the bone adjustment method tends to get further from KXRF values by overestimating background levels, which is from an overcorrection of the Compton scattering peak. Bone calibration has a similar correlation, but with only 4 points on the calibration line and the highest point at 31.4 ppm the actual values tend to deviate from KXRF. Higher concentration standards are necessary to get visible signal while defining our function to correct for the inverse square and attenuation signal degradation as soft tissue increases. Background subtraction was the most reliable calibration method for higher Lucite thicknesses and

lower Pb concentrations, which was determined using the correlation values for the cadaver bone evaluated at different Lucite thicknesses.

Table 2.4 Bone Pb concentrations for bare cadaver bone calculated using different calibration methods.

Cadaver Bone ID	KXRF	Background Subtraction	Bone Calibration	Bone Adjustment
6900	23.12	23.44	23.63	22.21
7202	22.17	19.23	19.94	18.48
6918	21.17	9.35	11.30	9.50
7131	20.77	25.59	25.53	24.34
7031	19.70	24.09	26.18	23.39
7162	18.36	17.91	18.81	17.48
7042	14.27	16.05	18.33	16.10
7002	13.54	15.29	16.48	15.15
6895	9.82	15.91	17.04	15.59
7168	3.64	1.08	3.82	-1.86

Table 2.5 Bone Pb concentrations for cadaver Bone covered with 3 mm Lucite

Cadaver Bone ID	KXRF	Background Subtraction	Bone Calibration	Bone Adjustment
6900	23.12	20.92	22.44	11.66
7202	22.17	16.72	18.53	8.14
6918	21.17	2.97	-1.35	-14.21
7131	20.77	18.10	11.76	9.61
7162	18.36	12.07	6.55	4.33
7002	13.54	10.80	13.55	3.25
6895	9.82	12.94	14.69	5.26

Figures 2.11-2.16 show the comparison of the correlations between goat bone Pb concentrations calculated by KXRF and portable XRF at Lucite thicknesses of 0-5 mm,

with the Pb concentrations for portable XRF being calculated using traditional peak fitting or background subtraction. From the correlations, one can see that traditional peak fitting does fairly well for bare bone or at lower Lucite thicknesses, but with higher Lucite thicknesses the correlation falls off quickly due to the high background leading to the Pb peak being highly distorted especially at low concentrations. The chi-squared values for all the spectral fittings are close to 1, with the average chi-squared and standard deviation of the chi-squared value for these fits being 1.1±0.4, which demonstrates that even for poor results the data is accurately represented by fitted function.

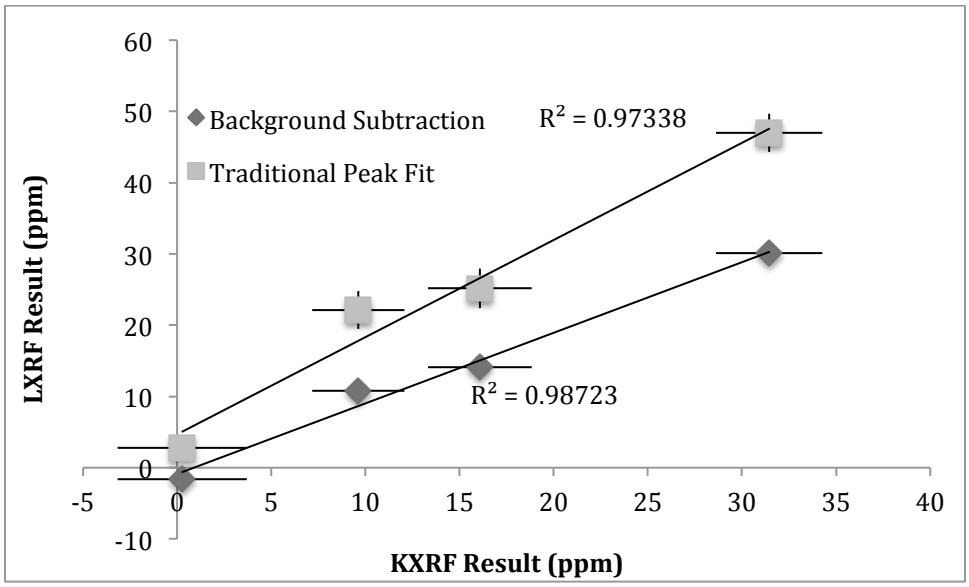

Figure 2.11 KXRF versus portable XRF bone Pb measurements for bare goat bone.

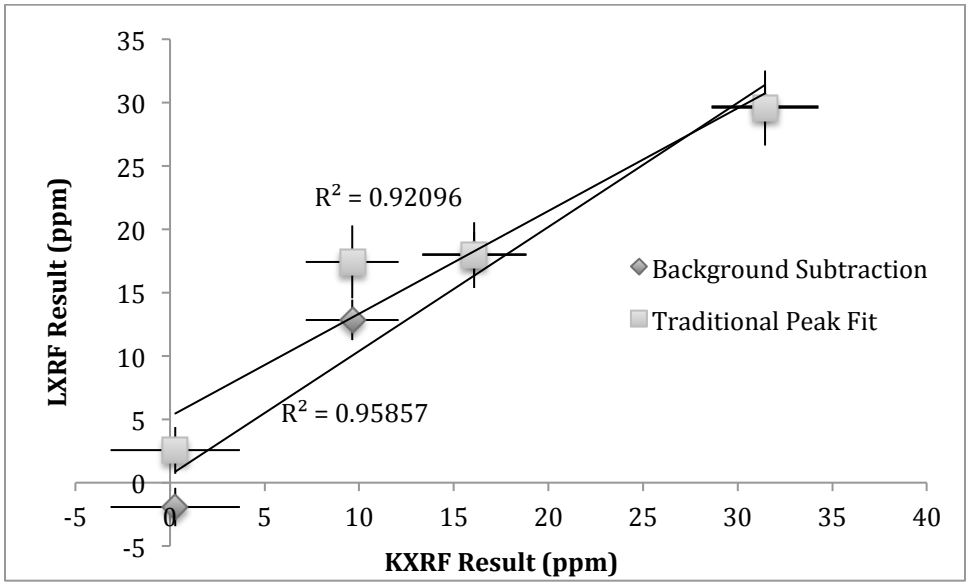

Figure 2.12 KXRF versus portable XRF bone Pb measurements for goat bone with 1 mm of Lucite thickness.

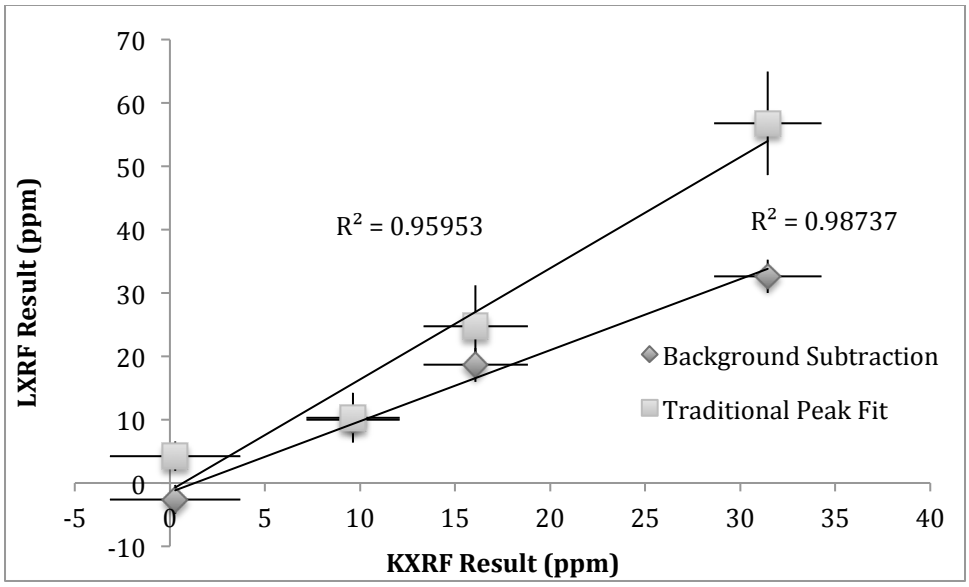

Figure 2.13 KXRF versus portable XRF bone Pb measurements for goat bone with 2 mm of Lucite thickness.

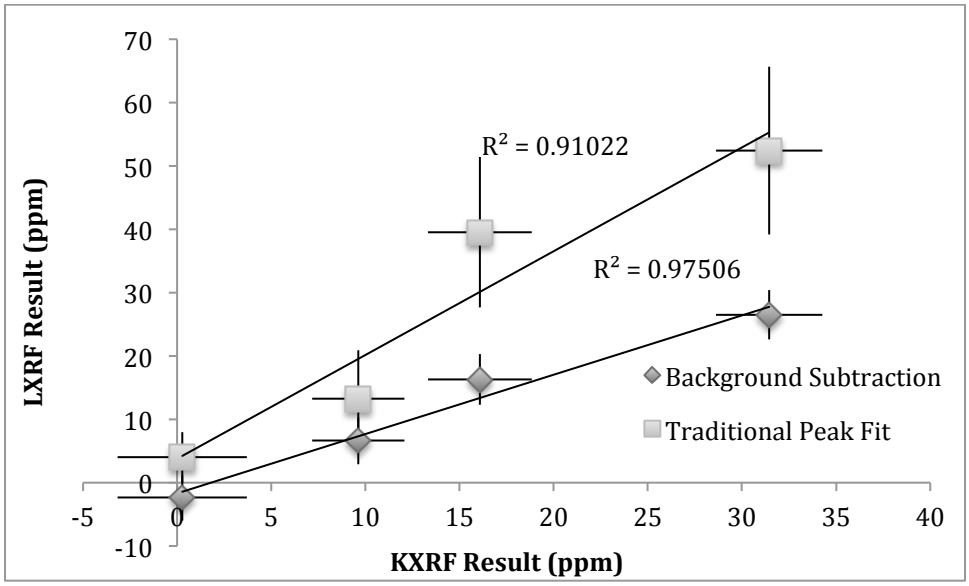

Figure 2.14 KXRF versus portable XRF bone Pb measurements for goat bone with 3 mm of Lucite thickness.

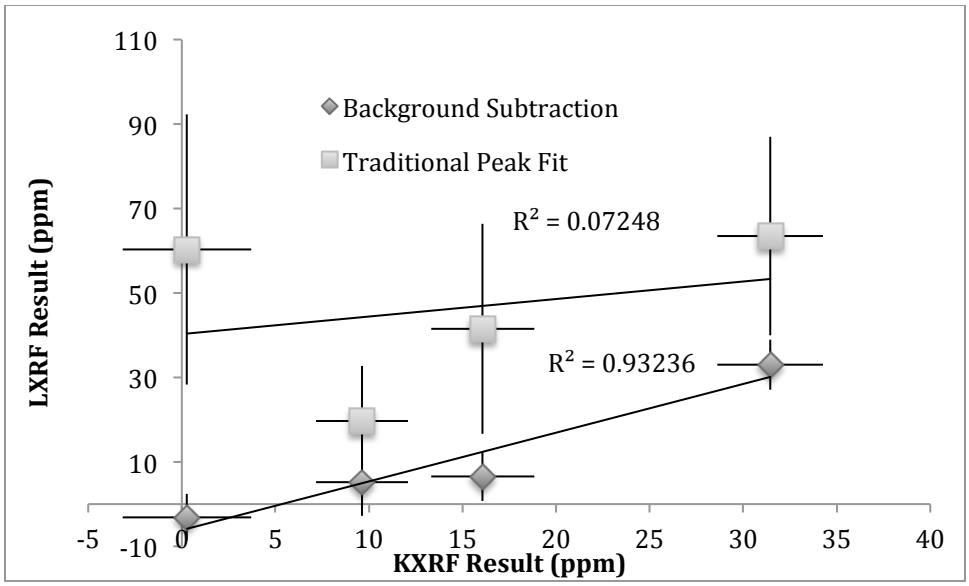

Figure 2.15 KXRF versus portable XRF bone Pb measurements for goat bone with 4 mm of Lucite thickness.

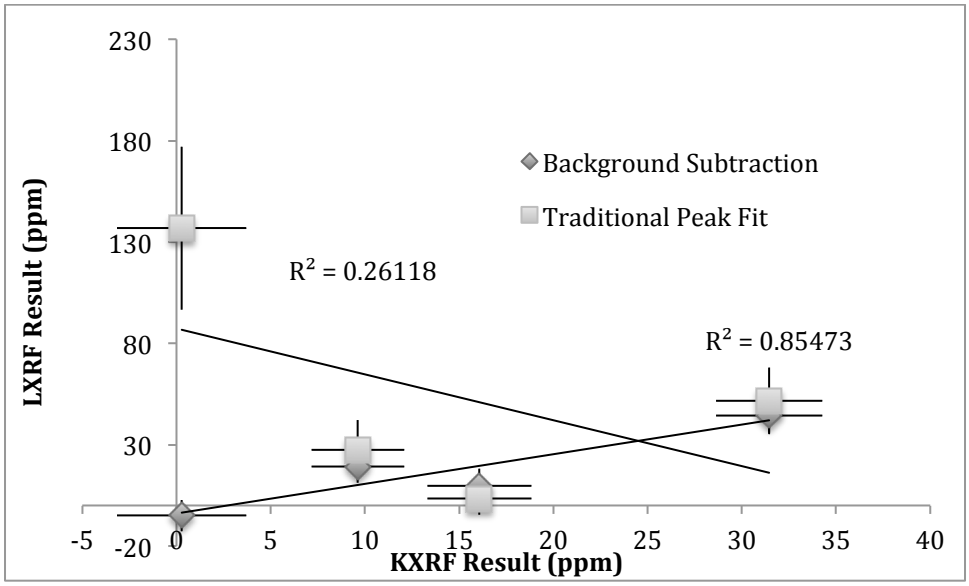

Figure 2.16 KXRF versus portable XRF bone Pb measurements for goat bone with 4 mm of Lucite thickness.

The data for cadaver bones with different Lucite thicknesses analyzed using the background subtraction method is presented in Table 2.6. The correlations (R-squared) between the concentrations obtained from KXRF and those from the portable XRF system range from 0.58 to 0.94 with Lucite thicknesses of 0 to 3 mm shown in Figures 2.17 and 2.18 respectively. The correlations between the Pb concentrations obtained from KXRF and portable XRF are worse for the cadaver bones than for the goat bones. This is mainly due to the lack of Pb concentration variation among the cadaver bones and geometric stability. Also, cadaver bone 6918 is an outlier (see discussion).

Table 2.6 Bone Pb concentrations for cadaver bones with different Lucite thicknesses calculated from the background subtraction method.

	Background Subtraction with Lucite Thickness				
Cadaver Bone	KXRF	0mm	1mm	2mm	3mm
6900	23.12	23.44	24.54	19.49	20.92
7202	22.17	19.23	22.02	14.56	16.72
6918	21.17	9.35	13.05	5.96	2.97
7131	20.77	25.59	20.9	21.68	18.1
7162	18.36	17.91	18.5	16.32	12.07
7002	13.54	15.29	14.48	14.54	10.8
6895	9.82	15.91	13.86	10.31	12.94

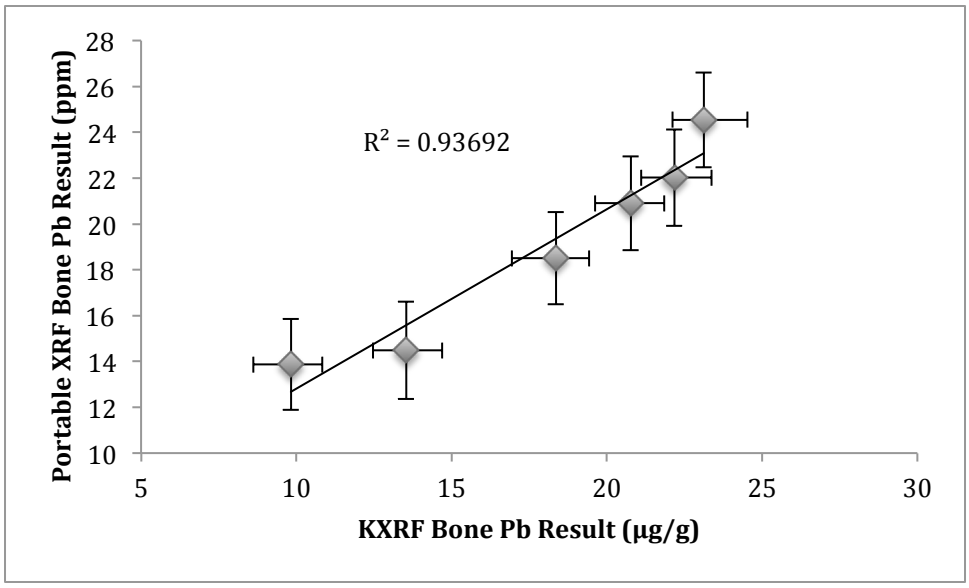

Figure 2.17 KXRF versus portable XRF bone Pb measurements for bare cadaver bone.

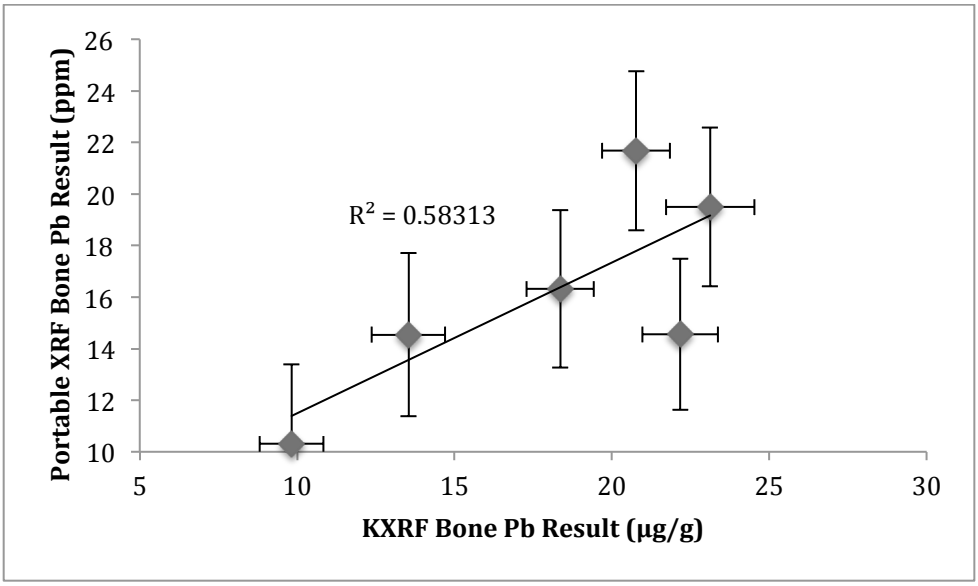

Figure 2.18 KXRF versus portable XRF bone Pb measurements for cadaver bone with 3 mm of Lucite thickness.

To test the reliability and reproducibility of the technology for *in vivo* measurement, the cadaver bones with intact soft tissue were measured repeatedly. Only three such cadaver bones were available in our lab, so there are limited data for this test. Table 2.7 shows the Pb concentrations from LXRF and KXRF for the three cadaver bones with intact soft tissue. The bones were measured nine times using the portable XRF device. The comparison in Table 2.7 demonstrates the abilities of the device in use through actual soft tissue. Using the Compton peak to determine soft tissue thickness, which was shown to be comparable to an ultrasound measurement, we found the intact soft tissue thicknesses for our three cadaver bone samples to be 1.3 mm for cadaver bone 7042, 4.1 mm for cadaver bone 7031, and 5.6 mm for cadaver bone 7168. The higher errors for individual measurements and higher standard deviation for grouped measurements are associated with larger soft tissue thicknesses, which is what we expect.

Table 2.7 Bone Pb concentrations for three intact cadaver bones measured by portable XRF for 9 times, comparing to those measured by KXRF.

	Cadaver Bone (ppm)		
Cadaver Bone ID	7042	7031	7168
KXRF	14.27±1.19	19.7±1.04	3.64±1.07
1	14.55±1.68	17.69±4.74	7.07±10.51
2	15.42±1.69	16.4±4.72	5±10.44
3	14.75±1.68	17.75±4.66	15.8±10.67
4	12.58±1.66	13.63±4.68	12.93±10.64
5	10.98±1.65	22.86±4.79	12.24±10.57
6	14.69±1.67	18.13±4.87	16.2±10.71
7	13.2±1.66	24.15±4.95	6.89±10.54
8	12.44±1.64	17.67±5	11.58±10.75
9	12.5±1.64	15.55±5.01	24.25±10.76
Average±SD	13.46±1.46	18.2±3.34	12.44±5.93
Soft Tissue Thickness (mm)	1.3	4.1	5.6

2.3.6 Discussion and Conclusions

This chapter investigated the optimized detection limit of a portable XRF system for in vivo bone Pb quantification and validated the system using phantoms, goat bones, and human cadaver bones. The improved system geometry and detector size greatly enhanced the detection limit of the device and the ability of the device to accurately determine the concentration of Pb in bone especially at the *in vivo* situation.

The comparison between simulation and experiment of phantom materials pointed out some potential flaws in using it as a comparison directly for our portable XRF. The main flaw with the simulation is verifying the geometry of the experimental device and inputting it correctly into the simulation. The angles between detector and sample are set rigidly in the experimental setup and result in slight differences in energy. Along with

that we do not know if they use some type of shielding surrounding the detector itself, which would help to lower background, and cannot input the exact detector parameters like resolution and resolving time into the simulation. These differences all led to slight changes in what could account for some of the error observed between Lucite and soft tissue in simulation versus our experimental result.

The detection limit for the portable XRF device is improved from the previous portable XRF device by a factor of about 2. Through soft tissue thicknesses of 4 mm the device has the capability of a detection limit of 8 ppm, which is comparable to detection limit of 6-10 ppm with KXRF bone Pb measurement systems in most labs. It is also relevant to point out that this was with a 3 minute measurement time, and that time could be increased by a factor of 2 or 3 to lower the detection limit further, while maintaining a reasonable radiation exposure. The main disadvantage of LXRF systems is the lack of penetration of the low energy x-rays and thus at depth, the ability of the system to determine concentration becomes limited. The average range for the energy of our x-ray tube in cortical bone is 1.3 mm and for soft tissue thickness is about 12.5 mm. With this system, it is shown that even at depths of 4 mm of soft tissue the portable XRF device now has the capability of obtaining measurements in 3 minutes, which would be equivalent to a KXRF device with a 30 minute measurement. In studies it has been shown that tibia measurement sites with tissue thickness of less than 4 mm can be found on most seniors and about half of the general population [47, 49]. One of our target populations for this device is the senior people whose mobility might be confined by their health conditions. Another point of clarification is the fact that with the low penetration depth of LXRF, the KXRF and portable XRF systems are sampling different sites of the bone.

KXRF would be sampling the whole bone and LXRF would be sampling the superficial 0.5-1 mm of the bone. It is not very clear how Pb distributes over the layer of tibia bone and the literature on this topic is limited. Todd et al. showed higher concentrations of Pb at 1-2 mm to the surface in bone [50], while Bellis et al. demonstrated a higher concentration of Pb at a much thinner layer [51]. While the bone Pb concentrations from KXRF and LXRF are highly correlated in our study, further investigation with larger amount of samples is needed on the comparison for the absolute bone Pb concentrations from these two methods. It is also relevant to point out that with measurements of bone Pb the goal is a correlation with health effect, which should be reflected in both surface and depth bone measurement sites.

Another point of potential difference is revealed in the units of measure of the results obtained for each device. The KXRF bone Pb measurement system has a unique normalization based on the energies of the excitation source, which allows it to be normalized specifically to the bone matrix that was irradiated during the measurement and can give results in μg/g bone mineral, which is equal to ppm units in most cases. The portable XRF calibration is done using phantoms of known concentrations in ppm; however, no normalization can be done to the irradiated portion of bone in particular since no spectral features are stable enough to be consistently changing with bone with no other relation to soft tissue or other compositional differences. This is due to the energy of the portable XRF. From past discussions comparing plaster-of-Paris and in vivo bone measurements, there should be a factor of about 1.5 between the two results. This factor converts the measured matrix from bone mineral to dry bone. In our measurements it appears that for the cadaver bone measurements this factor is non-existent, which should

not be the case. The portable XRF device with results from the phantom calibration should be in μg/g dry bone, which should need to be converted to μg/g bone mineral; however, plaster-of-Paris is not exactly equivalent to dry bone, which could further influence this relation. The units will need more investigation, but will not influence the relevance of our correlations, as the values should still correlate well regardless of unit conversions.

The Pb concentrations found through KXRF and portable XRF measurements of bare bone show good correlation. In order for our device to determine the *in vivo* Pb concentration, our analysis methods should prove to be accurate with bone. Bone has different density and effective atomic number compared to our calibration phantoms, which led to differences in its resultant XRF spectrum. Our results with simulation and then measurement of cadaver and goat bones show that our calibration methods adequately address these differences as the results are well correlated with KXRF data. In comparison, the traditional peak fitting calibration method results are shown with goat bones, and at larger Lucite thicknesses this method is worse than the background subtraction method especially for low concentrations of Pb. It is relevant to point out that other studies exploring the validity of LXRF for Pb studies used traditional peak fitting methods and showed that the results were not reliable especially at higher soft tissue thicknesses [32]. The main issue is with the fitting program's ability to discern background from the Pb peak region, which is increasingly difficult at higher background levels. It is much more difficult to fit the alpha region in these cases as well, since the alpha region tends to have much more noise from surrounding elemental characteristic x-rays like selenium and zinc, which further confound the area where the peak should be.

Beta regions tend to have less interaction with other characteristic x-rays and showed a better ability to be fit in low concentration and high tissue thickness situations, although still with limited accuracy.

The background subtraction calibration method performed the best in our study. The bone adjustment method did correct the Compton peak to phantom values for a more equal comparison, but it fails to take into account the balance between the Compton peak, background, and signal, and because of this, at higher Lucite thicknesses it exaggerates the problems seen with background subtraction of overestimating the background under the Pb peak regions. This is because the calibration itself is just trying to fix the Compton peaks to reflect phantom values, but the extent of this difference is not just from bone and will not be reflected only in the Compton scattering peak. If the interaction cross section of the bone should change for Compton scattering, it will also change for photoelectric absorption thus changing our signal. The bone calibration only adjusted for changes in Compton scattering, which did not reflect the bigger picture of what was happening in our spectra. Bone calibration should be the best calibration method in theory since it is a comparison of two bone matrices, but due to the lack of standard bones with higher Pb concentrations, the calibration line for this method tended to produce results that were less accurate than the background subtraction method. There were only 4 goat bone standards we could use for this and with that only a 31.4 ppm maximum concentration. Using this method effectively lowers our ability to detect low levels of Pb. A 31.4 ppm standard can only be accurate to a certain Lucite thickness. Reviewing the sample spectrum in Figure 2.5 gives you a sense of this. That sample spectrum is with 14 ppm and 1.3 mm, so at about 3 mm the Pb x-ray peaks will be almost invisible with the

background noise. Similarly, a 31.4 ppm phantom at 5 mm of Lucite thickness will be almost invisible. This will limit the statistical value you can place on your calibration line at 5 mm of Lucite thickness and the uncertainty will be much higher than if a 100 ppm phantom was used.

The correlation of bone Pb concentrations between KXRF and portable XRF is very good for phantoms and goat bones with Lucite thickness up to 5 mm, while the R-squared degraded slightly for our cadaver bone measurements. This is mainly due to the small variation of the Pb concentration for these cadaver bones, as well as the difficulty to adjust the geometry of the bare bones. In measuring cadaver bones, the geometry presented issues if not strictly monitored. We found that the cadaver bones were prone to air gaps in the geometry, which led to significant changes in the spectrum caused by the increased distance without significant attenuation. This can cause significant drops in our quantification. From Figure 2.19 below, we can see that a 2 mm gap could cause a drop from inverse square law effects of almost 50% of the signal, which would introduce an error of ~50% in our measurement. Although this effect was visible in the cadaver bone data, given the geometry of *in vivo* measurements this effect would not be present as the bone is covered in soft tissue, so there will not be air gaps between the soft tissue and bone *in vivo*. The geometry will always be conserved with the portable XRF pushed against the soft tissue covering the bone. Attenuation by soft tissue is accounted for with our calibration by determining the soft tissue thickness from the Compton peak, which in-turn corrects for distance, as the gap between the detector and bone is filled with soft tissue. The main issue with the cadaver bones was this gap was not filled with anything and thus could not be accounted for unless we knew the exact air gap.

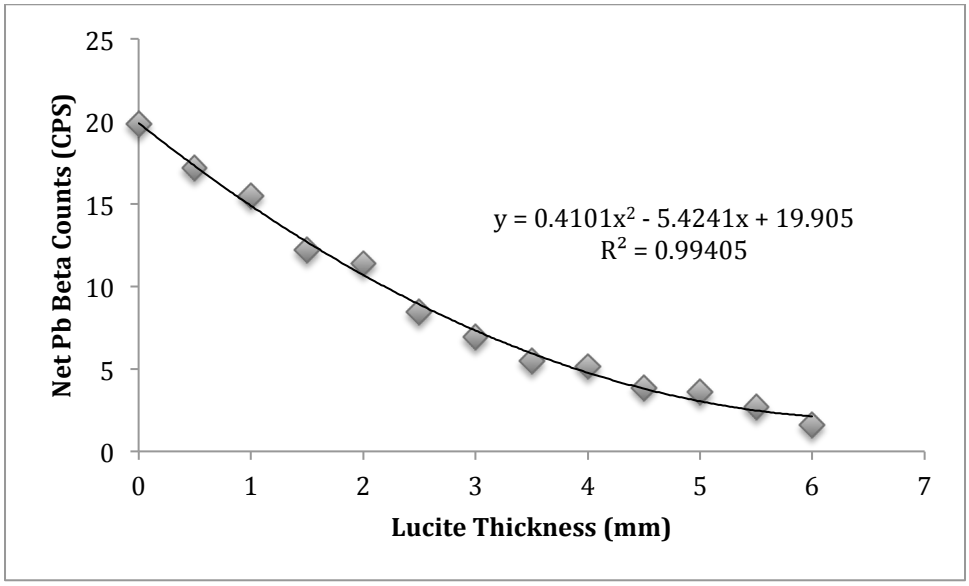

Figure 2.19 Net Pb beta counts versus Lucite thickness

Although only three intact cadaver bones were used to test the reproducibility of the system for bone Pb quantification and to validate the system in a real *in vivo* situation, several conclusions can be drawn from these limited data. First, this set of data confirmed the validity of the system for *in vivo* measurements, especially for the measurements with soft tissue thicknesses less than 5 mm. Second, the data confirmed that the thickness of the soft tissue significantly affect the uncertainties of the resultant concentrations. The standard deviations from the repeat measurements are lower than the uncertainties for individual measurements, which indicate the uncertainties for individual measurements maybe overestimated. In addition, the detection limit of the measurements calculated from the Pb concentration uncertainties (DL = 2 x sigma) for cadaver bones listed in Table 2.7 would be higher than those listed in Table 2.2 for corresponding soft tissue

thicknesses. This is because the uncertainty calculated in Table 2.7 includes the error on the gross count and net count of the signal under the Pb L x-ray peak, while the DL calculated in Table 2.2 only includes error associated with the background of a blank phantom covered with a corresponding thicknesses of Lucite. Nonetheless, this data set shows an excellent agreement of bone Pb concentrations for cadaver bones at thickness of 1.3 and 4.1 mm, while the agreement deteriorates at 5.6 mm. The disagreement between standard deviation of measurements and calculated uncertainty likely arises from a number of different places. As stated previously the measurement uncertainty calculation takes into account the uncertainty of gross and net counts, which is likely staying similar since it is the same measurement site. The same measurement site will have the same physical properties and interaction cross-sections for our portable XRF, which is why it reflects similar measurements. In reality we will be comparing different in vivo measurement sites for different individuals, which will need to be reflected in an associated uncertainty for these potential differences.

In the cadaver bone measurements, there is one bone (cadaver bone 6918), which we considered an outlier in our dataset. This bone came from a 100 year old female, and presents further challenges with the LXRF device. The spectrum from the bone had a much higher than normal Compton peak, which we attributed to the bone appearing more like soft tissue with respect to the spectral features. This resulted in a more pronounced overestimation of the background, and worse signal quantification. In general the background subtraction method should overcome slight variations in bone between individuals, as the Compton peak will also relate back to the material of the bone. The relationship we had derived between the Compton peak and the Pb signal broke down for

this particular bone. We found that the density of this bone was significantly different than the others, but have not identified a way to counteract this difference with our calibration methods. Although bone 6918 has a Compton peak that is significantly different, other spectral features show differences that may be able to be exploited to correct the issues with the Compton peak in this spectrum.

The portable XRF system, now with a significantly lower detection limit, has its main advantages over KXRF with its portability, acquisition times, and ease of use. The new system can achieve a minimum detection limit equivalent to a KXRF measurement through tissue thicknesses up to 5 mm. The portable XRF system also has the advantage of using an x-ray tube, which can be turned off when it is not in use and is less complicated for radiation licensing than a radioisotope source. The portable device lends itself for use in epidemiologic studies because of its quick measurement times and portability. The device allows for on-site Pb surveys and risk assessments of the environment, while performing exposure assessment of the community members.

CHAPTER 3. XRF MEASURED BONE PB AS A BIOMARKER FOR A PB POISONED PEDIATRIC POPULATION

3.1 Introduction

Despite strict standards for Pb use in many countries, childhood Pb poisoning remains a worldwide issue. This problem is more prevalent in heavily industrialized areas. China, in particular, presents unique exposure issues: pollution, alternative medicines with large amounts of Pb used to treat various diseases, and ever-increasing consumer and industrial usage of Pb containing products. Recent studies show that Pb exposure results in significant decline in intellectual ability even at low-levels, and that the Pb associated intellectual decrement was steeper at low blood Pb levels than at higher blood Pb levels [5, 6, 52]. These studies use blood Pb as a biomarker, which assesses recent exposure and has a half-life of about one month in adults [44]. Cd-109 based K-shell x-ray fluorescence (KXRF) has been used to study bone Pb for over two decades, but not many studies have been performed on children using a bone Pb biomarker, and the studies that do exist have a relatively high uncertainty and were not able to detect bone Pb in most of the subjects due to the high uncertainty of the conventional bone Pb measurement system [53, 54]. There is a significant gap in understanding children's bone Pb measurements

and their relationship to blood Pb, as well as the usefulness of bone Pb as a biomarker for Pb exposure and toxicity among children, which are addressed in this chapter.

This chapter focuses on a study of a group of Pb poisoned children recruited from Xinhua Hospital in Shanghai, China. The children were tested for bone Pb with the modern cloverleaf KXRF measurement system and the portable XRF bone Pb measurement system. With the low detection limit of the advanced KXRF system we can identify the role of bone Pb in children's Pb biokinetics, and using a comparison with portable XRF results we can assess the ability of its use in measuring children's bone Pb levels. This addresses the need for identification of Pb's roles in development and how it stores in the body of children.

3.2 Materials and Methods

3.2.1 Study Population

The study participants were Pb-exposed children and controls recruited through Xinhua Hospital, Shanghai Jiaotong University, China. The Pb-exposed group was recruited from children who were diagnosed as Pb poisoned with blood Pb levels >25μg/dL. Some of these children had already undergone multiple treatments prior to our first measurements, and some were measured at the time of their first treatment. The controls were recruited from children who visited the clinic for non-Pb related diseases. Xinhua Hospital has a specialized environmental health department, so children from all over the country in need of treatment would come to this hospital. The parents of the subjects completed a

questionnaire, and the subjects had their blood samples taken, and their bone measured for Pb concentration using an advanced cloverleaf Cd-109 KXRF as well as a portable x-ray fluorescence (XRF) system. Blood Pb was also measured for these children. Some of the Pb-exposed children were treated using ethylenediaminetetraacetic acid (EDTA) chelation. These treatments were done at the hospital and the patients were monitored during the process that lasted a few days. After treatment, some patients would return after 41.5±30.0 days for another round of treatments and they would be measured again for bone Pb using the Cd-109 KXRF system.

The study received IRB approval from Purdue University and Xinhua Hospital. When recruited, a trained research assistant would present the subjects and their parents with the details of the study and the consent forms. Signed consent forms were received from the parents of each subject, as well as an assent form from any child age 7 or older.

3.2.2 KXRF Bone Pb Measurement System

The KXRF bone Pb measurement system was used to measure tibia bone Pb as a metric of each individual's cumulative Pb exposure. The system was the same as described in Chapter 2. Before measurement, the subjects' legs were cleaned using alcohol and EDTA cotton swabs to remove any Pb contamination. For the KXRF measurement the subject would sit on a wooden chair. The subject's leg was immobilized by using two Velcro straps to attach their leg to the leg of the chair at the ankle and just below the knee. The measurement site was mid-tibia with the source at a distance to maintain ~30% dead time during the measurement. The system was on a moveable platform that could be used to

adjust to different placements for each individual. The measurement was taken for 30 minutes while the subject watched a movie. Finally, the spectra were analyzed using the in-house peak-fitting program, which gave results and error for each of the four detectors [55-57]. This error and result was combined using inverse variance weighting [58]. XRF provides a point estimate of Pb concentration, which can be negative if an individual's bone Pb is close to zero. It is important to include these negative values, as with their associated uncertainties they are still a point estimate of that individual's bone Pb. The negative values also give us a sense of how well the system is working with the population. Since children have typically demonstrated to be a population with measurement problems for bone Pb, it is important to identify the associated uncertainties in our measurements and the lowest limit for measurement in this population.

3.2.3 Portable XRF Bone Pb Measurement System

The portable XRF used in this study was the XL3t GOLDD+ system identified in Chapter 2. We used the optimized x-ray tube settings discussed in Chapter 2 for this study and used a two-minute measurement time. Before measurement, the subjects' legs were cleaned using alcohol and EDTA cotton swabs to remove any Pb contamination. We again chose the measurement site to be mid-tibia. In placing the device on the subject's leg, we used non-Pb based ink to make a dot on the measurement site. This dot could then be found using a camera mounted in the head of the portable XRF, which ensured a consistent measurement location. This was also the same site the KXRF measurement was taken from, since the portable XRF measurement was done first in

most cases. The subject's leg was held horizontally with their foot resting in the operator's lap during the measurement. The spectra were analyzed using traditional peak fitting as described in detail in our previous work in Chapter 2. Based on our previous study, by adjusting values for increased measurement time and tube current we estimated the entrance skin dose of the system was 21 mSv to a 1 cm^2 area and the whole body effective dose was 2.4 μSv [47]. This dose is less than that of the KXRF system and is the same for the adult and child subjects. The low energy x-rays used with the portable XRF do not penetrate into the bone marrow and thus do not have the increased tissue-weighting factor of bone marrow in children, which results in a lower radiation dose.

3.2.4 Blood Pb Analysis

Blood Pb analysis for this study was done at Xinhua Hospital. The blood of the subjects was collected in a Pb-free environment. We cleaned the subjects' skin using alcohol swabs before sampling. The blood collection tubes along with the EDTA-K2 anticoagulants were measured to be Pb free before sampling. All the samples were frozen and kept at -80^0 C immediately after the collection. Blood Pb concentrations were measured and analyzed by an Atomic Absorption Spectrometer (AAS) (AA900Z, PE) [59]. The sensitivity of our device was 0.01μg/dL, and inter and intra assay variability was 5%.

3.2.5 Statistical Methods

Linear regressions were used to determine correlation values and levels of significance of relationships between KXRF and portable XRF bone Pb measurements and KXRF bone Pb and blood Pb. The KXRF bone Pb data was excluded from our analysis if the final uncertainty was >10ug/g. This would indicate an excessive amount of movement during the measurement or a measurement taken for less than 30 minutes. Portable XRF data was excluded if the measurement time was <2 minutes.

3.3 Results

The study had 269 participants (181 male and 88 female), ranging in age from 1 to 15 years old with a mean of 5.7±3.1 years. Of these participants, 175 were Pb poisoned subjects and 94 were controls.

3.3.1 Bone and Blood Pb Concentrations from the Study Population

The bone and blood Pb concentrations for the exposed and control groups are listed in Table 3.1. The average uncertainty in this study for in vivo KXRF bone Pb measurement was 2.66 ± 1.05, and is shown for each group in Table 3.1 under Bone Pb Sigma. Blood Pb data shown in this table was taken at the time of the first bone Pb measurement, which for some exposed subjects was after multiple treatments. Table 3.2 shows the blood and bone Pb data separated by sex of the participants in the study. There was a non-significant difference between male and female groups with a p-value of 0.146, but a

trend of more bone Pb with females was observed. The uncertainty between males and females was not observed to have any differences.

Table 3.1 Bone and blood Pb statistics for exposed and control groups in the study population.

Exposed	N	Minimum	Maximum	Mean	Std. Deviation
Blood Pb (μg/dL)	182	0.80	91.60	20.78	14.08
Bone Pb (μg/g)	175	-22.64	244.33	22.40	31.65
Bone Pb Sigma	175	1.49	9.78	3.42	1.70
Control					
Blood Pb (μg/dL)	77	0.80	9.90	2.91	2.18
Bone Pb (μg/g)	94	-9.59	9.38	-0.95	3.50
Bone Pb Sigma	94	1.67	7.79	2.73	0.86

Table 3.2 Bone and blood Pb statistics for male and female subjects in the study population.

		Bone Pb (μg/g)			
	N	Mean	Minimum	Maximum	Standard Deviation
Male	181	12.6	-22.6	186.0	24.8
Female	88	17.6	-8.4	244.3	33.3
Total	269	14.2	-22.6	244.3	27.9

3.3.2 Blood Pb Correlations with Age

We performed a regression of blood Pb versus age and found a significant negative correlation as seen in Figure 3.1. Figure 3.2 shows this correlation to be weaker, but still

significant for KXRF bone Pb and age. The p-value for both of these correlations was <0.001.

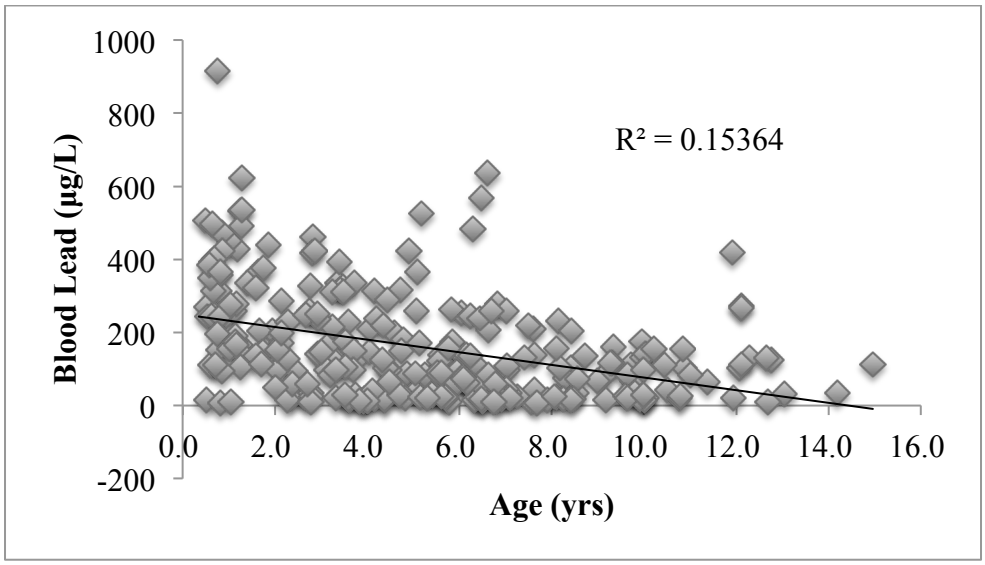

Figure 3.1 Age versus blood Pb for our study population.

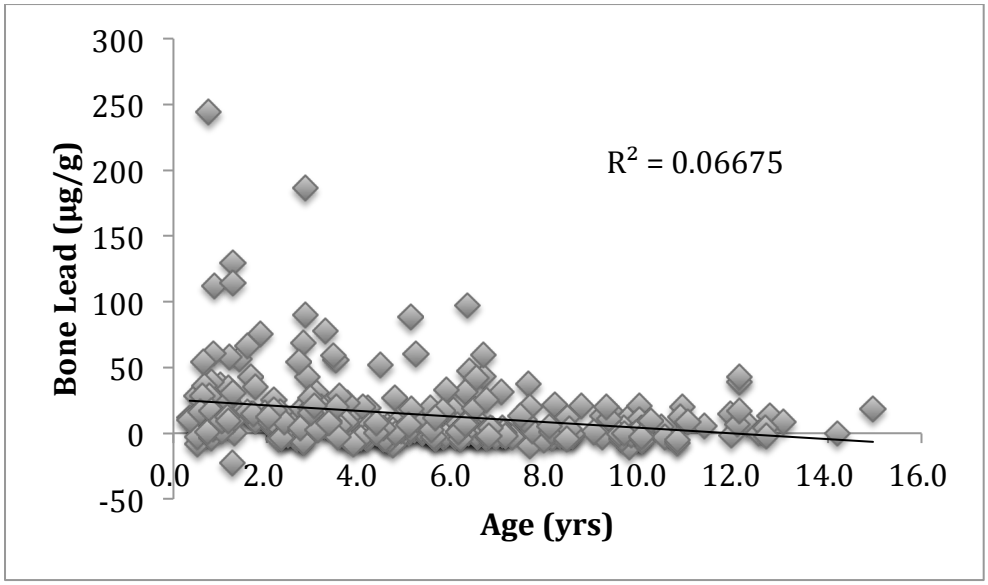

Figure 3.2 KXRF bone Pb versus age for our study population.

3.3.3 Correlations Between Bone and Blood Pb Concentrations

Figure 3.3 shows the correlation between bone Pb concentrations obtained from KXRF and blood Pb concentrations using all subjects. No correlation was found in this relationship when using only control subjects, and only a slight positive change in correlation value when using only exposed subjects (R^2=0.612). Figure 3.4 shows the significant correlation for portable XRF measured bone Pb and blood Pb using only exposed subjects. This is a weaker correlation for reasons explained in the discussion. No correlation was found in this relationship when using only control subjects, and only a negative change in correlation value when using only exposed subjects (R^2=0.07). The p-value of both regressions was <0.001.

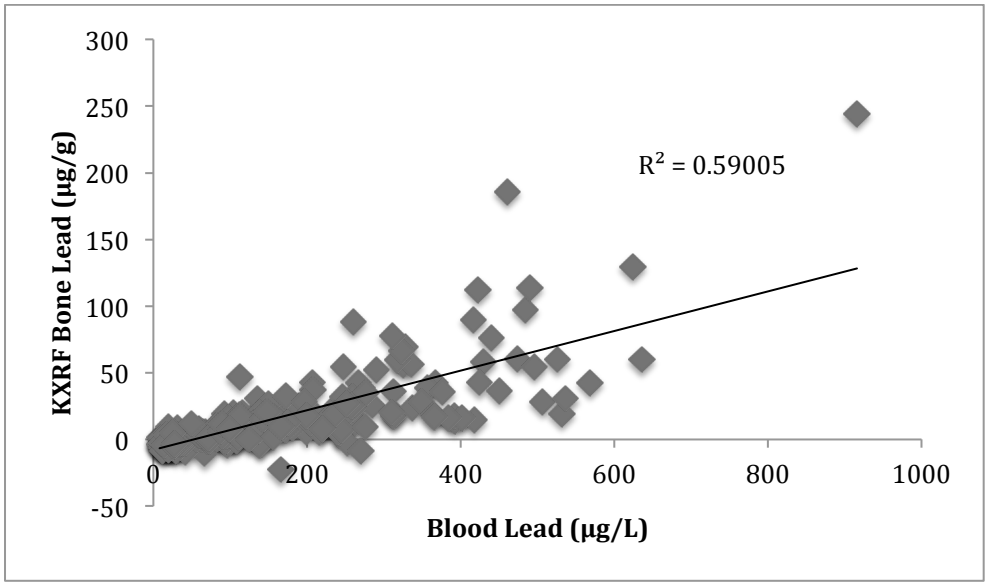

Figure 3.3 KXRF bone Pb versus blood Pb measurements for exposed patients.

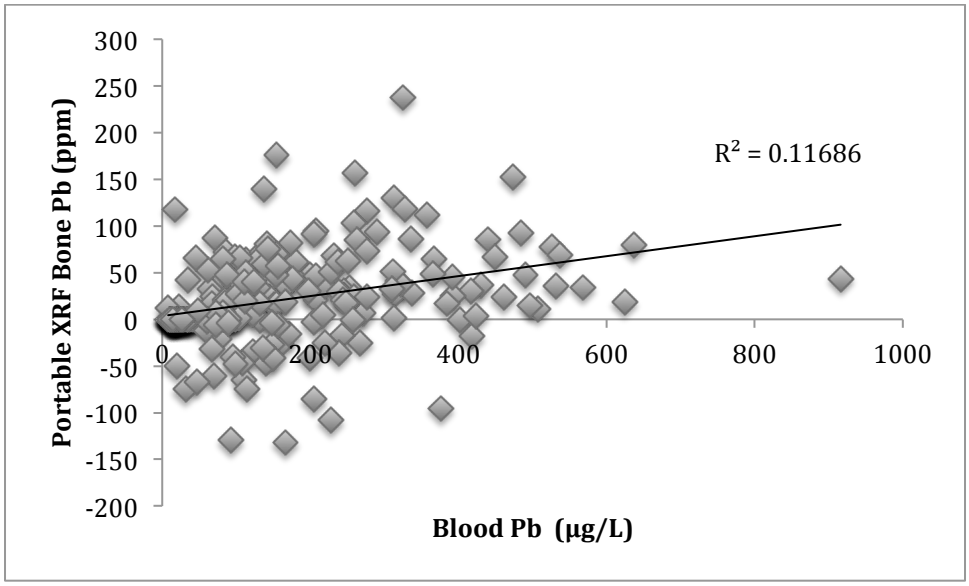

Figure 3.4 Portable XRF bone Pb measurement versus blood Pb.

3.3.4 Correlations Between KXRF and Portable XRF Measured Bone Pb

Figure 3.5 shows the correlation of bone Pb obtained by KXRF versus that obtained by portable XRF using only exposed subjects. Again with this relationship, no correlation was found when using only control subjects. The p-value of this regression was <0.001.

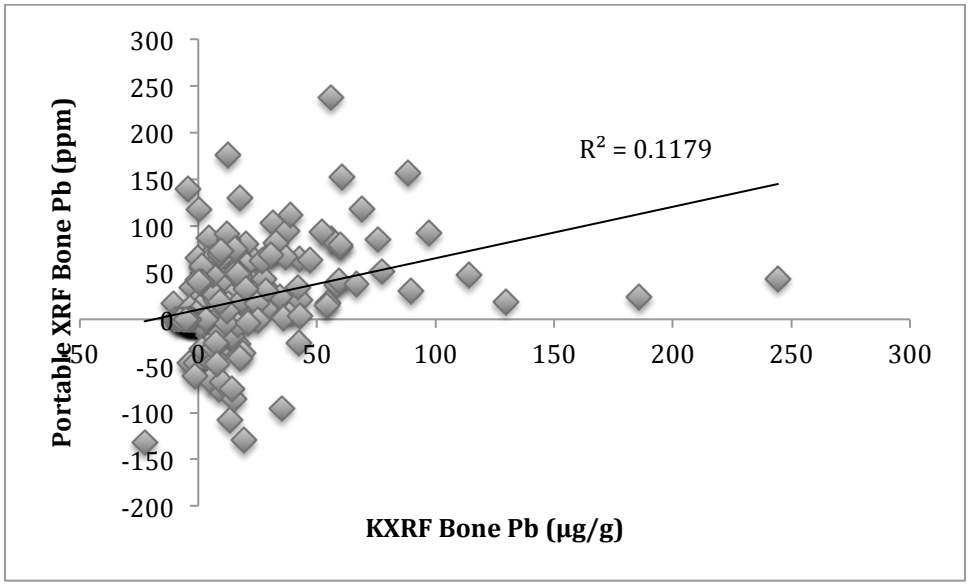

Figure 3.5 Portable XRF bone Pb result versus KXRF bone Pb result.

3.3.5 Bone Pb and Blood Pb Biokinetics

With the bone Pb and blood Pb concentration data obtained from the study, we can estimate the percentage of bone Pb over the total Pb amount in blood and bone, which are two of the largest Pb storage sites in the human body, as well as the Pb transfer rate between bone and blood. Total bone Pb and blood Pb amount were calculated by multiplying bone and blood concentrations and the bone mineral amount and blood volume. The total bone mineral was calculated from the data shown in Specker et al.'s paper [60]. Specifically, it was calculated using a combination of age, height, weight, and other variables as shown in the paper. The age, height, and weight of the subjects were collected in our study. The other variables were estimated from the average values

corresponding to our age group. The calculation was done by first using their equations for calculating total body bone area (TBBA) as shown below with our substitutions.

$$TBBA = -359.66 + 7.89 * H + 25.26 * W + 54.255 + 19.21$$

,where -359.66 was intercept, 54.255 was their averaged value for body fat percentage, 19.21 was their averaged value for calcium intake, H is height, and W is weight for our study participants. Then we can input the results from that equation into our final formula for total body bone mineral content (TBBMC).

$$TBBMC = 153.25 + 0.81 * TBBA + 16 * A - 3.52 * H + 4.09 * W - 113.15$$

, where 153.25 is the intercept, A is age, and 113.15 is their value for body fat percentage combined with its respective weighting factor. The total blood volume (TBV) for each child was calculated from the data shown in Linderkamp et al.'s paper [61]. Specifically, it was calculated using an age dependent logarithmic model, which relates blood volume to weight and height. Again, the age, height, and weight were collected in our study. The final formula used is shown below.

$$Log(TBV) = 0.6459 * LogW + 0.002743 * H + 2.0324$$

Then, using the 49 subjects that met the previous criteria and had sufficient data to calculate the total body bone mineral content and blood volume levels, we found that

total bone Pb on average accounted for 96±5% of total blood and bone Pb burden. The maximum and minimum values calculated for each individual exposed subject were 99.5% and 69.7% total body Pb burden from bone Pb respectively. Separating the subjects by age we see larger variation in this value with exposed subjects of 1-3 years old with 92.3±11% bone Pb and exposed subjects 3+ years with 96.5±4% bone Pb.

Throughout the course of the study some subjects returned for one to three treatments, there was a time gap of 41.5±30.0 days (minimum: 7; maximum: 97) between these treatments. We can assume that bone and blood Pb had reached equilibrium by the second visit, which then allowed us to calculate an estimated half-life of blood Pb. Possible sources of Pb exposure were removed from these children after their first treatment and the effects from chelation should have worn off, so the calculated half-life is expected to be the biological half-life without significant external exposure sources or effect from chelation therapy. The bone-remodeling rate (BMR) for children was calculated from the data shown in ICRP 70 [62]. We plotted the bone-remodeling rate versus age for children 0-15 years old, fitted the data with second-degree polynomial function, and calculated the bone-remodeling rate for each child from the fitted line. The formula for this function is below.

$$BMR = 0.469 * A^2 + 13.417 * A + 116.08$$

Assuming that bone and blood Pb were in equilibrium, that the Pb from other organs to blood is negligible compared to the Pb from bone to blood, and that there was negligible exposure from external sources, the Pb transferred from bone to blood would be equal to

the Pb transferred from blood to urine, feces, and other organs per unit time. This can be expressed as:

$$\lambda_{Blood\ Pb} \times T_{Blood\ Pb} = \lambda_{Bone \rightarrow Blood} \times T_{Bone\ Pb}$$

Where $T_{Bone\ Pb}$ is total body Pb in bone (total bone mineral × bone Pb concentration obtained from KXRF in unit of μg/g bone mineral), $T_{Blood\ Pb}$ is total body blood Pb (blood volume × blood Pb concentrations obtained from AAS), $\lambda_{Blood\ Pb}$ is the percentage of Pb in blood which would be transferred to urine, feces, and other organs per day, and $\lambda_{Bone \rightarrow Blood}$ is the percentage of Pb in bone which would be transferred to blood per day. Because the bone resorption rate represents the percentage of bone that would be resorbed to blood, $\lambda_{Bone \rightarrow Blood}$ is equivalent to bone resorption rate, which can be calculated as described before. From these we can calculate $\lambda_{Blood\ Pb}$:

$$\lambda_{Blood\ Lead} = \frac{\lambda_{Bone \rightarrow Blood} \times T_{Bone\ Pb}}{T_{Blood\ Pb}}$$

Given that

$$\lambda_{Blood\ Pb} = \frac{Ln(2)}{T_{1/2,blood}}$$

where $T_{1/2,blood}$ is the biological half-life of Pb in blood. The half-life of Pb in blood can be calculated as $Ln(2)/\lambda_{Blood\ Pb}$. The half-life was calculated for all the exposed subjects that had all the necessary measurements to perform the calculation, which resulted in 17 calculations of the half-life. The data and results for those subjects are shown below in Table 3.3 and 3.4.

Table 3.3 Exposed subject data for blood Pb half-life calculations.

Age (years)	Weight (kg)	Height (cm)	Total Blood Volume (L)	Total Bone Mineral (g)	Bone Pb (μg/g)	Second Blood Pb (μg/L)	Total Bone Pb (mg)	Blood Pb Half Life (days)
1.3	10	80	0.79	303.9	129.6	758	39.4	3.74
1.4	10	79	0.79	303.1	56.0	238	17.0	2.90
1.6	10.9	80.5	0.84	333.0	17.5	195	5.8	8.16
1.9	11	82	0.85	343.4	75.7	223	26.0	2.33
2.8	12.5	92	0.98	423.6	69.1	291	29.3	4.13
2.8	17	92	1.20	534.7	89.6	309	47.9	3.30
2.8	14	95	1.08	469.9	186.0	615	87.4	3.25
2.9	12	91	0.95	411.3	19.3	173	8.0	9.13
3.4	20.5	108	1.50	675.5	34.9	245	23.6	5.09
3.4	17.5	106	1.34	596.5	13.8	195	8.2	15.36
4.7	22.5	116	1.67	769.3	33.9	238	26.1	7.19
4.9	16	103	1.24	575.2	19.0	228	10.9	9.35
5.2	16	110	1.29	599.9	60.0	420	36.0	9.88
6.6	25	132	1.98	906.9	59.8	461	54.3	13.05
6.8	35	125	2.36	1135.4	53.2	247	60.4	8.65
11.9	36	150	2.81	1313.2	14.4	294	18.9	51.13

Table 3.4 Blood Pb half-life split by age group for exposed subjects.

Group	N	Average Blood Pb Half Life (days)	Standard Deviation
Age 1-3	8	4.62	2.56
Age 3+	9	16.27	14.47
Total	17	10.45	11.71

Along with this data, we estimated the change in bone Pb before and after treatment for each patient that came back for multiple visits after chelation therapy. This data is shown below in Table 3.5. There was a non-significant difference between bone Pb before and after treatment with this data, but we believe this would be more significant with more cases.

Table 3.5 Bone Pb changes after chelation therapy for different groups in our study population.

Group	N for Each Group	Average Bone Pb Value Before Treatment (μg/g)	Standard Deviation	Average Bone Pb Value After Treatment (μg/g)	Standard Deviation	Total Bone Pb Before	Total Bone Pb After
Age 1-3	20	38.5	43.4	34.1	34.1	770.8	682.4
Age 3-6	19	17.6	16.6	16.9	16.4	334.7	321.2
Age 6+	14	16.9	16.7	15.7	15.7	236.5	220.5
Male	37	27.5	35.6	25.3	32.7	1018.9	934.6
Female	22	36.4	52.7	29.9	37.3	800.0	658.1
Total	59	30.8	42.6	27.0	34.2	1818.9	1592.6

3.4 Discussion and Conclusions

This chapter demonstrated the capabilities of *in vivo* XRF bone Pb measurement on children. The average uncertainty for the KXRF bone Pb measurement for this population is 2.66 ± 1.05, which is slightly higher than that for an adult population. This is expected because there is on average more fatty tissue in a child's bone and the bone density is lower for a child's bone. The portable XRF has a higher detection limit than the KXRF device used in this study. The detection limit for the portable XRF heavily depends on the soft tissue of the subject and thus varies more throughout the study [38]. An issue associated with the anatomical structure of the bone in children, which is illustrated below, further deteriorated the detection limit for portable XRF.

Correlations between bone and blood Pb and age could have a number of implications. One possible reason for this observation would arise because the patients were exposed populations and the short half-life of Pb in blood. The blood half-life is relatively short compared to bone and thus will have a better reflection of recent exposures from behavioral differences in ages, such as foot and hand to mouth behaviors. This can influence the blood Pb values to be higher in the lower age group.

The correlation between KXRF bone Pb and blood Pb shows a higher slope and stronger r-squared than similar studies with adults [63-66]. One of the reasons for both these differences could be that children have a higher bone resorption rate, which indicates a more frequent transition of Pb between bone and blood, and hence their bone Pb is more significantly correlated with their blood Pb. The more significant correlation also indicates that for this population the majority of Pb in blood comes from bone. This

is expected since there is a significant store of Pb in these children's bones, children's bones are well known to have turnover rates higher than that of adults, and the exposure source has been removed from most cases viewed in this study.

The portable XRF in comparison to the KXRF results gave a correlation less than what we would expect based on previous observations in adults and lab samples, as well as what we would have expected given the high Pb concentrations in this study. Since KXRF is a gold standard for *in vivo* bone Pb measurement, the correlation between KXRF and portable XRF demonstrates the limited ability of the portable XRF with current calibration methods to quantify bone Pb in children. In a previous paper, we detailed calibration methods and found the best calibration method as determined by in-lab samples [35]. In that study we found that the best calibration utilized the Compton scattering peak in relation to the soft tissue thickness over bone. This technique, although valid for adults, has complications with children. The Compton scattering peak is much larger than anticipated with children and thus overestimates soft tissue thickness and background from our spectrum. We attribute this to differences in composition and structure of the bone in children. Children are known to have changing bone composition and density as their bones are developing. Although our phantoms are designed to give accurate calibration for bone in adults, the differences in children's may affect our XRF spectra than we attempted to correct for with calibration [62]. Given this issue, we applied an alternative calibration for the results shown here, which used traditional peak fitting of the beta Pb peak, which is also detailed in the previous study of the device [35]. We chose to do this because when looking at the individual spectrum there was a visible Pb peak in this region with no surrounding elemental peaks for distortion of the signal.

Calibration could be improved with proper calibration phantoms to reflect the appropriate anatomy of children's bone. It is relevant to point out that a similar situation arose with one particular bone pointed out in Chapter 2. Bone 6918 had been found to have a significantly different density and gave values for the portable XRF that differed greatly from the superior KXRF measurement results. Given that the calibration of the portable XRF used for adults is not suitable for a pediatric population, future measurements of children using this technology may be feasible, but further investigation on the effect of bone composition and an improved calibration method would be necessary to obtain more accurate results.

The effect of bone density on the portable XRF is reflected in two spectral features, the Compton scattering of the Ag target peaks and the degradation of signal from characteristic x-rays from bone. The main issue would be the degradation of signal from characteristic x-rays. We had accounted for a partial degradation from the overlying soft tissue thickness, but this would be in addition to that by changing the cross section of interaction in bone directly from the lower density values. One possible solution to this would be to find some element in bone that produces a characteristic x-ray and has levels known to be consistent among individuals. We could use that peak then to normalize the Pb peaks and determine the interactions that actually occurred in the bone. There is no obvious element for this process, and thus we have used our conventional calibration for this part of the study, which did prove to show some significance in comparison between portable XRF and KXRF data. Another possible solution to our calibration problem with children could be identifying spectral differences in the coherent and Compton scattering peaks relating to density and composition. This method would rely upon using the known

cross-section of phantom data for the two interactions based on effective Z and density to determine a ratio for correction. This would require precise calculation of this ratio and could possibly utilize simulation to be more effective; however, this has the difficulty of needing to have known compositional and density differences that one could simulate in the first place, and unfortunately the exact bone changes that cause the issues are unknown.

The relationships between KXRF bone Pb and blood Pb and KXRF bone Pb and portable XRF bone Pb measurements became slightly more positive when isolating based with only the exposed group. This is because the controls in the study all had values of nearly zero for both blood and bone Pb. The same relationships with only controls show no correlation, which can again be caused by the values being close to zero with uncertainties higher than measured bone Pb values.

The Pb body burden of the children assessed in our study is much higher than that suggested in other studies, which is expected because these children were Pb poisoned [53]. Our proportion of grams bone Pb to grams bone and blood Pb results are in agreement with previous studies of Pb body burden [19], and demonstrates the value of bone Pb measurements even with children to better reflect body Pb burden.

Only few studies in literature investigated half-life of Pb in blood in children [67, 68]. The half-life of Pb in blood calculated in our study lies in between results from these previous studies. Manton et al. reported a half-life of Pb in blood ranging from 8-11 months to 2-3 years [67]. This study did not isolate bone Pb from blood Pb and thus may reflect the long half-life of Pb in bone, since Pb stored in bone would gradually be

released to blood endogenously. In addition, because the blood Pb levels in those children were relatively low, a continuous external exposure, even at low level, could contribute to a prolonged half-life. Duggan's study reported a much shorter half-life of Pb in blood of 3.35±1.34 days using blood and urine Pb data [68]. However, the data are based on only two subjects. The half-life of blood Pb in our study is calculated from bone Pb and blood Pb data using the best bone and blood parameters we could find from the literature. The data used are the ones taken as far from chelation as possible (41.5±30.0 days after chelation) to reduce the effect of chelation. However, chelation may still affect the equilibrium of Pb in bone and blood at that point of time and hence affect half-life of blood Pb calculated. Also, for our study we were able to isolate the exposure source for most children, but it is possible some continued to be exposed during this period. A potential source of error in our study was the bone resorption rate we estimated from previous studies. Changes in this rate could impact our results by almost a factor of 2 in extreme cases for the youngest subjects. Even considering this, the value we calculate would still be much lower than the adult blood Pb half-life published in literature.

The trend of decrease in bone Pb before and after treatment demonstrates the need for bone Pb assessment for these types of patients. This also has implications on whether chelation will be able to remove Pb from bone as well as from blood. Monitoring bone Pb in patients is vital to identifying whether body burden levels will decrease. This is important as bone Pb could serve as a source of continuing exposure for years to come for long-term exposed individuals.

In conclusion, bone is a major storage site for Pb in children, and serves as an indicator of total body Pb burden. KXRF is a viable measure of bone Pb in children with

detection limits capable of measuring even environmental exposures. Portable XRF has limitations for bone Pb measurements in children based on calibration, which need to be addressed before being used further in pediatric populations. Bone Pb contributes significantly to blood Pb levels in Pb poisoned children and the blood Pb half-life in children is calculated to be 10.45±11.71 days. The results from the study indicate that bone Pb may be a better marker for determination of chelation efficacy.

CHAPTER 4. IN VIVO QUANTIFICATION OF SR IN BONE AMONG A PB POINSONED PEDIATRIC POPULATION

4.1 Introduction

Strontium (Sr) is a metal that is closely related to calcium (Ca) in the body, which may have beneficial or toxic effects on bone formation. 99% of strontium is stored in the teeth and bones after uptake in the body [12, 13]. Low doses of Sr have been reported as being beneficial to bone and Sr supplementation has been used to treat osteoporosis and osteopenia [69]. Women have higher probability of developing bone diseases, and treatment with Sr ranelate had led to a reduced risk of fractures in postmenopausal women affected by osteoporosis [15, 16]. High levels of Sr have been correlated to skeletal abnormalities in animals and children, and associated with osteomalacia [11, 70]. Sr exposure is generally limited to oral exposures with Sr chromate being more dangerous for inhalation because of chromium. The skeletal abnormalities would occur in malnourished children lacking in sufficient protein and calcium in their diets with the exposure coming from food grown in soil with >350 ppm Sr [11]. Bone should be a long-term storage site for Sr, and bone is the superior marker for treatment efficacy in Sr treated patients [15]. Measuring bone Sr is traditionally done using a bone biopsy, which is a painful procedure unlikely to be completed multiple times [14]. Blood Sr can be used to measure exposure levels, but it is unlikely to correlate with long-term exposures [71].

X-ray flourescence (XRF) has been used to measure bone Sr, but this device uses a radiosotope source, has bulky equipment requiring liquid nitrogen cooling, and a 30-minute measurement time [10]. Another technique utilizing the differences in absorption of photon energies called dual photon absorptiometry (DPA) was able to non-invasively measure bone Sr, but this device was also fairly large, required 10-minute measurement times, immersion in water, and produced results in percentage Sr [22]. These systems both use radioisotope sources, bulky equipment, and require longer acquisition times. The portable XRF used to measure bone Pb can be similarly applied for measurement of bone Sr. This chapter demonstrates a calibration of Sr for the portable XRF and uses the data collected in chapter 3 to verify bone Sr in vivo measurements using a group of children in Shanghai, China.

4.2 Materials and Methods

4.2.1 Strontium Phantoms

Sr phantoms were made using Mowial-88 and bone meal. This is a similar approach to that used previously for hand bone phantoms and has been proven to be effective for calibration phantoms [72]. Mowial-88 acts as a binding agent for the bone meal and is Sr free. Bone meal easily replicates the bone matrix, since it is ground cow bone. The bone meal was determined to have a Sr contamination level of around 74 ppm. Sr contamination in traditional methods using plaster-of-paris lead to Sr levels of greater than 1000 ppm. A method for producing chemically pure phantoms was found, but

requires weeks to complete, and requires advanced chemical manipulations [73]. Our Mowial-88 phantoms had added concentrations of Sr of 0, 5, 10, 15, 20, 30, 50, 75, 100, and 200 ppm in order to get a calibration line and accurately determine the detection limit of Sr. Lucite slabs were then used as a soft-tissue equivalent phantom and measurement of the Sr phantoms at different Lucite thickness was used in the calibration and detection limit calculations. Measurements were made by using the flat bottom portion of the Sr phantom with lucite slabs placed between the phantom and the portable XRF.

4.2.2 Portable XRF Bone Sr Measurement System

The system used here was the same as used in chapter 3. We used the same optimized settings for Pb for our Sr measurements, and this should be appropriate for two reasons: 1) the Sr binding energy is higher than Pb and we already have the maximum energy output and filter combination to maximize the high energy x-ray spectrum, and minimize the low energy part of the spectrum to the best of the current devices capabilities; and 2) we wanted to validate the study using in vivo data already produced from the Pb poisoned pediatric population assessed for Pb in chapter 3, which requires a calibration using the same device settings used for the Pb measurements. Sr typically has a higher average concentration in bone, which should make measurement easier.

4.2.3 Spectrum Analysis

The spectra were analyzed using traditional peak fitting as for Pb measurements for this population in chapter 3. The traditional peak fittings method is described in detail in chapter 2. The analysis used a Gaussian with an exponential background to estimate net counts. Then we used the Compton scattering peak to estimate soft-tissue thickness, which was found from a calibration line based on soft tissue thickness. The soft tissue thickness could then be used to identify the relationship between soft tissue corrected net counts and concentration. With this process we used the peak energy of Sr at 14.2 keV instead of Pb peak energies. The other Sr peak at 15.8 keV has a significant amount of background from the characteristic x-rays produced by the Ag target in the x-ray tube that underwent Compton scattering in the sample. The 15.8 keV peak also only represent 14% of the total characteristic production with the majority being from the 14.2 keV peak. Thus 14.2 keV was the only peak we used in our analysis procedures. Negative values for bone Sr are left as such because they represent the point estimate of bone Sr with uncertainty in the measurement. If an individual measurement is close to zero then the point estimate from that individual can be negative with the associated uncertainty.

Linear regressions were used to determine correlation values and levels of significance of relationships between age, sex, and portable XRF bone Sr. The portable XRF data was excluded if the measurement time was <2 minutes.

4.3 Results

4.3.1 Bone Sr Calibration Curve

The portable XRF was calibrated for in vivo bone Sr measurement by measuring Sr phantoms of varying concentration at different Lucite thicknesses. Figure 4.1 shows the results of the calibration curve obtained at 0 mm Lucite thickness. Figure 4.2 shows the calibration line for 0, 1, 3, 5, 7.5, and 9 mm of Lucite thickness. This demonstrates the degradation of signal to background ratio with increasing Lucite or soft tissue thickness.

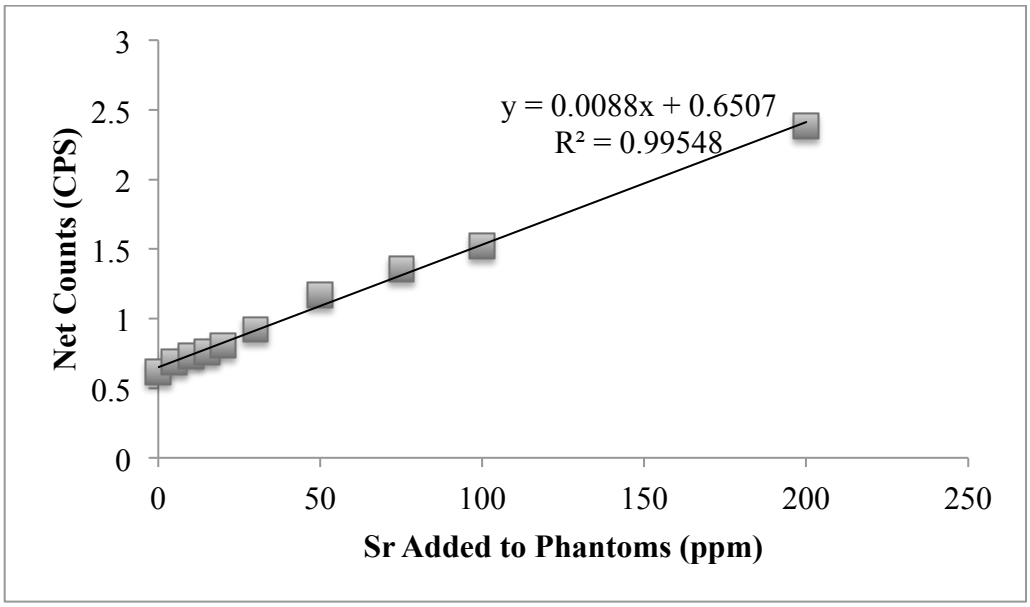

Figure 4.1 Calibration Curve for Sr at 0 mm Lucite thickness.

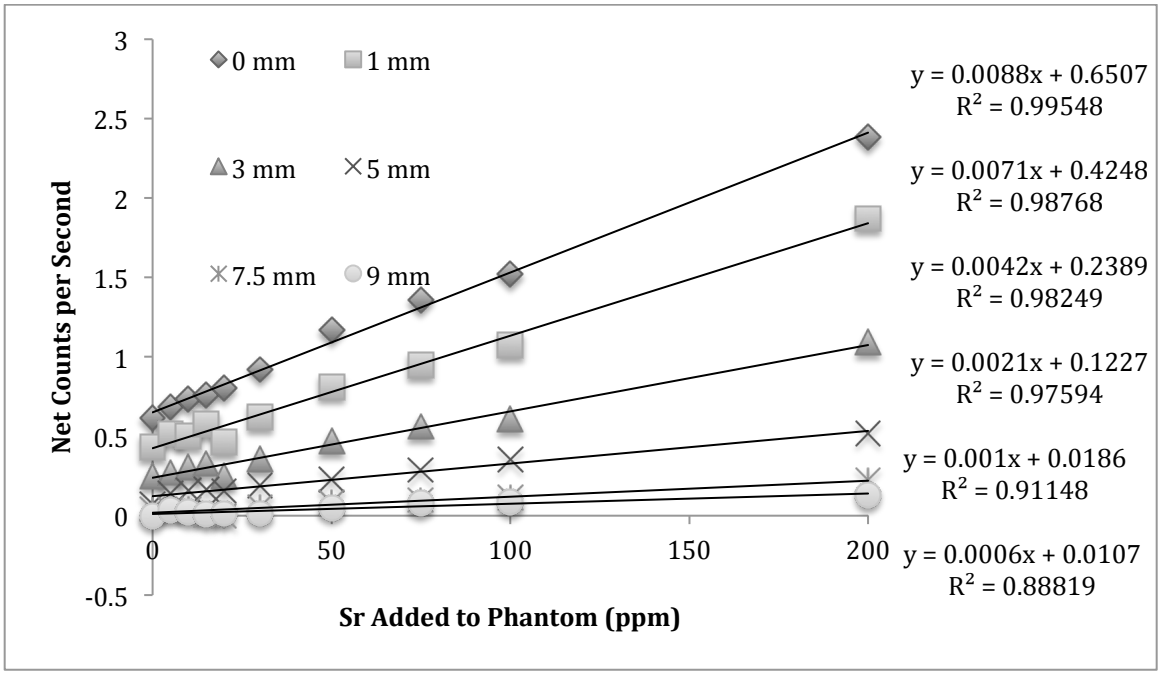

Figure 4.2 Calibration lines for Sr phantom measurements from 0 mm to 9 mm of Lucite thickness.

4.3.2 Calibration Function for Measurement of Bone Sr at Different Soft Tissue Thicknesses

The function in Figure 4.3 below shows the calibration of the net Sr counts change with increasing Lucite or soft tissue thickness for our 274 ppm phantom. This relation takes into account the attenuation of soft tissue and inverse square degradation of the signal as shown from our previous work in chapter 2.

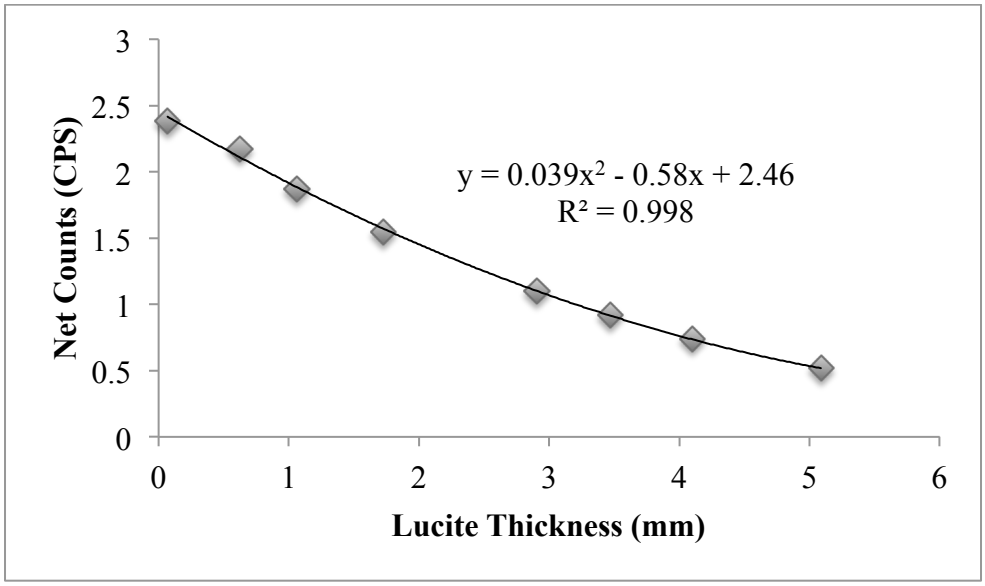

Figure 4.3 Calibration function for Sr counts at different Lucite/soft tissue thicknesses with 274 ppm phantom

4.3.3 Minimum Detection Limit for Portable XRF Bone Sr Measurements

The MDL was calculated by measuring our standard phantoms of varying concentrations of Sr with different Lucite thicknesses and using the following equation:

$$MDL = \frac{2 \times \sqrt{BKG}}{Slope}$$

, where BKG is the background under the 14.2 keV Sr peak estimated from our fitting program and the slope is taken from the calibration curve of all 10 phantoms at a particular Lucite thickness. The resultant MDL is displayed in Figure 4.4.

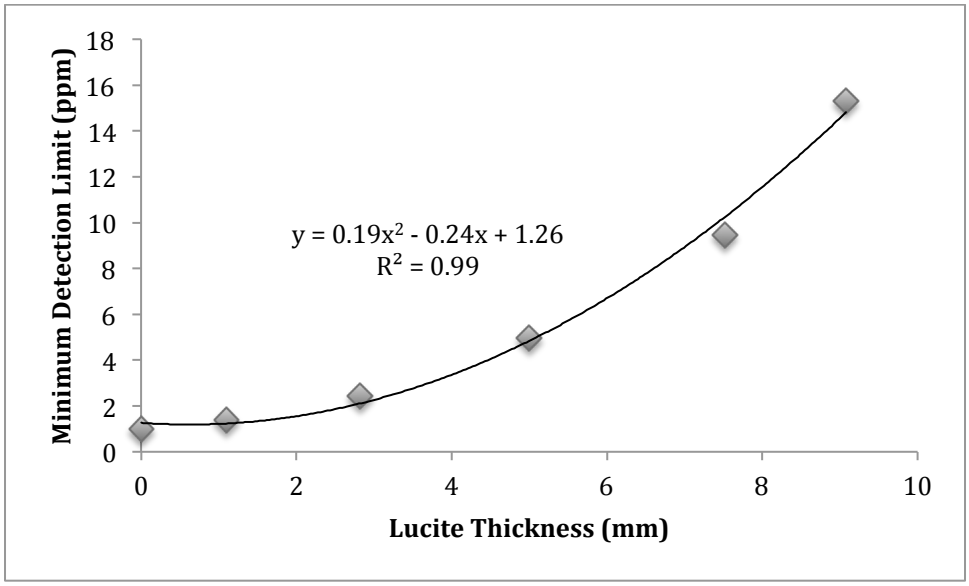

Figure 4.4 Minimum detection limit change over increasing Lucite thickness.

4.3.4 Portable XRF In Vivo Bone Sr Measurements

Table 4.1 shows summary statistics for the population measured for in vivo bone Sr. The average age of the children measured was 5.7 ± 3.1 years. The difference between male and female subjects for average bone Sr level was found to be non-significant with a p-value of 0.25.

Table 4.1 Statistics of Bone Strontium and Age for the Population

	Bone Strontium (ppm)				
	N	Average	Minimum	Maximum	Standard Deviation
Male	165	45.9	-30.4	347.6	56.9
Female	72	36.6	-32.3	248.6	59.3
Total	237	43.2	-32.3	347.6	57.6
Age (yrs)	237	5.7	1.0	15.0	3.1
Age (M)	165	5.6	1.0	15.0	2.8
Age (F)	72	6.0	1.0	14.2	3.7

4.3.5 Correlations Between Bone Sr and Age

Figures 4.5, 4.6, and 4.7 show correlations of bone Sr concentrations with ages. Figures 4.5 and 4.6 show significant correlations between age and bone Sr for a combined group and then just females respectively with p-value<0.05. Figure 4.7 shows a non-significant correlation between age and bone Sr for males. The slope of the correlations demonstrates the estimated accumulation of Sr in bone per year in ppm.

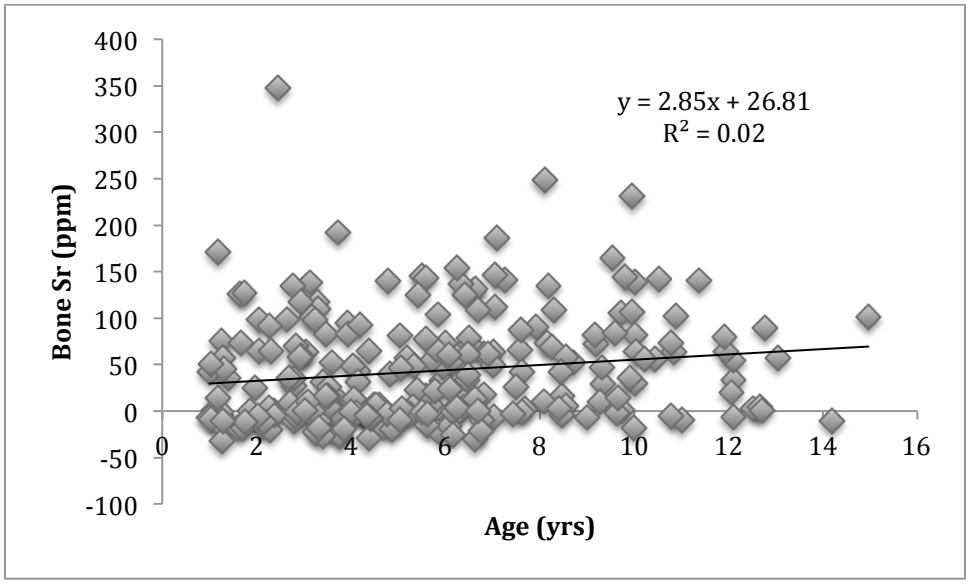

Figure 4.5 Significant correlation between bone Sr and age with combined male and female subjects.

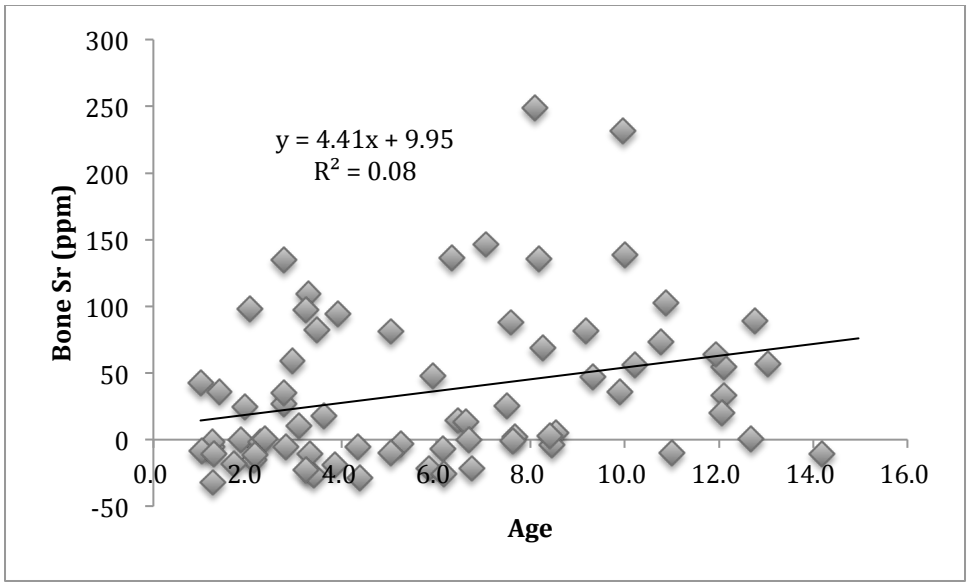

Figure 4.6 Significant correlation between bone Sr and age for female subjects only.

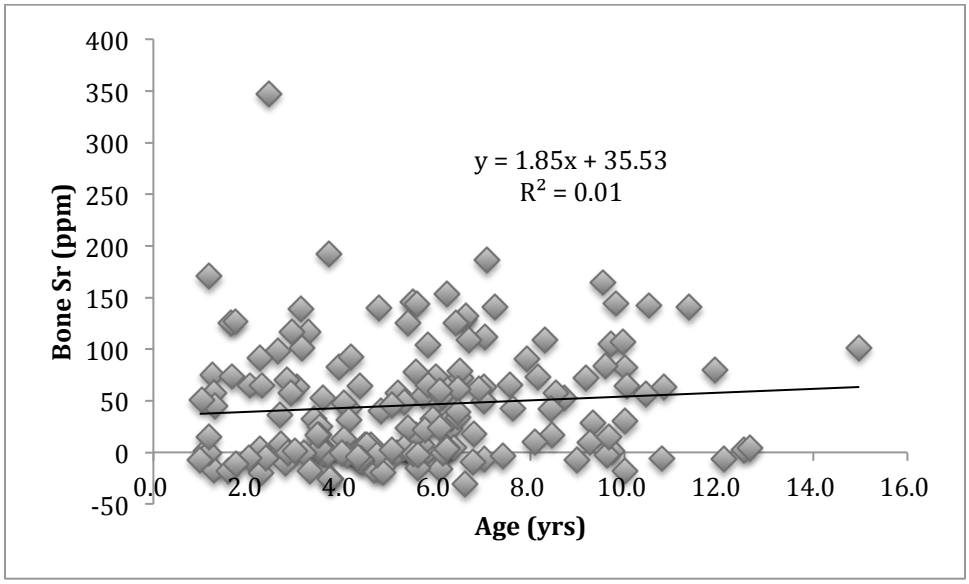

Figure 4.7 Non-significant correlation between bone Sr and age for male subjects only.

4.3.6 Age and Sex Differences in Accumulation of Bone Sr

We then investigated differences when splitting age groups depending on an estimation of puberty status. A previous study estimated the ages in which puberty began in males and females as 8-14.9 and 9.7-14.1 respectively [74]. We separated our results into these age groups and determined if there were further significant differences between these groups. Table 4.2 summarized statistics for the separated groups. The female groups had significant differences of average bone Sr between the age groups with p-value<0.01. The male groups had a non-significant difference of average bone Sr level for the age groups, but showed an increasing trend with p-value of 0.165.

Table 4.2 Bone Sr differences with puberty age and sex.

		Bone Sr (ppm)			
	N	Average	Min	Max	Standard Deviation
Female >8yrs	23	66.2	-10.3	248.6	69.4
Female <8yrs	49	22.6	-32.3	146.7	48.6
Male >9.7yrs	18	60.8	-17.7	144.0	55.6
Male <9.7yrs	147	44.1	-30.4	347.6	57.0

4.4 Discussion and Conclusions

This chapter demonstrated the ability of a portable XRF for measurement of in vivo bone Sr levels within a 2-minute measurement. The device was calibrated using standard Sr phantoms and Lucite and used to measure bone Sr in a group of Pb poisoned children. We found that Sr does accumulate in bone and bone Sr has a significant relation with age, which indicates that bone may be a long-term storage site for Sr. Accumulation of bone Sr can be accurately monitored with the portable XRF. This technique can then be used to monitor health effects associated with Sr exposure as well as monitoring patients using Sr supplementation to treat osteoporosis.

Our calibration line demonstrated the linearity of the device with respect to Sr levels. The contamination of the phantoms was evenly distributed throughout the bone matrix, and with this level of contamination our calibration line was accurate to the amount of Sr added to our phantoms. The contamination did increase the uncertainty of the bone Sr concentrations which results from the increased uncertainties of the parameters for the calibration line we obtained using our phantoms. In the future, we can improve upon this calibration by using standards with less contamination from Sr.

The calibration lines at different Lucite thicknesses are useful to visually assess the detection limit of the device. Our MDL was calculated using slope to demonstrate the change in signal from one concentration to another. The slope in Figure 4.2 clearly decreases as the Lucite thickness increases, and at a certain point will have a very limited difference between each concentration. This helps to demonstrate the limitations of the portable XRF.

We determined the background estimation from the peak fitting was the most acceptable means to estimate the MDL in our case without the ability to produce a 0 ppm phantom. This was done using the background estimation from the fitting procedure, which produced an exponential function. We used the area under the exponential corresponding to two sigma of the Sr peak to estimate the background level for a particular measurement. The calculated MDL was at a level low enough to detect Sr in most subjects with less than 5mm skin thickness, as the average bone Sr level was found to be 43.2 ± 57.6 ppm. Soft tissue thickness does have a significant effect on the detection limit as seen in Figure 4.4. The soft tissue thickness increases uncertainty in the measurement by decreasing our signal to background ratio as shown in our calculation of detection limit. This is where the negative values in our study arise, because bone Sr levels close to zero with high uncertainty from soft tissue thickness have a greater possibility to be negative. Children in general will have thicker overlying soft tissue than adults, and will have higher uncertainty in their measurements.

The correlations with age likely reflect the natural development of the children's bones. There are several factors here that could affect the correlation. We did not have any information on the Sr exposure for each subject, so the possibility of someone being

more or less exposed could be involved. Since diet plays a role in Sr metabolism, it is also probable that some of the children had a higher metabolism of Sr due to less vitamin D and protein in their diets.

Studies from Popovic et al 2005 and Mostafaei et al 2015, on Pb and fluorine, demonstrated that differences in bone metabolism between sexes could influence bone metal concentrations [75, 76]. Our study demonstrates similar sex differences in accumulation of bone Sr. The female subjects were more likely to accumulate Sr with age than the male subjects. Both male and female subjects showed an increase in Sr after puberty age; however, the male data showed a non-significant difference. We attribute the non-significance seen in our male subjects to the fact that there were only 18 subjects older than 9.7 years, and we think a noticeable difference would be identifiable in studies with more subjects. Since this was an estimation of puberty status based on age, there could be further limitations. A better group distinction could be made using a questionnaire for puberty status. The female results, which were much more noticeable in our subjects, could be an indication of the influence of estrogen versus testosterone on bone metabolism. Steroids are responsible for the maintenance of bone growth and density until menopause in women [77]. A better test for these differences would be to compare the bone Sr accumulation with age before and after puberty age, but due to the small sample size of older subjects, we were unable to do this type of analysis. A pilot study in adults with wider age ranges would help to further illuminate the differences seen in this study.

In conclusion, Sr in bone is a valid biomarker for Sr accumulation and can be used to assess the effectiveness of treatments or health effects associated with Sr intake or

exposure. Our data shows that the portable XRF can be used to measure Sr in bone and accurately determine bone Sr concentration for most subjects with a 2-minute measurement time. The results also suggest possible sex differences in accumulation and metabolism of Sr in bone.

CHAPTER 5. HIGH ENERGY X-RAY TUBE BASED XRF MEASUREMENT SYSTEM FOR IN VIVO QUANTIFICATION OF PB AND OTHER METALS

5.1 Introduction

K-shell x-ray fluorescence (KXRF) bone Pb measurement systems have widely expanded our knowledge of Pb and its health effects over the past few decades. The most advanced system using Cd-109 and a cloverleaf detector geometry has a detection limit of 2-3 μg/g bone mineral. The KXRF measurement system has had many upgrades over the years, but overall remains the same with the same limitations in portability, lengthy measurement times, and a radioisotope source. The KXRF measurement system uses liquid nitrogen cooled high-purity germanium detectors, which make the system itself very large, especially when including the amplifiers and computer system to take the measurement. This presents a problem for populations without the ability to go to a location for a measurement. A portable XRF system using an x-ray tube and Si drift detector has overcome these disadvantages, but introduced problems for other potential populations. The portable XRF has limitations with the detection limit increasing dramatically with thicker soft tissue thicknesses. Advances in detector and x-ray tube technology would allow for the combination of the advantages for both the KXRF and portable XRF bone Pb measurement systems to be transferred to a device that excluded the main disadvantages of both. Using an x-ray tube source and different detector

material would allow a system to be on the portable scale, which opens the possibility of measurement of at risk populations such as the elderly who are not easily accessible to a stationary device. Then, using the high-energy x-rays for KXRF measurements eliminates any issues with soft tissue thickness. X-ray tubes have the capabilities of producing high-energy spectra through the use of high Z materials, such as Uranium, as targets. Alternative detector materials, such as Cadmium Zinc Telluride (CdZnTe) or Silicon (Si), offer advantages of operation at room temperature with trade-offs in detector resolution and efficiency. This chapter demonstrates how we used Monte Carlo simulations to determine the feasibility of an in vivo portable x-ray tube based KXRF bone Pb measurement system and find its estimated sensitivity in comparison to the current Cd-109 based KXRF and portable XRF measurement systems.

5.2 Materials and Methods

5.2.1 Monte Carlo Simulations

The Monte Carlo simulation program, Monte Carlo N-Particle transport code (MCNP), used in our study was developed by Los Alamos National Lab and distributed by the Radiation Safety Information Computational Center. This software has recently been updated to more accurately depict interactions at lower energies, using its default database for interaction cross-sections. This includes Doppler interactions and all the main interactions observed in XRF previously discussed in this dissertation. This gives us the ability to simulate an x-ray tube source with electron to photon conversions in the

target. MCNP has the ability to set unique materials, densities, geometries, and sources in order to reproduce an experimental setup.

We first wanted to verify the ability to replicate experimental setups using MCNP, and then we could use it to optimize system parameters in this study of a high-energy x-ray tube for XRF applications.

5.2.2 Validation of MCNP Using a Portable XRF Experimental Comparison

We first tested the abilities of MCNP to accurately reproduce an x-ray tube spectrum by simulating the portable XRF device. This device should be a good validation for MCNP's ability to depict the electron photon conversions in an x-ray tube. We measured the x-ray tube output using a high-purity germanium (HPGe) detector. To reduce dead time of the detector, we placed the x-ray tube 10 cm away. We recreated this setup in MCNP. We started with electrons hitting the x-ray Ag target and proceeding through the filters and collimators inherent in the device. We also needed to take into account the attenuation of the x-rays through air and the aluminum window of the HPGe detector before being detected. By taking the experimental measurement and comparing it to our simulation result by looking at spectral features we can validate the ability of MCNP to reproduce an x-ray tube source. Successful validation of this comparison allows us to use MCNP in other applications of x-ray tube simulations and reproduce potential experimental results for x-ray tube systems.

5.2.3 High-Energy X-ray Tube Based KXRF Measurement System

The x-ray tube based KXRF system we modeled had specifications chosen based on simulation and calculations shown in the results section, and has geometry shown in Figure 5.1 below. The system utilized a 90-degree geometry between the x-ray source and detector. The x-ray tube had an accelerating voltage of 220 kV, a 0.56 mm transmission Uranium target, and a 1 cm tungsten collimator. The target thickness was modeled and found to maximize K-shell fluorescence from the Uranium target, while minimizing the low energy bremsstrahlung interactions creating excess background in the Pb peak areas and radiation dose. The detector was modeled as silicon, cadmium zinc telluride (CdZnTe), and HPGe with 1 cm thickness and a 3.2 cm diameter. The leg was modeled with tibia bone of diameter 1.3 cm based on data in ICRP 70, with soft tissue with a radius of 50 mm and thickness of 4.8 mm at the thinnest point surrounding the bone [49].

The leg was simulated with an approximate distribution where the thickness increased around the leg with the thinnest portion at the shin as shown in Figure 5.1. The geometry of the leg was optimized using a comparison of changing the thinnest soft tissue from pointing towards the source to pointing towards the detector. Figure 5.1 shows the thinnest section of soft tissue being about halfway between source and detector. This geometry is used as a conservative estimate of the tibia bone and soft tissue, as the thinnest portion of soft tissue would be longer than we have shown in this simulation. The tibia bone close to the surface of the leg is flatter with respect to the surface and has a triangular prism shape, shown in Figure 5.2, rather than the cylinder depicted in our

simulation shown in Figure 5.1. The tibia bone we simulated had a Pb concentration of 100 ppm, which would be used to compare signal between different materials and experimental devices using standards of the same concentration.

Two separate simulations were performed: 1) to get the initial spectra of x-rays from the x-ray tube source and 2) to simulate the XRF interaction in leg and collect signal in the detectors. The results from the first simulation were used to create the x-ray source in the second. This allowed us to get much better statistics on the final spectra collected in the detectors. The final simulation used Si, Ge, and CdZnTe detectors separately to demonstrate differences between them. The detectors were all modeled with the same standard size of 3.2 cm diameter and 1 cm thickness to match the standard KXRF detector [9].

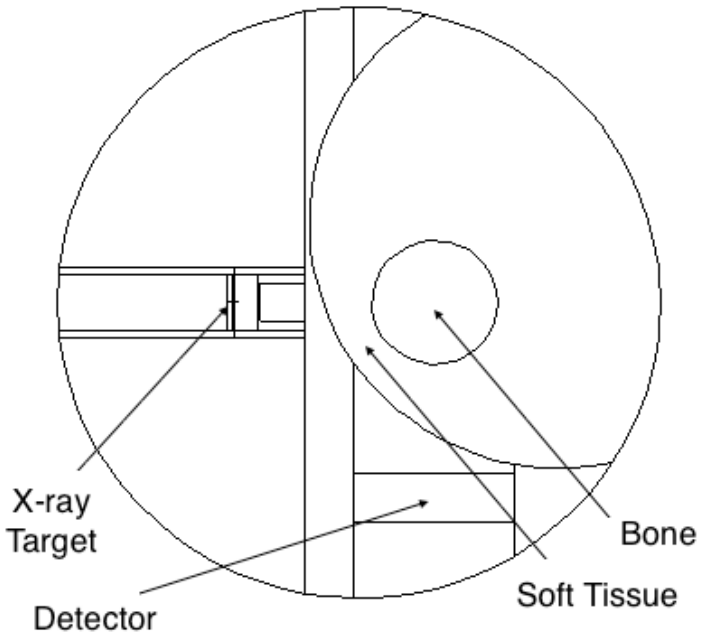

Figure 5.1 Simulated KXRF setup with x-ray tube source and detector in 90 degree geometry and bone shown in the ‘halfway’ geometry.

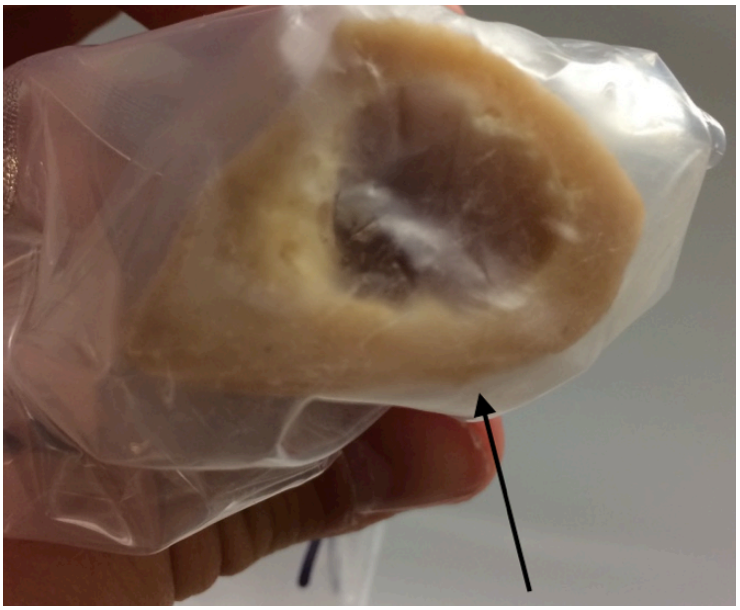

Figure 5.2 Human cadaver tibia bone cross-section to demonstrate the actual shape of the tibia bone with the arrow depicting the portion towards the surface of the shin.

5.2.4 Normalization of Simulation Data to Experimental Results

The normalization of the simulation data is critical to getting accurate results when comparing with experimental data. For the validation section of this study, ideally one would do an assessment of dose starting from a given number of electrons or amperes in the x-ray tube, but given the amount of geometry variables and unknown area of beam from the portable XRF x-ray tube, this was too difficult. Thus for this simulation we used a ratio of low energy and high-energy spectral features to find a normalization factor. A similar method is used in other studies using MCNP [78]. The main interest for our simulation would be the shape of the spectral features, which would confirm the x-ray production, filtration, and attenuation of the beam. These would be the key features

needed to identify a good comparison between simulation and experiment for our further tests.

In our simulation for the high-energy x-ray tube based KXRF system, the normalization is easier. For this simulation, we can instead do a normalization to dose of the Cd-109. We used dose normalization to compare our x-ray tube based XRF to Cd-109 based systems using a skin dose of 40mSv to a $1cm^2$ area as our limiting factor and target for normalization since this is the dose associated with the peak activity source of a Cd-109 based KXRF system. Normalizing our simulation to the same dose as with a Cd-109 KXRF measurement would then give an accurate comparison of the signal from Pb collected by either system without accounting for detector resolution, resolving time, and background. We did a dose simulation for our x-ray tube and found a skin dose of 9.8e-13 Sv per particle. We then normalized our dose based on the number of particles it would take in the x-ray tube to reach a skin dose of 40 mSv, and found we needed to use 4.1e10 particle in our simulation to reach this dose. The simulation gave us values for the probability of any starting particle actually being absorbed in the detector, which varied for each detector material around ~13%. We then had to correct for the 230 energy bins we had been using. Finally we could multiply this number, which varied based on the detector material around ~3e6, by the known probability distribution from the simulation to get a final normalized spectrum.

5.3 Results

5.3.1 Validation of MCNP Using Experimental and Simulation Comparison of the Portable XRF

The Monte Carlo simulations gave us comparisons between simulated spectra and experimental spectra, which can be seen normalized to the experimental spectrum in the 30 keV to 50 keV energy range in Figure 5.3 below. The agreement for the overall spectrum comparison of the x-ray tube output was about what was expected. The normalization shown in this has no relation to dose matching, but is solely based on area to demonstrate the correct shape acquired by the simulation in this case. Figure 5.3 demonstrates some limitations in the simulation in reproducing the background at lower energies. The mismatch in the Compton scattering peak from the Ag target comes from the detector resolution, and other effects discussed later in this chapter.

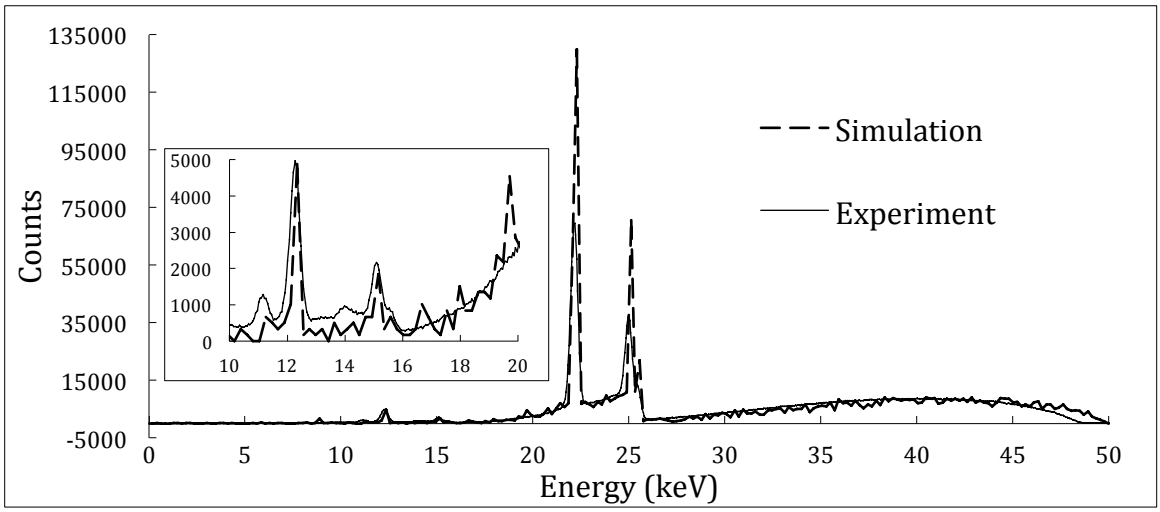

Figure 5.3 Experimental versus simulation spectrum comparison for x-ray tube output from portable XRF.

5.3.2 High-Energy X-ray Tube Target Optimization

Uranium and thorium were chosen as possible targets because of the energies of characteristic x-ray production as well as being explicitly cited as target materials in patents for high z target x-ray tubes [79]. A comparison of the energy of the characteristic x-rays from these targets after undergoing Compton scattering at various angles is seen in Tables 5.1 and 5.2 below. Table 5.3 shows the Pb characteristic x-ray energies.

Table 5.1 Thorium target characteristic x-ray energies after undergoing Compton scattering at various angles.

Thorium	Scattered Energy (keV)		
Angle	K-alpha1	K-alpha2	K-beta
75	83.9	79.6	91.3
90	80.5	76.5	87.3
105	77.3	73.7	83.6
120	74.6	71.2	80.4
135	72.4	69.2	77.9
150	70.8	67.7	76.0
165	69.9	66.9	74.9
180	69.6	66.6	74.6
Relative Intensities	100	62	36

Table 5.2 Uranium target characteristic x-ray energies after undergoing Compton scattering at various angles.

Uranium	Scattered Energy (keV)		
Angle	K-alpha1	K-alpha2	K-beta
75	86.2	83.4	94.0
90	**82.6**	**80.0**	**89.8**
105	79.3	76.9	85.9
120	76.5	74.2	82.6
135	74.2	72.1	79.9
150	72.5	70.5	78.0
165	71.5	69.5	76.8
180	71.1	69.2	76.4
Relative Intensities	100	62	37

Table 5.3 Pb characteristic x-ray emission energies.

Pb	K-alpha1	K-alpha2	K-beta
Energy (keV)	75.0	72.8	84.9
Relative Intensities	100	62	35

From the comparison of this data, the target and detector source angle was chosen to not conflict with characteristic Pb x-rays. Thus, a 90-degree geometry using a Uranium target was chosen as the optimal setup for our simulation.

The next step was to optimize the target thickness. The optimization was done by maximizing the x-rays with energy greater than the binding energy of Pb and minimizing the radiation dose. This method incorporated a way to identify which x-rays created in the tube would ultimately be useful versus the x-rays just increasing our dose without further use. Since we are also using dose as a normalization factor, it is of the utmost importance that we minimize it in the optimization process.

In doing this optimization, it was most useful to create functions to define the results to get a more precise calculation for the optimized target thickness. Using a simulation for about 5 varying target thicknesses we could actually form a function that would define the relationship over target thicknesses about equal to those already simulated. The functions found for this optimization are presented below in Figures 5.4 and 5.5.

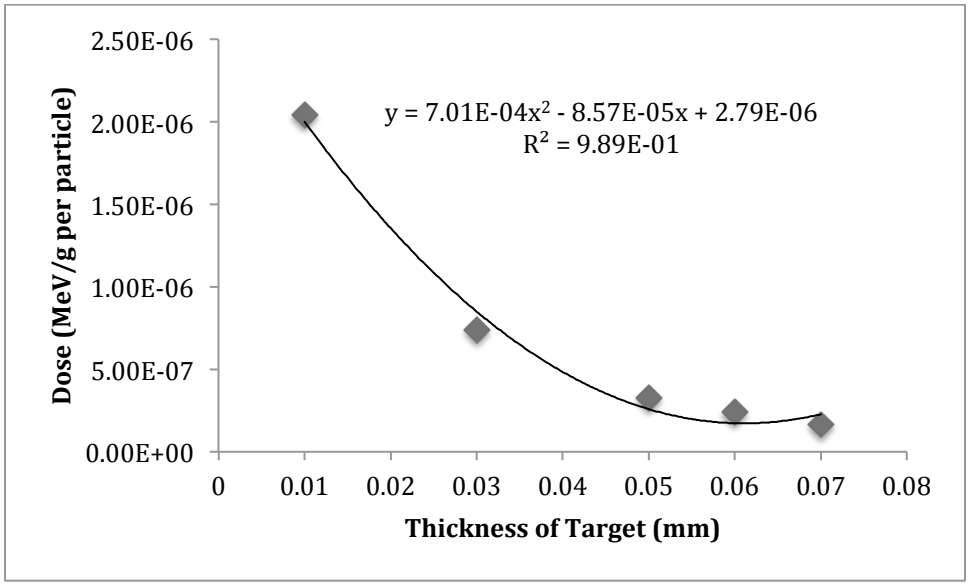

Figure 5.4 Radiation dose for an XRF measurement versus the thickness of the Uranium target in centimeters.

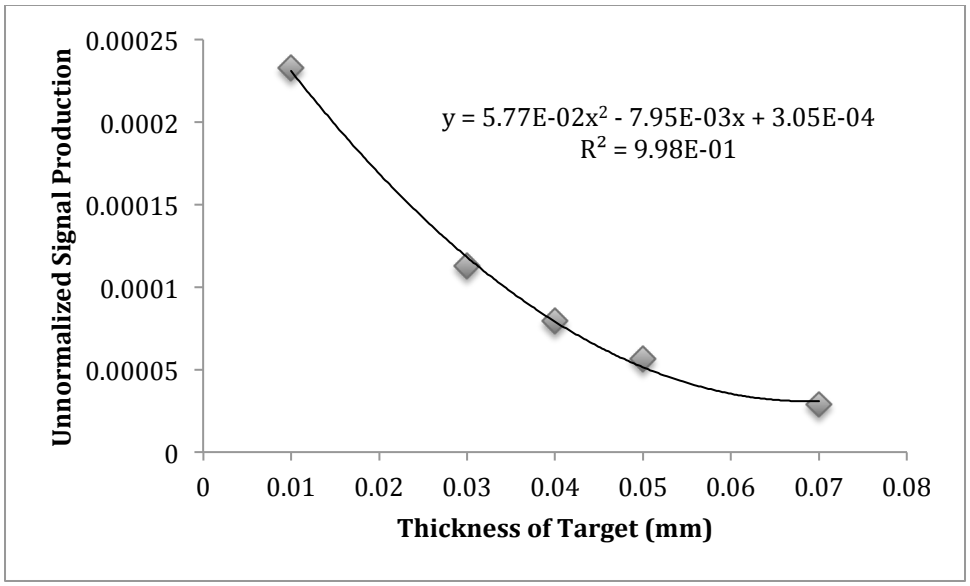

Figure 5.5 X-ray production with energy greater than 88 keV versus Uranium target thickness in centimeters.

Finally, these functions were compared as a ratio. We used a ratio since both dose and potential signal should linearly affect our final characteristic yield in our simulation. This

ratio was then maximized to find the most potential signal versus the least radiation dose, and the optimal target thickness was found to be 0.56 mm. A visual representation of this is seen in Figure 5.6 below. The final optimized spectrum with 0.56 mm target thickness is shown in Figure 5.7.

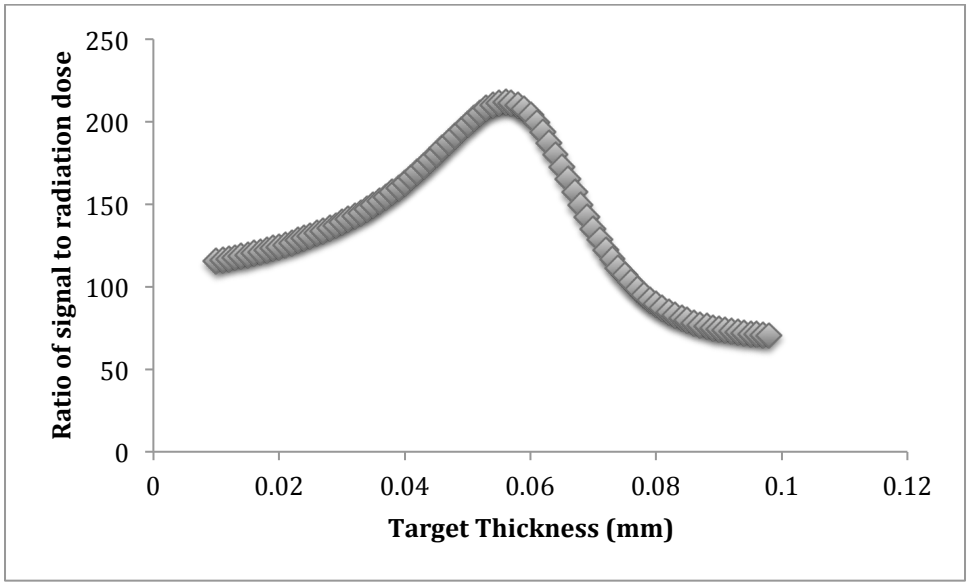

Figure 5.6 Potential x-ray signal divided by radiation dose versus Uranium target thickness in centimeters.

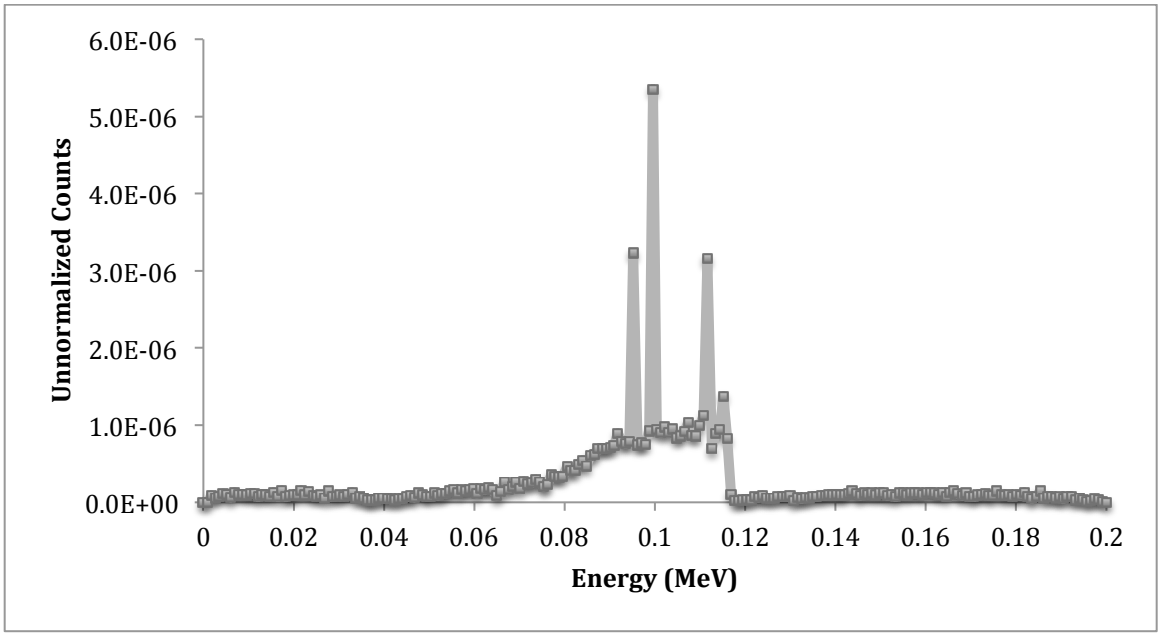

Figure 5.7 Optimized spectrum obtained using the 0.56 mm Uranium target thickness.

5.3.3 High-Energy X-ray Tube Geometry Optimization

Using our uranium target with a 90-degree geometry, we wanted to determine which setup of three would be most optimal for the source detector geometry: 1) thinnest skin at the x-ray tube source, 2) thinnest skin halfway between source and detector, and 3) thinnest skin at the detector. The comparison between these situations can be seen in Table 5.4 as a percentage of the signal from the optimized geometry with the thinnest skin at the detector. To further clarify this comparison Figures 5.8 and 5.9 show an example of the geometry for thinnest skin at the source and detector respectively.

Table 5.4 Detector geometry optimization in terms of the thinnest skin direction.

Source	Halfway	Detector
0.326	0.644	1.000

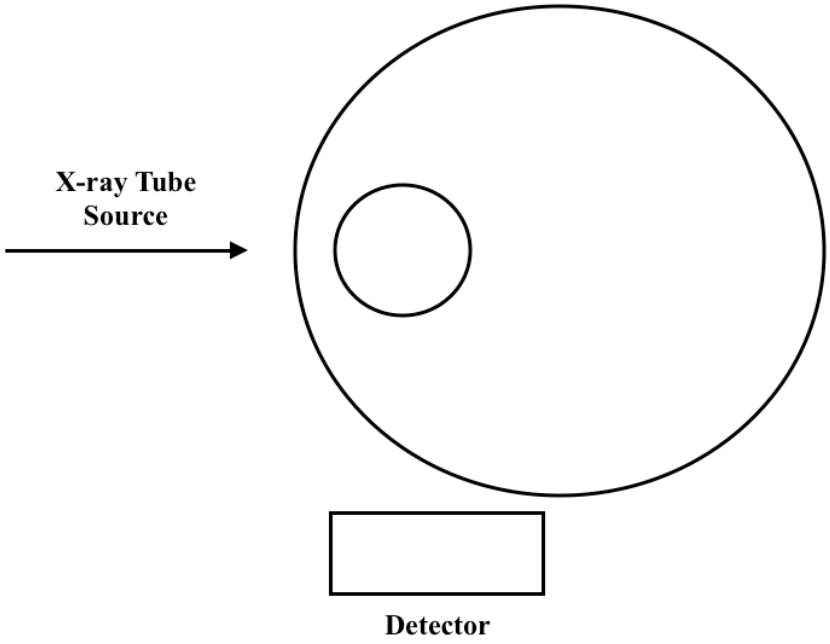

Figure 5.8 Example of geometry with thinnest skin at the x-ray tube source.

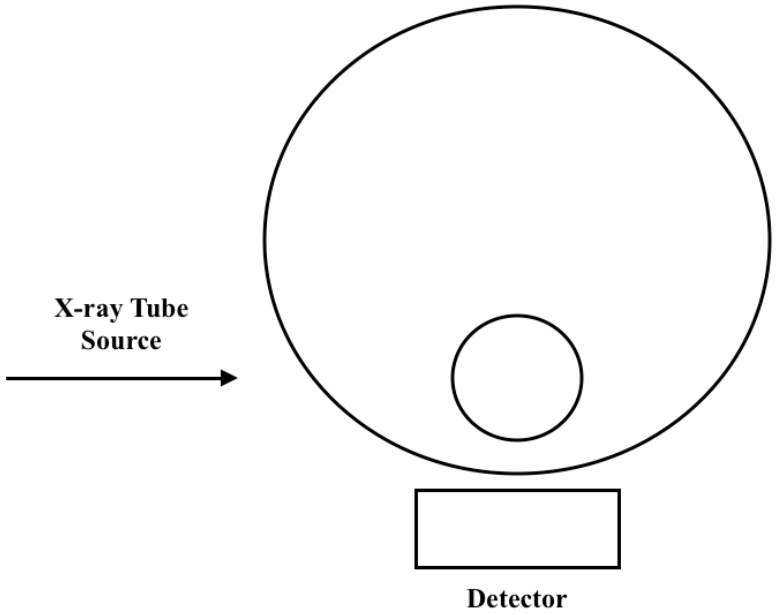

Figure 5.9 Example of geometry with thinnest skin at the detector.

5.3.4 Comparison Between the High-Energy X-ray Tube KXRF and Cd-109 KXRF Bone Pb Measurements

The results from the simulation are shown in Table 5.5 below. A sample spectrum as taken from the CdZnTe detector with 100 ppm phantom is shown below in Figure 5.10. The simulation signals are normalized to the skin dose for Cd-109 based KXRF systems. The signal ratio (SR) is a ratio of the simulated signal versus Cd-109 experimental signal and is calculated as follows:

$$SR = \frac{N_{\beta-x} + N_{\alpha-x}}{N_{\beta-Cd} + N_{\alpha-Cd}}$$

where $N_{\beta-x}$ and $N_{\alpha-x}$ are the net signals from simulation of K beta and alpha peaks, and $N_{\beta-Cd}$ and $N_{\alpha-Cd}$ are the net signals from Cd-109 based KXRF of K beta and alpha peaks. All signals are taken from measurements of simulated or experimental 100 ppm phantoms.

Table 5.5 Dose normalized signal comparison and MDL estimate of materials for KXRF x-ray tube system.

	Si	CdZnTe	Ge	Cd-109 based
Pb K Beta Signal (counts)	31	980	800	920
Pb K Alpha Signal (counts)	162	3406	3092	4400
MDL Estimate (μg/g bone mineral)	82.61	3.64	4.10	3

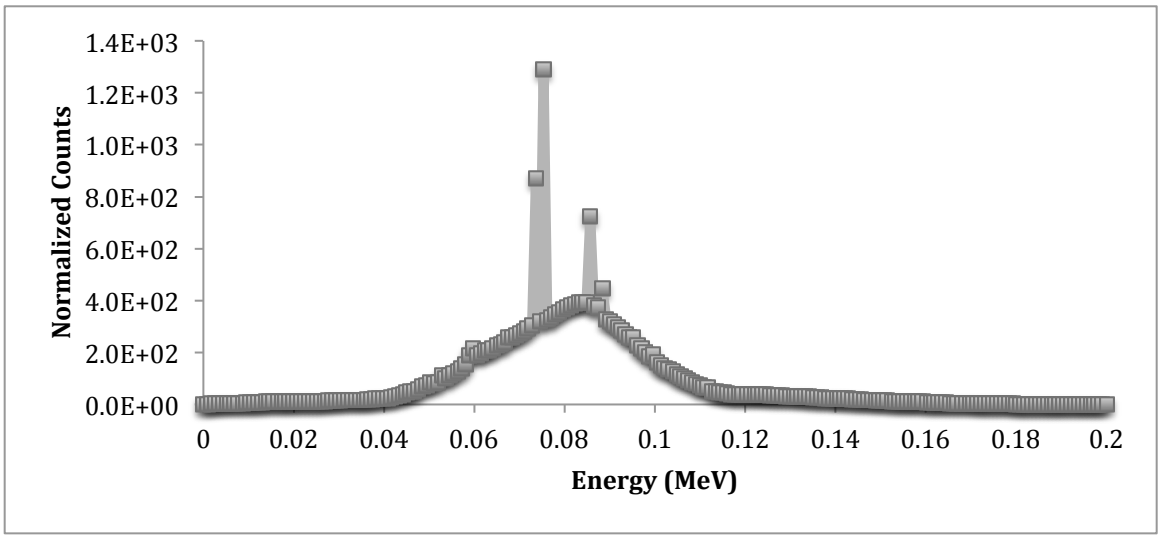

Figure 5.10 Sample spectrum as taken from the CdZnTe detector simulation for the 100 ppm phantom.

5.4 Discussion and Conclusions

The results from this study show that it is feasible to use an x-ray tube based KXRF system. Although there would be many obstacles to overcome in comparison to the Cd-109 based system in terms of signal degradation by using a different geometry, using a different material detector with lesser detector resolution, and using a source that has non-optimal properties for exciting Pb energies in materials. Even considering these initial problems, the system would still be viable for measurement albeit with a detection limit greater than current modern Cd-109 based systems. The system would also have advantages of current portable XRF technology because it would not have the significant issues with skin thickness degrading the measurement. Our study also shows the validity of using MCNP for x-ray tube and XRF simulations through comparison with experimental work.

MCNP simulations showed good agreement with experimental results from our Ag target x-ray tube based system. The simulation matched the shape of the experimental spectrum well, demonstrating its ability to accurately determine electron interactions in the target and filters through attenuation and absorption; however, one thing the simulation lacked was an appropriate amount of background in the low energy areas of the spectrum. With underestimation of the background, it is difficult to do a calculation of detection limit, since normally the background counts are an integral component in the calculation. Hence, this study uses signal to do a comparison of detection limit, because we do not know whether or not the background is accurate. The Ag characteristic peaks also matched poorly. Visually this was mostly a result of detector resolution. Numerically,

this was because of the way the experimental spectrum was measured. Since characteristic production is isotropic and bremsstrahlung production is mostly in the forward direction, there will be more of a dependency on distance from the target in the x-ray tube for characteristic production. Thus, being 10 cm away from the x-ray tube for our measurement of the spectra impacted the resultant comparison between the characteristic yield in the target versus the bremsstrahlung production, which would be mostly in the forward direction. When correcting the spectrum this way, the percent error between the Ag characteristics peaks for simulation and experiment goes to 0.4%.

The target thickness was optimized using potential signal production and radiation dose. The use of potential signal production rather than actual signal production was chosen to minimize time for simulations and to minimize the effect of the differences between the two simulations. The first simulation of x-ray production has a different source definition than the second simulation used to determine signal production for our in vivo measurement. If we were to use actual signal production we would be using both simulations, but by using only the potential of signal production with x-rays of >88 keV we only used the initial x-ray tube simulation. Doing this helped to minimize any potential differences between the simulations.

The choice of geometry is different from traditional Cd-109 systems with a 180-degree geometry. A 180-degree geometry has both the source and detector centered on the tibia bone with least amount of soft tissue interference. The 90-degree geometry was chosen to limit any interference with Compton scattering from the uranium target. Uranium characteristic energies from the uranium target scattered at 180-degrees would be the same energy of the K-alpha characteristic energies of Pb, so these two different

peaks would likely be indistinguishable. The uranium characteristic energies scattered at 90-degrees are 5 keV higher than Pb K-alpha energies The K-alpha Pb peaks will be the main source of signal for determining Pb concentration. Peaks from scatter will surround the K-beta energy peak, but that peak only has 35% intensity and will contribute much less to overall signal than the alpha peaks.

Optimizing the in vivo measurement for 90-degree geometry is less straightforward than for the 180-degree geometry on the Cd-109 system. There are three different geometries we tested using the simulation. Each setup pointed the shin, or the portion of the leg with least soft tissue over the tibia bone, in different directions: at the x-ray tube source, 45-degrees between source and detector, and at the detector. This comparison determined the maximum signal to arise from the geometry pointing the thinnest skin section towards the detector. Although my simulated geometry used a crude ellipsoid for the skin thickness and a less accurate cylinder for the tibia bone, this is likely a true observation. By aligning the thinnest skin thickness with the detector, you will collect the most Pb signals. When the x-ray tube irradiates the leg, the energy of the beam is high enough to penetrate through the surfaces and successfully ionize elements in the bone to create the initial Pb signal. That creation of signal would then serve as a secondary isotropic source in the bone of the leg, which would by definition of the inverse square law, have most signal collection by placing the detector closest to the bone where the source is located. Thus, the optimized geometry with the thinnest skin at the detector is justified.

The 90-degree geometry should work in our favor in terms of background levels. Background, which will primarily come from a photon undergoing multiple Compton

scattering interactions, should be minimized with a 90-degree geometry. Although, other scattering angles will each contribute small amounts to the background, looking at the Klein-Nishina formula reveals that the majority of scattering will be in the forward direction of the x-ray tube. Since 90-degree Compton scatter interactions at the energies of our x-ray tube would have the lowest cross-section of any angle, the background would be minimized in our 90-degree geometry, which would help lower the detection limit of the device, especially since our analysis assumes equivalent background between the Cd-109 system and our high energy x-ray tube system. One of the main reasons 180-degree geometries are used is for convenience. It is significantly more convenient to have the source mounted on the front of the detector and prevents interaction between the two, as well as helping to isolate the geometry, but the 90-degree geometry has the potential for lower background and better detection limit. When moving towards experimental designs, the isolation of a consistent geometry will be the utmost concern for this system.

The detection limit calculation is crude since it assumes background to be the same as for a Cd-109 system. A calculation of the detection limit using standard methods with our simulated background yields a detection limit result less than Cd-109 systems, which is false. Our calculation yields a more conservative estimate. Although these detection limit estimates are crude, they do give us insight into the difference the detector materials will make in our proposed system. It is also important to keep in mind the detectors may differ in size from the estimates used for the simulation, and these simulations did not take into account dead time or detector resolution, which will be another area where signal loss will occur. The silicon detector from our simulation is larger than anything currently available and thus unrealistic for consideration, but helps

to demonstrate the material differences in detectors contributing to the detection limit changes. Overall an experimental comparison will likely vary from the results shown here, which tried to take a conservative estimate for the detection limit, but the results should be consistent in verifying the feasibility of the system.

Although simulations leave out certain challenges the experimental setup will face, we believe these results demonstrate the feasibility of a KXRF x-ray tube based system based on the signal and detection limit estimates. There are numerous advantages of a KXRF system that is much more portable without the hindrance of liquid nitrogen cooling, using an x-ray tube source without degradation or complicated licensing, and using k-shell energies for Pb measurement.

MCNP has been shown to be a validated method in properly simulating x-ray tube physics by producing spectra of the same quality as experimental x-ray tubes of the same design. A high-energy x-ray tube based KXRF system using a transmission target made of uranium, has the ability to measure Pb in bone samples with a detection limit similar to second-generation radioisotope based KXRF bone Pb measurement systems. By using the high-energy of KXRF we can avoid the substantial limitations of soft tissue thickness that are prevalent in the portable XRF, but still maintain relative portability with an x-ray tube source. Based on these findings, development of a portable x-ray tube based KXRF system is feasible for in vivo measurement of bone Pb.

CHAPTER 6. CONCLUSION

A portable XRF device for quantification of Pb and Sr in vivo was developed in this work. The device was calibrated using standard phantoms and validated in lab using samples of cadaver and goat bone. The detection limit of the device for Pb was found to be less than 10 ppm for soft tissue thicknesses less than 5 mm, which is on par with conventional KXRF devices in most labs. The correlation between our cloverleaf Cd-109 KXRF and portable XRF bone Pb measurements for in lab samples correlated well and demonstrated the device capabilities for in vivo measurement.

The device was used in tandem with our cloverleaf Cd-109 KXRF for validation and measurement of bone Pb in a Pb poisoned children study in Shanghai, China. The device was shown to have difficulties with particular anatomical differences in the developing bones of children, but still maintained a significant correlation with the Cd-109 KXRF measurements. We found blood Pb to have a higher correlation value with our Cd-109 KXRF bone Pb measurements, which we associated with higher bone turnover in children. We found the children to store most of their body burden of Pb in their bone, and bone Pb to be a good biomarker for exposure in children. We were able to measure the half-life of Pb in blood in select cases for our study and calculated the half-life to be 10.45±11.71 days, which is significantly different from adult blood Pb half-life values.

We found a trend of decreased bone Pb values after chelation therapy, but the difference was non-significant, which may point towards the efficacy of chelation in removing the body Pb burden located primarily in bone. Since total Pb body burden is centralized in the bone and the half-life of Pb in blood for children is much shorter than adults we infer that bone Pb is a much better marker for monitoring Pb exposure and determining chelation efficacy in children.

We then calibrated the portable XRF for measurements of Sr in vivo. We produced a set of standard Sr phantoms using a new technique with Mowial-88 and bone meal, which produced phantoms we could use for calibration and MDL calculations appropriately. We found the MDL for Sr measurements to be about 15 ppm at about 9 mm of soft tissue thickness, which would be detectable for most subjects. We used the data collected in our study of Pb poisoned children to determine the Sr levels of these children and found an average of 43.2 ± 57.6 ppm of bone Sr. We correlated these values with age and found a significant relation in the whole group and females, but not in males. We then separated the groups by puberty age to identify any changes that may occur due to increased sex hormones and found significant differences in girls before and after puberty age. During this study we found that the portable XRF was able to measure bone Sr in vivo for most subjects and could be used clinically in determining the efficacy of Sr supplementation or toxicity of Sr exposure.

We finally explored the feasibility of creating a high-energy x-ray tube based KXRF bone Pb measurement system. We validated the use of MCNP for determination of experimental x-ray tube output. We determined a uranium target to be the most appropriate to measure Pb in vivo. We found an optimized uranium target thickness of

0.56 mm by minimizing radiation dose and maximizing potential signal. We then estimated the detection limit of our high-energy x-ray tube bone Pb measurement system to be 3.6 ppm by comparing the signal collected in the cloverleaf Cd-109 KXRF system for a 100 ppm phantom. We determined that the device would be feasible for bone Pb measurement with a detection limit about equivalent to a second-generation Cd-109 KXRF system.

In the future, the portable XRF can be applied for use in identifying other metals and tissues for in vivo measurement, such as Mn and Hg in toenail. The portable XRF can be applied to studies of subjects exposed to multiple metals for identification of synergistic health effects. The calibration of the portable XRF can be further optimized if a relation between composition and density changes in bone and spectral features can be identified and manipulated for use in our measurements. Further studies of Pb in children can reveal more information on the biokinetic differences observed in our study and may shed light on further differences between adults and children in this respect. The high-energy x-ray tube based KXRF measurement system can be developed for measurements of Pb and other metals in vivo with potential to overcome disadvantages seen in both portable XRF and KXRF systems.

LIST OF REFERENCES

LIST OF REFERENCES

1. Rabinowitz, M.B., *Toxicokinetics of bone lead.* Environ Health Perspect, 1991. **91**: p. 4.
2. Navas-Acien, A., et al., *Lead exposure and cardiovascular disease--a systematic review.* Environ Health Perspect, 2007. **115**(3): p. 472-82.
3. Weisskopf, M.G., et al., *Biased Exposure-Health Effect Estimates from Selection in Cohort Studies: Are Environmental Studies at Particular Risk?* Environ Health Perspect, 2015. **123**(11): p. 1113-22.
4. Weuve, J., et al., *Cumulative exposure to lead and cognition in persons with Parkinson's disease.* Mov Disord, 2013. **28**(2): p. 176-82.
5. Jusko, T.A., et al., *Blood lead concentrations < 10 microg/dL and child intelligence at 6 years of age.* Environ Health Perspect, 2008. **116**(2): p. 243-8.
6. Lanphear, B.P., et al., *Low-level environmental lead exposure and children's intellectual function: an international pooled analysis.* Environ Health Perspect, 2005. **113**(7): p. 894-9.
7. CDC., *Very High Blood Lead Levels Among Adults - United States 2002-2011*. 2013, Morbidity and Mortality Weekly. p. 967-971.
8. Bryan, C. *US leads Avgas effort for lead-free air*. 2014 [cited 2016 April 15].
9. Chettle, D.R., M.C. Scott, and L.J. Somervaille, *Lead in bone: sampling and quantitation using K X-rays excited by 109Cd.* Environ Health Perspect, 1991. **91**: p. 49-55.
10. Pejović-Milić, A., et al., *Quantification of bone strontium levels in humans by in vivo x-ray fluorescence.* Med Phys, 2004. **31**(3): p. 528-38.
11. Ozgür, S., H. Sümer, and G. Koçoğlu, *Rickets and soil strontium.* Arch Dis Child, 1996. **75**(6): p. 524-6.
12. Cabrera, W.E., et al., *Strontium and bone.* J Bone Miner Res, 1999. **14**(5): p. 661-8.
13. Dahl, S.G., et al., *Incorporation and distribution of strontium in bone.* Bone, 2001. **28**(4): p. 446-53.
14. Boivin, G., et al., *In osteoporotic women treated with strontium ranelate, strontium is located in bone formed during treatment with a maintained degree of mineralization.* Osteoporos Int, 2010. **21**(4): p. 667-77.
15. Meunier, P.J., et al., *The effects of strontium ranelate on the risk of vertebral fracture in women with postmenopausal osteoporosis.* N Engl J Med, 2004. **350**(5): p. 459-6

16. Reginster, J.Y., et al., *Strontium ranelate reduces the risk of nonvertebral fractures in postmenopausal women with osteoporosis: Treatment of Peripheral Osteoporosis (TROPOS) study.* J Clin Endocrinol Metab, 2005. **90**(5): p. 2816-22.
17. *The world health report 2004: changing history*. 2004, World Health Organization: Geneva.
18. Sakai, T., *Biomarkers of lead exposure.* Ind Health, 2000. **38**(2): p. 127-42.
19. Barry, P.S., *A comparison of concentrations of lead in human tissues.* Br J Ind Med, 1975. **32**(2): p. 119-39.
20. Mushak, P., *Gastro-Intestinal Absorption of Lead in Children and Adults: Overview of Biological and Biophysico-Chemical Aspects.* Chemical Speciation and Bioavailability, 1991. **3**(3-4): p. 18.
21. Arlot, M.E., et al., *Histomorphometric and microCT analysis of bone biopsies from postmenopausal osteoporotic women treated with strontium ranelate.* J Bone Miner Res, 2008. **23**(2): p. 215-22.
22. Nielsen, S.P., et al., *Noninvasive measurement of bone strontium.* J Clin Densitom, 2004. **7**(3): p. 262-8.
23. PB, H., et al., *Fluorescent thyroid scanning: a new method of imaging the thyroid.* Radiology, 1968. **90**: p. 18.
24. Ahlgren, L., et al., *X-ray fluorescence analysis of lead in human skeleton in vivo.* Scand J Work Environ Health, 1976. **2**(2): p. 82-6.
25. LK, S., C. DR, and S. MC, *In vivo measurement of lead in bone using X-ray fluorescence.* Phys Med Biol, 1985. **30**: p. 14.
26. Gordon, C.L., D.R. Chettle, and C.E. Webber, *An improved instrument for the in vivo detection of lead in bone.* Br J Ind Med, 1993. **50**(7): p. 637-41.
27. Nie, H., et al., *A Study of MDL Improvements for the In Vivo Measurement of Lead in Bone.* Nuclear Instruments and Methods in Physics Research B, 2004. **213**: p. 4.
28. Nie, H., et al., *In vivo investigation of a new 109Cd gamma-ray induced K-XRF bone lead measurement system.* Phys Med Biol, 2006. **51**(2): p. 351-60.
29. Wielopolski, L., et al., *Feasibility of noninvasive analysis of lead in the human tibia by soft x-ray fluorescence.* Med Phys, 1983. **10**(2): p. 248-51.
30. Wielopolski, L., et al., *In vivo bone lead measurements: a rapid monitoring method for cumulative lead exposure.* Am J Ind Med, 1986. **9**(3): p. 221-6.
31. Wielopolski, L., et al., *In vivo measurement of cortical bone lead using polarized x rays.* Med Phys, 1989. **16**(4): p. 521-8.
32. Todd, A.C., et al., *L-shell x-ray fluorescence measurements of lead in bone: accuracy and precision.* Phys Med Biol, 2002. **47**: p. 20.
33. Todd, A.C., *L-shell x-ray fluorescence measurements of lead in bone: system development.* Phys Med Biol, 2002. **47**: p. 15.
34. Todd, A.C., *L-shell x-ray fluorescence measurements of lead in bone: theoretical considerations.* Phys Med Biol, 2002. **47**: p. 14.
35. Specht, A.J., M. Weisskopf, and L.H. Nie, *Portable XRF technology to quantify Pb in bone in vivo.* Journal of Biomarkers, 2014. **2014**: p. 9.

36. Specht, A.J., et al., *XRF-measured bone lead (Pb) as a biomarker for Pb exposure and toxicity among children diagnosed with Pb poisoning.* Biomarkers, 2016: p. 1-6.
37. Rosen, J.F., et al., *Sequential measurements of bone lead content by L X-ray fluorescence in CaNa2EDTA-treated lead-toxic children.* Environ Health Perspect, 1991. **93**: p. 271-7.
38. Specht, A.J., M. Weisskopf, and L.H. Nie, *Portable XRF Technology to Quantify Pb in Bone In Vivo.* J Biomark, 2014. **2014**: p. 398032.
39. Royce, S., *Lead Toxicity*. 1990, U.S. Dept. of Health and Human Sevices, Public Health Service, Agency for Toxic Substances and Disease Registry.
40. Navas-Acien, A., et al., *Bone lead levels and blood pressure endpoints.* Epidemiology, 2008. **19**: p. 8.
41. Navas-Acien, A., et al., *Blood cadmium and lead and chronic kidney disease in US adults: a joint analysis.* Am J Epidemiol, 2009. **170**(9): p. 1156-64.
42. Schaumberg, D.A., et al., *Accumulated lead exposure and risk of age-related cataract in men.* JAMA, 2004. **293**: p. 4.
43. Shih, R.A., et al., *Cumulative lead dose and cognitive function in adults: a review of studies that measured both blood lead and bone lead.* Environ Health Perspect, 2007. **115**(3): p. 9.
44. Leggett, R.W., *An age-specific kinetic model of lead metabolism in humans.* Environ Health Perspect, 1993. **101**: p. 18.
45. Todd, A.C., et al., *Validation of X-ray fluorescence-measured Swine femur lead against atomic absorption spectrometry.* Environ Health Perspect, 2001. **109**(11): p. 1115-9.
46. Hubbell, J.H. and S.M. Seltzer. *NIST: X-ray Mass Attenuation Coefficients*. 1982 [cited 2016 April 20].
47. Nie, H., et al., *In vivo quantification of lead in bone with a portable x-ray fluorescence system--methodology and feasibility.* Phys Med Biol, 2011. **56**(3): p. N39-51.
48. Nie, H., et al., *Dosimetry study for a new in vivo X-ray fluorescence (XRF) bone lead measurement system*. 2007: Nuclear Instruments and Methods in Physics Research B. p. 225-230.
49. Pejović-Milić, A., et al., *Ultrasound measurements of overlying soft tissue thickness at four skeletal sites suitable for in vivo x-ray fluorescence.* Med Phys, 2002. **29**(11): p. 2687-91.
50. Todd, A.C., et al., *Individual variability in human tibia lead concentration.* Environ Health Perspect, 2001. **109**(11): p. 1139-43.
51. Bellis, D.J., et al., *Measurement of the microdistribution of strontium and lead in bone via benchtop monochromatic microbeam X-ray fluorescence with a low power source.* J Anal At Spectrom, 2009. **24**(5): p. 622-626.
52. Canfield, R.L., et al., *Intellectual impairment in children with blood lead concentrations below 10 μg per deciliter.* N Engl J Med, 2003. **348**(16): p. 26.
53. Nie, L.H., et al., *Blood lead levels and cumulative blood lead index (CBLI) as predictors of late neurodevelopment in lead poisoned children.* Biomarkers, 2011. **16**(6): p. 517-24.

54. Behinaein, S., et al., *Factors influencing uncertainties of in vivo bone lead measurement using a (109)Cd K X-ray fluorescence clover leaf geometry detector system.* Environ Sci Process Impacts, 2014. **16**(12): p. 2742-51.
55. Bevington, P. and D. Robinson, *Data reduction and error analysis for the physical sciences*. 2003, New York, NY: McGraw-Hill.
56. Nie, H., *Studies in bone lead: A new cadmium-109 XRF measurement system. Modeling bone lead metabolism. Interpreting low concentration data*. 2005, McMaster University (Canada), 2005. p. 191 p.
57. Somervaille, L.J., et al., *In vivo measurements of bone lead-a comparison of two x-ray fluorescence techniques used at three different bone sites.* Phys Med Biol, 1989. **34**(12).
58. Todd, A.C., *Calculating bone-lead measurement variance.* Environ Health Perspect, 2000. **108**(5): p. 383-6.
59. Liu, K.L., *[Review of atomic spectroscopy].* Guang Pu Xue Yu Guang Pu Fen Xi, 2005. **25**(1): p. 95-103.
60. Specker, B., et al., *Total body bone mineral content and tibial cotrical bone measures in preschool children.* Journal of Bone and Mineral Research, 2001. **16**(12).
61. Linderkamp, O.V., H. T.; Riegel, K. P.; Betke, K., *Estimation and Prediction of Blood Volume in Infants and Children.* European Journal of Pediatrics, 1977. **125**: p. 227-234.
62. ICRP, *Publication 70, Basic anatomical and physiological data for use in radiological protection - the skeleton.* Annals of the ICRP, 1995. **25**(2).
63. Bleecker, M., et al., *Relationship between bone lead and other indices of lead exposure in smelter workers.* Toxicology Letters, 1995. **77**: p. 241-248.
64. Fleming, D.E., et al., *Accumulated body burden and endogenous release of lead in employees of a lead smelter.* Environ Health Perspect, 1997. **105**(2): p. 224-33.
65. Gerhardsson, L., et al., *In vivo measurements of lead in bone in long-term exposed lead smelter workers.* Arch Environ Health, 1993. **48**(3): p. 147-56.
66. Nie, H., et al., *Bone lead and endogenous exposure in an environmentally exposed elderly population: the normative aging study.* J Occup Environ Med, 2009. **51**(7): p. 848-57.
67. Manton, W.I., et al., *Acquisition and retention of lead by young children.* Environ Res, 2000. **82**(1): p. 60-80.
68. Duggan, M.J., *The uptake and excretion of lead by young children.* Arch Environ Health, 1983. **38**(4): p. 246-7.
69. Marie, P.J., et al., *Mechanisms of action and therapeutic potential of strontium in bone.* Calcif Tissue Int, 2001. **69**(3): p. 121-9.
70. Cohen-Solal, M., *Strontium overload and toxicity: impact on renal osteodystrophy.* Nephrol Dial Transplant, 2002. **17 Suppl 2**: p. 30-4.
71. Pors Nielsen, S., *The biological role of strontium.* Bone, 2004. **35**(3): p. 583-8.
72. Mostafaei, F., et al., *Design of a phantom equivalent to measure bone-fluorine in a human's hand via delayed neutron activation analysis.* Physiol Meas, 2013. **34**(5): p. 503-12.

73. Da Silva, E., et al., *Pure hydroxyapatite phantoms for the calibration of in vivo X-ray fluorescence systems of bone lead and strontium quantification.* Anal Chem, 2013. **85**(19): p. 9189-95.
74. Lee, P.A., *Normal ages of pubertal events among American males and females.* J Adolesc Health Care, 1980. **1**(1): p. 26-9.
75. Popovic, M., et al., *Impact of occupational exposure on lead levels in women.* Environ Health Perspect, 2005. **113**(4): p. 478-84.
76. Mostafaei, F., et al., *Measurements of fluorine in contemporary urban Canadians: a comparison of the levels found in human bone using in vivo and ex vivo neutron activation analysis.* Physiol Meas, 2015. **36**(3): p. 465-87.
77. Clarke, B.L. and S. Khosla, *Female reproductive system and bone.* Arch Biochem Biophys, 2010. **503**(1): p. 118-28.
78. Salgado, C.M., C.C. Conti, and P.H. Becker, *Determination of HPGe detector response using MCNP5 for 20-150 keV X-rays.* Appl Radiat Isot, 2006. **64**(6): p. 700-5.
79. F, E.L., T.U. Clayton, and W.M. John, *Composite x-ray target*. 1929, Google Patents: United States.

VITA

VITA

Aaron Specht

Doctoral Student, Medical Physics Program
College of Health and Human Sciences
School of Health Sciences,
Purdue University

EDUCATION

2008-2012 Purdue University West Lafayette, IN
- B.S. Honors Physics
- GPA 3.7/4.0

2012-Present Purdue University West Lafayette, IN
- Medical Physics Doctoral Student
- GPA 3.9/4.0

RESEARCH EXPERIENCE

5/2011-Present Purdue University, Medical Physics West Lafayette, IN
- Created a MCNP simulation model of a portable x-ray fluorescence device to quantify metals in bone in vivo.
- Developed several calibration techniques and calibrated a portable LXRF device for use in quantifying bone lead in vivo.
- Conducted a lead poisoning study in China among a pediatric population.
- Conducted a pilot study in China to measure bone lead concentration in an Alzheimer's disease (AD) population.
- Initiated a project to develop a portable KXRF system to measure lead and other metals in bone.
- Participated a study using synchrotron micro-XRF to determine the metal distribution in tooth samples
- Published 2 papers, submitted 1 paper, and 2 manuscripts in preparation

1/2011-5/2011 Purdue University, Medical Physics West Lafayette, IN

- Created a MCNP simulation of a CT scanner to explore dose information with phantoms.
- Familiarized myself with protocols and standards in practice in modern CT imaging.

1/2009-5/2011 Purdue University, Physics West Lafayette, IN

- Searched for Correlation between Nuclear Decay Rates and Earth-Sun Distance with Professor Virgil Barnes.
- Used NaI detectors to measure decay of isotopes over long periods of time.
- Studied equipment sensitivity to environmental effects, such as temperature for use in data correlations.
- Created a simulation of the NaI(TI) detector using Java and FORTRAN

HONORS AND AWARDS

2008-2012 Dean's List and Semester Honors all semesters at Purdue University
2008 Gianni Ascarelli Student Award Physics Research Fellowship
2011 Spira Undergraduate Research Award
2012 Ross Fellowship
2013 Purdue Doctoral Fellowship
2013 International Society of Exposure Sciences (ISES) Poster Award
2014 Purdue Research Foundation (PRF) research grant
2015 SOT Graduate Student Travel Award

PROFESSIONAL AND SCHOLARLY ASSOCIATIONS

2014 – present International Society of Exposure Sciences (ISES)
2013 – present Society of Toxicology (SOT)
2013 – present Health Physics Society (HPS)

PUBLICATIONS

1. Specht, A. J., Weisskopf, M. & Nie, L. H. 2014. Portable XRF technology to quantify Pb in bone in vivo. *Journal of Biomarkers,* Volume 2014 (2014), Article ID 398032, http://dx.doi.org/10.1155/2014/398032
2. Specht A. J., Lin Y, Weisskopf M, Yan CH, Hu H, Xu J, Nie LH. 2016. KXRF-measured bone lead (Pb) as a biomarker for Pb exposure and toxicity among children diagnosed with Pb poisoning. Biomarkers, e-pub ahead of print: http://dx.doi.org/10.3109/1354750X.2016.1139183
3. Wang Y, Specht A, Liu Y, Finney L, Maxey E, Zheng W, Weisskopf M, Nie LH. Micro-distribution of lead in human teeth using synchrotron-µXRF. X-ray Fluorescence, submitted
4. Specht A, Mostafaei F, Lin Y, Xu J, Nie LH. Measurements of strontium levels in bone in vivo using x-ray fluorescence (XRF) among a pediatric population. Manuscript in Preparation.
5. Specht A and Nie LH. Feasibility of x-ray tube based KXRF bone lead measurement system. Manuscript in Preparation.

My Bibliography link:
http://www.ncbi.nlm.nih.gov/sites/myncbi/aaron.specht.1/bibliography/49161815/public/?sort=date&direction=a scending

ABSTRACTS, CONFERENCES, AND PRESENTATIONS

1. Specht A, Weisskopf MG, and Nie LH. Portable XRF Technology to Quantify Lead and Strontium in Bone *in vivo* – Calibration and Validation, abstract Published in "The Toxicologist" (2013) and project presented at the 2013 Annual SOT meeting Mar. 10-14, San Antonio, Texas
2. Specht A, Weisskopf MG, and Nie LH. Calibration and improvements of a portable XRF technology to quantify lead in bone *in vivo*, abstract Published in "The Toxicologist" (2014) and project presented at the the 2014 Annual SOT meeting Mar. 23-27, Phoenix, Arizona
3. Specht A, Weisskopf MG, and Nie LH. Improvements in portable XRF technology to quantify lead in bone in vivo, abstract published and podium presentation for the 2014 Lead Collaborative Consortium June 5-7, Hamilton, ON, Canada
4. Specht A, Weisskopf MG, and Nie LH. Calibration and improvements of a portable XRF technology to quantify lead in bone in vivo, abstract published and project presented at the 2014 Annual ISES meeting Oct. 12-16, Cincinnati, Ohio.
5. Specht A, Lin Y, Weisskopf M, Yan CH, Hu H, Xu J, Nie LH. KXRF-measured Bone Lead (Pb) As A Biomarker For Pb Exposure And Toxicity Among Children Diagnosed With Pb Poisoning, abstract accepted for presentation at the 2016 Annual SOT meeting Mar. 13-17, New Orleans, LA.
6. Specht A, Weisskopf MG, and Nie LH. Calibration and improvements of a portable XRF technology to quantify lead in bone in vivo, College of Health and Human Sciences Research Day, 2014.
7. Specht A, Weisskopf MG, and Nie LH. Calibration and improvements of a portable XRF technology to quantify lead in bone in vivo, College of Health and Human Sciences Research Day, 2015.
8. Specht A. Calibration and improvements of a portable XRF technology to quantify lead in bone in vivo, Seminar in School of Health Sciences, Jan. 28 2014.
9. Specht A. XRF technology to quantify lead in bone in vivo, Seminar in School of Health Sciences, Nov. 3 2015.

GRANT PENDING

1F32ES027330-01, PI 08/01/2016 –07/31/2019

A novel portable KXRF bone lead (Pb) measurement system for use with the assessment of Pb associated psychiatric symptoms
To test the viability of an x-ray tube based portable KXRF device to measure lead in bone and study lead associated change of psychiatric symptoms.

TEACHING EXPERIENCE

HSCI 574 Medical Health Physics — Spring 2013
Teaching Assistant to Dr. Mark Richard

HSCI 514 Radiation Instrumentation Lab — Spring 2014
Teaching Assistant to Drs. Linda Nie and Jim Schweitzer

MENTORING EXPERIENCE

Supervising MS Graduate Research; Student supervised:

Xinxin Zhang

Project title: Development and Validation of Portable XRF Technology to Measure Manganese in Toenail *In Vivo*

Supervising Undergraduate Research; Students supervised:

Scott Blake

Project title: Design and Build a Customized Moderator/Reflector/Shielding Assembly for *In Vivo* Measurement of Manganese in Bone Using NAA Technology

Austin Trout

Project title: Dosimetry Study of *In Vivo* Neutron Activation Analysis of Metals in Bone

Jacob Wilson

Project title: In Vivo Measurement of Fluorine in Bone using IVNAA Technology: Monte Carlo Simulations

Nikola Plavsa

Project title: Monte Carlo (MC) Simulation of In Vivo Measurement of Metals in Bone using a Portable XRF Device

Zheng Gu

Project title: Development of Metal Doped Phantoms for *In Vivo* Metal Measurements of Metals in Toenails

Emma Wallens

Project title: Feasibility Study of Measurement of Lead in Condor Bones *In Vivo* Using Portable XRF Technology